DANIEL JONAS DEZAN

HEAT TRANSFER ENHANCEMENT AND OPTIMIZATION OF FLAT-TUBE MULTILOUVERED FIN COMPACT HEAT EXCHANGERS WITH DELTA-WINGLET VORTEX GENERATORS

São Paulo – SP
2015

DANIEL JONAS DEZAN

HEAT TRANSFER ENHANCEMENT AND OPTIMIZATION OF FLAT-TUBE MULTILOUVERED FIN COMPACT HEAT EXCHANGERS WITH DELTA-WINGLET VORTEX GENERATORS

Thesis Submitted in Partial Fulfillment of the Requirements for the Degree of Doctor of Science in Mechanical Engineering

Graduate Program of
Mechanical Engineering

Advisor:
Prof. Dr. Jurandir Itizo Yanagihara

São Paulo
2015

Este exemplar foi revisado e corrigido em relação à versão original, sob responsabilidade única do autor e com a anuência de seu orientador.

São Paulo, _____ de _____ de _____

Assinatura do autor: _____

Assinatura do orientador: _____

Catalogação-na-publicação

ACKNOWLEDGMENTS

RESUMO

Esta pesquisa visa a análise da contribuição de cinco variáveis de entrada e a otimização do desempenho termo-hidráulico de trocadores de calor com venezianas combinados com geradores de vórtices *delta-winglets*. O desempenho termo-hidráulico de duas geometrias distintas, aqui nomeadas por GEO_1 e GEO_2, foram avaliadas. Smoothing Spline ANOVA foi usado para avaliar a contribuição dos parâmetros de entrada na transferência de calor e perda de carga. Considerando aplicação automotiva, foram investigados números de Reynolds iguais a 120 e 240, baseados no diâmetro hidráulico. Os resultados indicaram que o ângulo de venezianas é o maior contribuidor para o aumento do fator de atrito para GEO_1 e GEO_2, para ambos os números de Reynolds. Para o número de Reynolds menor, o parâmetro mais importante em termos de transferência de calor foi o ângulo das venezianas para ambas as geometrias. Para o número de Reynolds maior, o ângulo de ataque dos geradores de vórtices posicionados na primeira fileira é o maior contribuidor para a tranfesferência de calor, no caso da geometria GEO_1, enquanto que o ângulo de ataque dos geradores de vórtices na primeira fileira foi tão importante quanto os ângulos das venezianas para a geometria GEO_2. Embora as geometrias analisadas possam ser consideradas como técnicas compostas de intensificação da transferência de calor, não foram observadas interações relevantes entre ângulo de venezianas e parâmetros dos geradores de vórtices. O processo de otimização usa NSGA-II (Non-Dominated Sorting Genetic Algorithm) combinado com redes neurais artificiais. Os resultados mostraram que a adição dos geradores de vórtices em GEO_1 aumentaram a transferência de calor em 21% e 23% com aumentos na perda de carga iguais a 24,66% e 36,67% para o menor e maior números de Reynolds, respectivamente. Para GEO_2, a transferência de calor aumentou 13% e 15% com aumento na perda de carga de 20,33% e 23,70%, para o menor e maior número de Reynolds, respectivamente. As soluções otimizadas para o fator de Colburn mostraram que a transferência de calor atrás da primeira e da segunda fileiras de geradores de vórtices tem a mesma ordem de magnitude para ambos os números de Reynolds. Os padrões de escoamento e as características de transferência de calor das soluções otimizadas apresentaram comportamentos

particulares, diferentemente daqueles encontrados quando as duas técnicas de intensificação de transferência de calor são aplicadas separadamente.

Palavras-chave: Intensificação da transferência de calor, Técnicas de intensificação compostas, Trocadores de calor compactos com venezianas, Geradores de vórtices, Otimização com modelos de superfície de resposta, Redes neurais artificiais, Algoritmo genético, Análise estatística.

ABSTRACT

This doctoral thesis focuses on screening analysis of five input parameters and heat transfer and pressure drop optimization of flat-tube multi-louvered fin heat exchangers combined with delta-winglet vortex generators. The thermal-hydraulic performance of two distinct geometries, GEO_1 and GEO_2, were evaluated. Smoothing Spline ANOVA was used to evaluate the contribution of the input parameters such as louver angle, angle of attack of the delta-winglet and streamwise position of the delta-winglet on heat transfer and pressure drop. Taking the automotive application into account, Reynolds numbers of 120 and 240, based on hydraulic diameter, were investigated. The results indicated that the louver angle is the main contributor to increase the Friction factor for GEO_1 and GEO_2 for both Reynolds numbers. For the lower Reynolds number, the most important heat transfer parameter was the louver angle for both geometries, while at the higher Reynolds number, the angles of attack of the first row of delta-winglets mostly contributed to GEO_1, and the angle of attack of the first row of delta-winglets was as important as the louver angle for GEO_2. Although those specific geometries can be considered a kind of compound enhancement technique, relevant interactions were not verified between louvers and delta-winglet vortex generators parameters. The surrogate-based optimization procedure uses NSGA-II method (Non-Dominated Sorting Genetic Algorithm) combined with artificial neural networks. The results showed that the addition of DWLs on GEO_1 increased the heat transfer of 21.27% and 23.52% with associated pressure loss increasing of 24.66% and 36.67% for the lower and the higher Reynolds numbers, respectively. For GEO_2, the heat transfer was increased 13.48% and 15.67% with an increase of the pressure drop of 20.33% and 23.70%, for the lower and the higher Reynolds numbers, respectively. The optimized solutions for the Colburn factor showed that heat transfer behind the second row of delta-winglets has the same order of magnitude of that behind the first row, for both Reynolds numbers. The flow patterns and heat transfer characteristics from optimized solutions presented some particular behavior, differently from the findings when those two heat transfer enhancement techniques are applied separately.

CONTENTS

LIST OF FIGURES

Chapter 3

Chapter 4

Chapter 5

LIST OF TABLES

LIST OF ABBREVIATIONS AND ACRONYMS

ANN — Artificial Neural Networks

ANOVA — Analysis of Variance

DOE — Design of Experiments

DWL — Delta winglet vortex generator

FVM — Finite Volume Method

GA — Genetic Algorithm

GEO_1 — Optimized geometry with louver height of 5.54 mm and DWL chord of 1.98 mm

GEO_2 — Optimized geometry with louver height of 8.00 mm and DWL chord of 1.76 mm

LHS — Latin Hypercubes Sampling

LVG — Longitudinal Vortex Generators

MLP — Multilayer-Perceptron

MLS — Moving Least Squares

NSGA-II — Non-Dominated Sorting Genetic Algorithm

RBF — Radial Basis Functions

RNG — Re-Normalization Group Theory

RMSE — Root Mean Square Error

RSM — Response Surface Methodology

SIMPLE   Semi-Implicit Method for the Pressure-Linked Equations

SS-ANOVA   Smoothing Spline ANOVA

SST   Shear-Stress Transport

SVR   Support Vector Regression

VG-F   Forward Vortex Generator

VG-B   Backward Vortex Generator

LIST OF SYMBOLS

Roman Symbols

A_C	Minimum flow cross-sectional area (m^2)
A_0	Total surface area (m^2)
A_{fr}	Fin frontal area (m^2)
b(v)	Sigmoid activation function (-)
C_{ij}	Cosines matrix on SS-ANOVA method
$D_h = \dfrac{4A_{fr}}{E}$	Hydraulic diameter (m)
E	Wet perimeter (m)
$Eu = \dfrac{2\Delta P}{\rho U_C^2}$	Euler number (-)
f	Friction factor
F_D	Flow depth (mm)
F_H	Fin height (mm)
F_P	Fin pitch (mm)
F_i	Fitness function
h	Convection heat transfer coefficient
j	Colburn factor
k	specific turbulent kinetic energy (m^2/s^2)
L_H	Louver height (mm)

L_P	Louver pitch (mm)
Re_{Dh}	Reynolds number based on hydraulic diameter
Re_{LP}	Reynolds number based on louver pitch
R^2	Coefficient of determination
St	Stanton number
T	Temperature (K)
T_P	Transverse tube pitch (mm)
$U_C = \dfrac{UA_{fr}}{A_C}$	Maximum air velocity (m/s)
x	Delta-winglet streamwise position (mm)
y	Delta-winglet spanwise position (mm)

Greek Symbols

ϕ	Louver angle (º)
θ	Delta-winglet angle of attack (º)
δ	Hydrodynamic boundary layer thickness (mm)
ε	Turbulent kinetic energy dissipation rate (m^2/s^3)
ω	Specific dissipation rate (m^2/s^3)
κ_k	Collinearity indice
λ	Stepness of the logistic function
ρ	Air density (kg/m^3)
η	Flow efficiency (%)

Γ^* Vector columns on SS-ANOVA method

Subscripts

in	Inlet
out	Outlet
o	Reference value
w	Tube or fin wall
1	First delta winglet placed on the first row
2	Second delta winglet placed on the first row
3	First delta winglet placed on the second row
4	Second delta winglet placed on the second row
*	Constant terms on vector columns are neglected

1 Introduction

Compact heat exchangers are widely used in several applications, such as in automotive and chemical industries, residential air-conditioning and refrigeration systems. The subject of heat transfer enhancement is of significant interest for developing compact heat exchangers to meet the demand for high efficiency and low cost with the smallest volume possible and as light as possible. Normally, the high surface area densities of compact heat exchangers lead to ducts with small aspect ratios. To avoid high pressure drops and pumping power for the fluid, low velocity flow are commonly used.

The heat transfer in air flow is much lower than in liquids flows and thus the great challenge is to enhance the convective heat transfer on air-side. Typically, air-side resistance to heat transfer is responsible for 80 – 90 percent of the total resistance to heat flow. Densely packed fins are commonly used to increase the air-side surface area and play the dual role of increasing the convection heat transfer coefficient (Mohammad et al., 2008). Aluminium and cooper are the most popular metal materials used on heat exchangers due to their high thermal conductivity.

Many techniques have been used to enhance the heat transfer over the years. Basically, there are two effective ways to enhance the heat transfer: (*i*). alterations to the main flow and; (*ii*). introduction or exploitation of secondary flows. In main flow enhancement, the gross characteristics of the flow are manipulated through pressure variations due to periodic interruption of the growth of the thermal boundary layers close to the heat transfer surfaces or due to geometric changes. Plate-and-fin extended surfaces such as louvered fins, offset-strip fin and pin fins are examples of elements which rely on the first enhancement technique. Secondary flows are vortical structures which are deliberately introduced in the local flow. This technique is used to increase of fluid mixing, fluid vorticity and turbulence intensity. Examples of devices which can generate secondary flows are the vortex generators (VGs) in form of protuberances such as delta-wings, rectangular wings and delta winglets.

The simultaneous combination of two or more techniques of heat transfer enhancement can produce better results than techniques applied separately. Both

louvered fins and vortex generators are recognized as enhancement techniques which have shown good results for heating, ventilation, air-conditioning and refrigeration applications. This combination is usually called *compound enhancement* technique (Bergles, 2002).

The benefits of heat transfer enhancement by using special surface geometries are due to an increase of the convective heat transfer coefficient or/and surface area. Three usual methods may be used to increase both (Webb and Kim, 2005):

1. Increase both convective heat transfer and surface area through the employment of interrupted fin geometries that provide a higher convective heat transfer than "*smooth*" surfaces.

2. Convective heat transfer augment without an appreciable surface area increase.

3. Increase of surface area without appreciable convective heat transfer augment.

1.1 Plate-and-fin extended surface geometries (louvered fins)

The enhanced performance of plate-and-fin extended surface heat exchangers have made them to be applied in a wide variety of single-phase applications and, normally, at least one of the work fluids used in the plate-and-fin geometry is a gas. The use of extended surfaces reduces the gas-side thermal resistance and thus provides an increase of the convective heat transfer coefficient. However, the heat transfer enhancement is always associated with pressure drop increasing. The main fin geometries used are: plain fins (rectangular and triangular shapes), perforated fins, wavy fins, pin fins, offset strip fins and louvered fins.

The first reliable study about louvered fins was published in 1950 by Kays and London (1984). Louvered fins are very popular in automotive applications and when combined with flat tubes they result in very compact heat exchangers. The louvers

interrupt the airflow and create a series of thin boundary layers that have lower thermal resistance. Figure 1-1 depicts a schematic of flat-sided tube and louvered plate fin heat exchanger, and the Figure 1-2 shows the side view with the main geometric parameters of the louvered fins. As it can be seen from Figure 1-2, experimental studies aimed at optimizing louvered fin geometries tend to be costly and time-consuming because of the amount of geometrical parameters involved. Thus, the amount of works based on numerical analysis to evaluate the heat transfer enhancement on louvered fins has increased over the years.

A distinct additional flow characteristic arises in louvered fins for low and high Reynolds numbers if compared with other types of geometries (T'Joen et al., 2011), (Malapure et al., 2007):

i. <u>Low Reynolds numbers</u>: thick boundary layers block the passage between the louvers, forcing the flow to pass between the different fins. This phenomenon can be attributed to the high flow resistance due to louvers. In most cases, the air temperature reaches the fin temperature in the initial part of the second half of the louvered array, and as a result the heat transfer performance of the fin is poor. Also, the second half of the louvers array only accounts for pressure loss without any significant heat transfer enhancement. This flow pattern is referred as duct-directed flow (Figure 1-3);

ii. <u>High Reynolds numbers</u>: the flow is deflected, lengthening the flow path. The fluid particles travel larger distances through the fin, resulting an increase of the heat exchange with a strong increase of pressure drop. The boundary layers around the louvers are thinner and the flow is nearly oriented with the louvers. Low pressure zones are created near the louvers due to formation of boundary layer. Large louver angles, small fin pitches, thin louvers and large louver pitches are conducive to called louver-directed flow, Figure 1-4 (Zhang and Tafti, 2003).
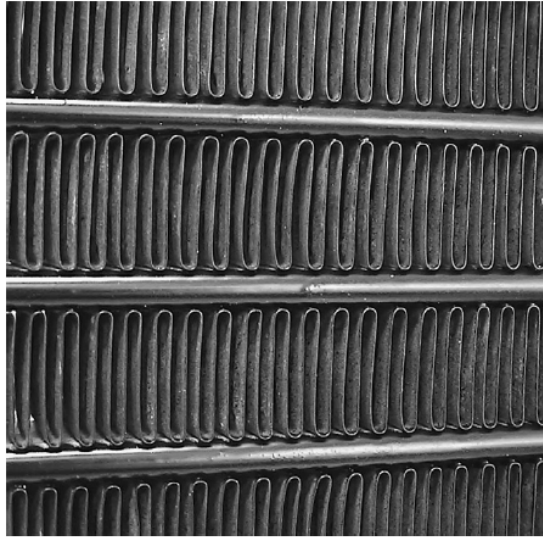
Figure 1-1 Louvered plate fin heat exchanger.
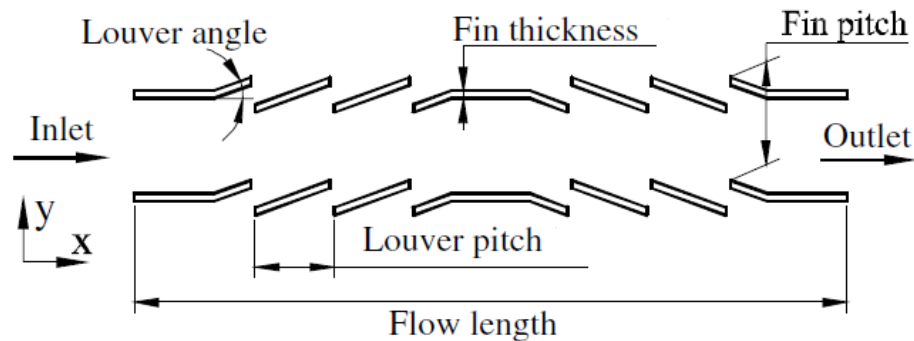
Figure 1-2 Main geometrical parameters of louvered fins (Hsieh and Jang, 2006).

According to Zhang and Tafti (2001), there are two primary mechanisms by which thermal wakes interfere with downstream louvers:

1. Intra-fin interference: thermal wakes of upstream louvers interfere with downstream louvers in the same fin. This mode of interference is divided in two types. The first one type is dominant in duct-directed flow, in which the thermal wakes of upstream louvers interfere with successive downstream louvers. The second type can commonly be identified in louver-directed flows for higher flow efficiencies. In this case, the wakes of upstream louver collide

on downstream louvers of the turnaround louver in the same fin row (Figure 1-5 a). This type of interference can be observed in large fin pitches, and small louver angles.

2. Inter-fin interference: this mode of interference is present in both louver-directed and duct-directed flows. However it is normally observed in louver- directed flow, when thermal wakes between fin rows interfere each to other (Figure 1- 5 b), increasing the heat transfer.
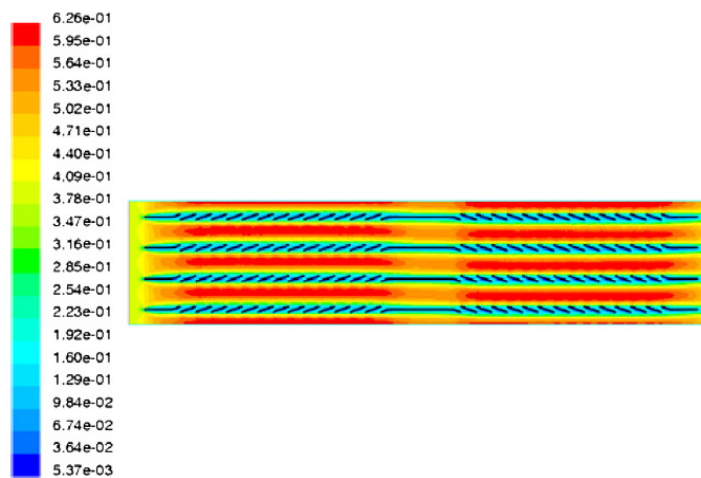
Figure 1-3 Example of "duct-directed flow" – Computed velocity in m/s (Malapure et al., 2007).
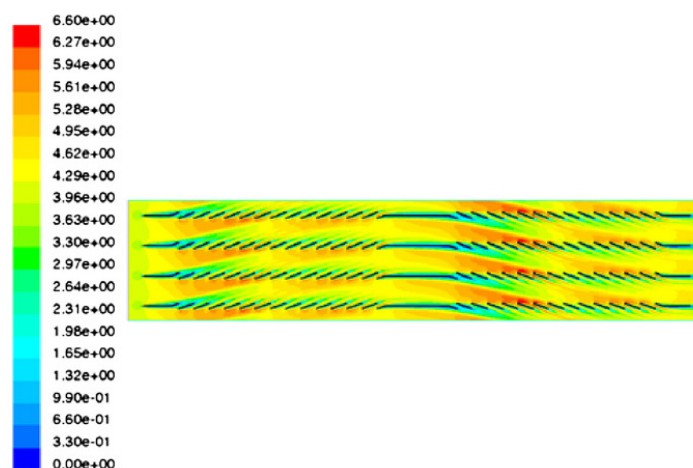
Figure 1-4 Example of "louver-directed flow" – Computed velocity in m/s (Malapure et al., 2007).
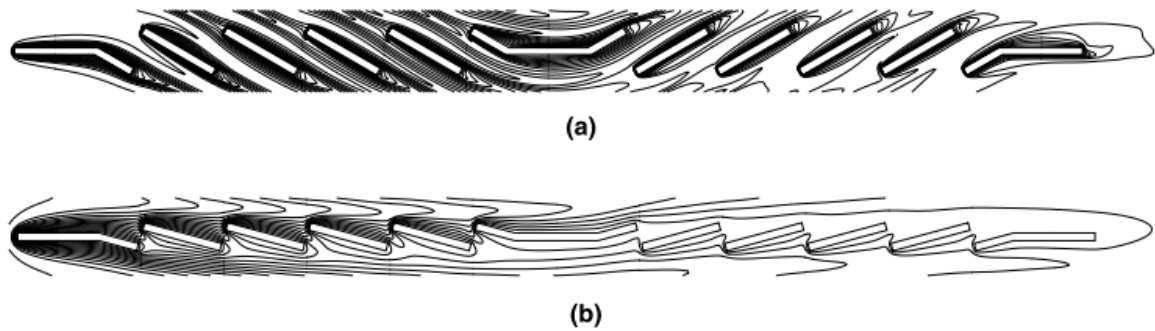
Figure 1- 5 Thermal wake effects: (a). intra-fin interference and; (b). inter-fin interference (Zhang and Tafti, 2001).

1.2 Longitudinal vortex generators (LVG)

In this technique, the heat transfer surface is modified to intentionally introduce secondary vortices that are carried by the main flow (Gentry and Jacobi, 1997). They have long been used to control de flow separation by increasing the near-wall momentum through the momentum transfer from the outer (free-stream) flow to the wall region (Lin, 2002).

The VGs can be regarded as a special kind of extended surface, which can be stamped on or punched out from the fin. Although the heat transfer surface area may not be changed before and after the set up of LVG, the fluid flow can be strongly disturbed because of the generation of vortices when fluid flows over it. In the conventional point of view, the LVG not only disturbs the flow field, disrupt the growth of the boundary layer, but also makes fluid swirling and causes a heavy exchange of core and wall fluid, leading to the enhancement of heat transfer.

Firstly, it is important to explain the different types of vortex shedding. There is a commom understanding among researchers that vortex is a swirling motion around an axis (FIEBIG, 1998). Basically, the vortices can be divided on transverse and longitudinal vortices. The vortices that have their axes perpendicular or spanwise to the flow direction and they are consistent with two-dimensional flow are called transverse. Figure 1-6 shows an example of transverse vortex generated behind ribs.

The longitudinal vortices have their axes in the flow direction or streamwise and they always imply three-dimensional flow. It is well accepted that longitudinal vortices provide higher heat transfer enhancement for the same pressure penalty than transverse vortices (Fiebig, 1995), (Fiebig, 1998), (Yanagihara and Torii, 1992).
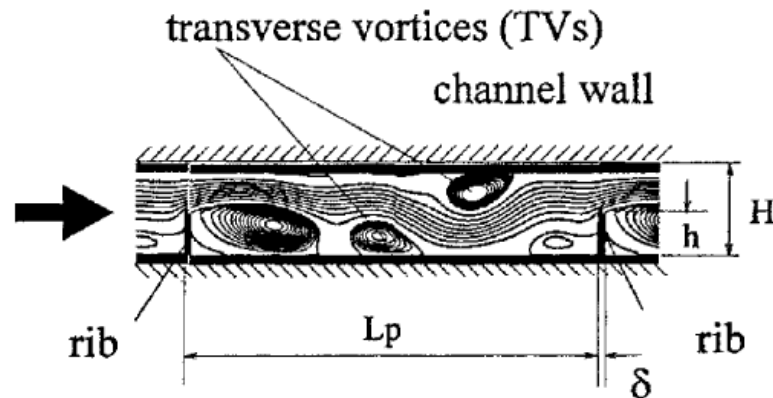
Figure 1-6 Transverse vortex behind ribs in a channel (FIEBIG, 1998).

Von Kárman vortex street behind a cylinder is a typical example of transverse vortices. As a fluid particle flows toward the leading edge of a cylinder, the pressure on the particle rises from the free stream pressure to the stagnation pressure. The high fluid pressure near the leading edge impels flow about the cylinder as boundary layers develop about both sides. The high pressure is not sufficient to force the flow about the back of the cylinder at high Reynolds numbers. Near the widest section of the cylinder, the boundary layers separate from each side of the cylinder surface and form two shear layers that trail aft in the flow and bound the wake. Since the innermost portion of the shear layers, which is in contact with the cylinder, moves much more slowly than the outermost portion of the shear layers, which is in contact with the free flow, the shear layers roll into the near wake, where they fold on each other and coalesce into discrete swirling vortices. A regular pattern of vortices, called a vortex street, trails aft in the wake. Von Karman vortices are named after Theodore von Karman, who first described the phenomenon in the atmosphere. Dr. von

Karman was a co-founder of NASA's Jet Propulsion Laboratory. Figure 1-7 shows the Von Kárman vortex street behind a cylinder.

Compared to a fully developed laminar channel flow, stationary transverse vortices transport additional thermal energy convectively from the wall to the core of the fluid and also from the core to the wall.
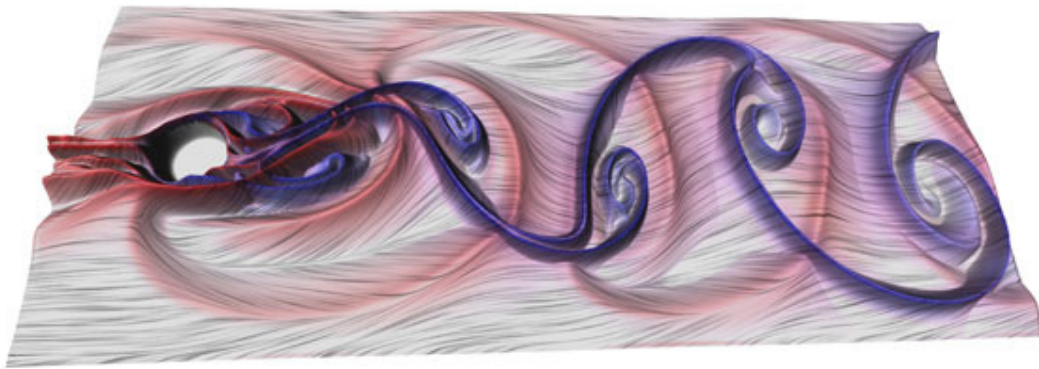
Figure 1-7 Von Karman vortex street behind a circular cylinder.

The unsteady transverse vortices increase the heat transfer by means "Reynolds" averaged transport. However, no substantial heat transfer enhancement can be observed for stationary transverse vortices.

According to literature, there are several types of vortex generators which have extensively been used as heat transfer enhancement techniques. The four basic vortex generators forms are: delta-winglet, delta wing, rectangular-winglet and rectangular wing (Figure 1-8).

In contrast to the common interrupted surfaces, the LVG not only improves the heat transfer performance but also reveals comparatively small pressure drops. They characterize the secondary flow pattern from the vortical motions that are caused by spanwise and normal velocities.
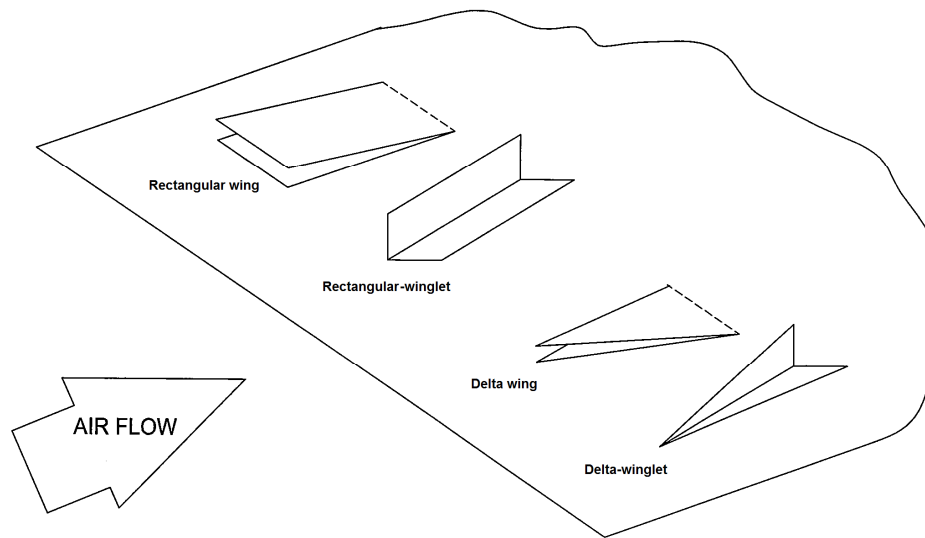
Figure 1-8 Types of vortex generators

Yanagihara and Torii (1993), Pauley and Eaton (1994) compared the results for laminar and turbulent boundary layers for the very similar delta-winglet vortex generators and flat plate geometry and they concluded, for the investigated parameter range, that:

1. Longitudinal vortices are extremely persistent in both laminar and turbulent boundary layers;

2. The heat transfer is strongly influenced by the interaction of the vortices with themselves and the base flow;

3. Global heat transfer augmentation increases with angle of attack (up to 45º), vortex generator height relative to boundary layer thickness and vortex generator height;

4. Heat transfer enhancement is due to boundary layer thinning mainly by the downward flow generated by the vortices, and generation of additional velocity fluctuations;

5. Heat transfer enhancement is higher in laminar boundary layers than in turbulent boundary layers.

For the present study, delta-winglets (DWLs) were adopted due to the recommendation that they generally produce the same heat transfer enhancement with less pressure penalty in comparison to the other LVGs showed at Figure 1-8 (Biswas et al., 1996), (Fiebig, 1995), Fiebig (1998), (Jacobi and Shah, 1995).

According to Yanagihara and Torii (1992), three types of longitudinal vortices can be generated by a delta-winglet (Figure 1-9):

1. **Main vortex**: it is formed due to flow separating at the tip of the delta-winglet and rolling up due to the lower pressure behind of the vortex generator which results in detached shear layers.

2. **Corner vortex**: it is a horseshoe-like vortice generated in the corner between front side of the delta-winglet and the plate. It develops in the stagnation region of the vortex generator and it may develop at the trailing edge of the vortex generator.

3. **Induced vortex**: it is created between the main and corner vortices

Some delta-winglet parameters are important and they have been extensively investigated over the years, such as aspect ratio (ratio of DWL length to DWL height), and both DWL angle of attack and position. According to Ferrouillat et al. (2006), the two most important dimensionless geometric parameters that control vortex characteristics are the LVG angle of attack and frontal area.
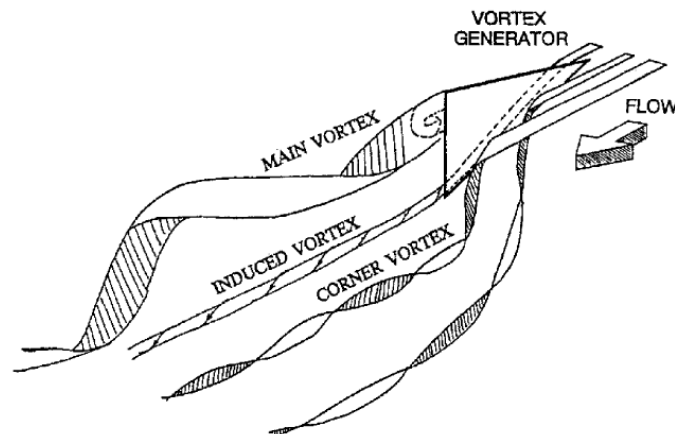
Figure 1-9 Sketch of longitudinal vortices generated by delta-winglet (Torii and Yanagihara, 1997)

The explanation of the three heat transfer enhancement mechanisms commonly observed on generation of longitudinal vortices is discussed below.

First, the enhancement mechanism of developing boundary layers is considered. New boundary layers are generated on each side of the winglet (if the vortex generators are stamped, additional boundary layers form at the stampings). For turbulent channel flow, the developing boundary layers on the winglets will be turbulent, otherwise they will be laminar. Moreover, the enhancement effect of developing boundary layers is much more pronounced in laminar than in turbulent flow, except when the development length becomes larger than the hydraulic diameter.

Enhancement by swirl is the most important mechanism in steady flow (Fiebig, 1995). The tangential velocity becomes as large as the average axial velocity, and the velocity field is strongly 3-D. The longitudinal vortices lead to a spiralling motion and an exchange of fluid between the wall layer and the core. As long as the flow is steady, transverse vortices do not improve convective heat transfer from the walls to the main stream, since the transverse vortices with their steady 2-D flow have no convective mechanism for heat transfer enhancement. Therefore, in steady flow, only longitudinal vortices can increase heat transfer significantly by generating a 3-D spiraling motion.

The third mechanism, flow destabilization, is finally considered. The transverse vortex leads to a recirculation region and profiles with reversed flow. They are less stable, and their critical Reynolds number is much lower than the critical Reynolds numbers of fully developed channel flow.

Pairs of DWL may be positioned on aligned or staggered configurations. Previous studies from Tigglebeck et al. (1992) and Tiggelbeck et al. (1993), at $\mathrm{Re} = 4600$, have indicated that the higher performance was obtained when DWLs were aligned. This better performance may be due to the tendency for an aligned pair to remain close to the surface, while a sttagered pair tends to move away from the surface. Figure 1-10 (a) and (b) ilustrates two DWLs pairs producing counter-rotating longitudinal vortices in aligned and sttagered arrangements, respectively.
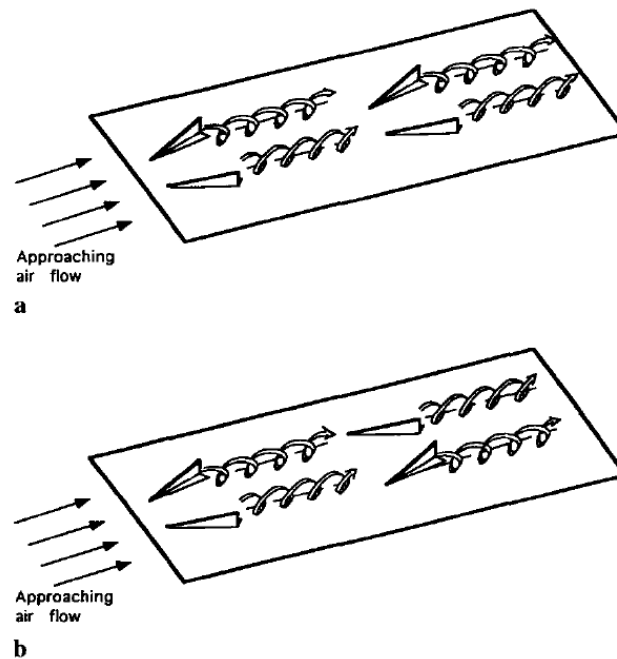
Figure 1-10 Two DWL pairs in (a) aligned and (b) sttagered arrays (Jacobi and Shah, 1995).

Apart from the work of Russel et al. (1982), in heat exchanger applications with ratios of flow length to channel height of at least 30, large heat transfer will require not one but several rows of DWL vortex generators. Also, it was observed that the streamwise spacing between the vortex generators is an important parameter. Based on this, they suggest that an optimization is necessary because the oncoming flow to the vortex generators in the rear side of the fin has higher vorticity and inhomogeneity.

1.3 Motivation and objective of this research

In order to improve heat transfer in compact heat exchangers in automotive industry, this research has focused on the use of flat-tube multilouvered fin combined with delta winglet vortex generators. Flow field and local heat transfer mappings are first necessary to obtain a throrough understanding of thermal and velocity fields in airflows passing through louvered fins and/or longitudinal vortices generators. Finally,

extensive optimization is required to apply effectively these compound techniques in actual heat exchangers.

To obtain input for optimization, either experiments or numerical simulations are required. Performing experimentally a parametric study is usually expensive and time consuming, because of the many models which must be fabricated and tested. Based on this, Computational Fluid Dynamics (CFD) tools allow for more versatility since the geometries can be easily adapted. Fluent 14.5 comercial software has been used as the CFD tool in the present work.

The first part of this research is the study of the contribution of louver angle, and DWL angles of attack and streamwise positions on heat transfer and pressure drop. It is investigated the contribution of these input parameters for two types of geometries, GEO_1 and GEO_2, and two Reynolds numbers, 120 and 240 (based on hydraulic diameter). This range of inlet velocities was chosen because the basic heat exchanger geometry used herein is based on radiators used on automotive application. It is well known that heat transfer is critical for very low inlet velocities and as consequence there is a need to increase the heat transfer surface area or the pumping power to attend the engine heat rejection.

For GEO_1, the louver height is smaller than the louver height for GEO_2 but with higher DWL frontal area than that of GEO_2. Figure 1-11 shows the top view of both geometries. The Smoothing Spline ANOVA method is used to provide an approach to semi-parametric function estimation based on an ANOVA type decomposition for understanding the main and interaction effects of the input parameters on heat transfer and pressure drop. Furthermore, there are no reports taking into account the interaction effects of these parameters on the Colburn and Friction factors applied to flat-tube multi-louvered fin heat exchanger with DWLs.

The second part of this research uses surrogate-based optimization procedure of those five input parameters of the GEO_1 and GEO_2 for both Reynolds numbers in order to maximize the heat transfer. The surrogate-based optimization uses NSGA-II method (Non-Dominated Sorting Genetic Algorithm) combined with back propagation artificial neural networks. The heat transfer maximization studies based on those five

input parameters applied to flat-tube multilouvered fins with DWLs were not found until this moment.

(a)   (b)
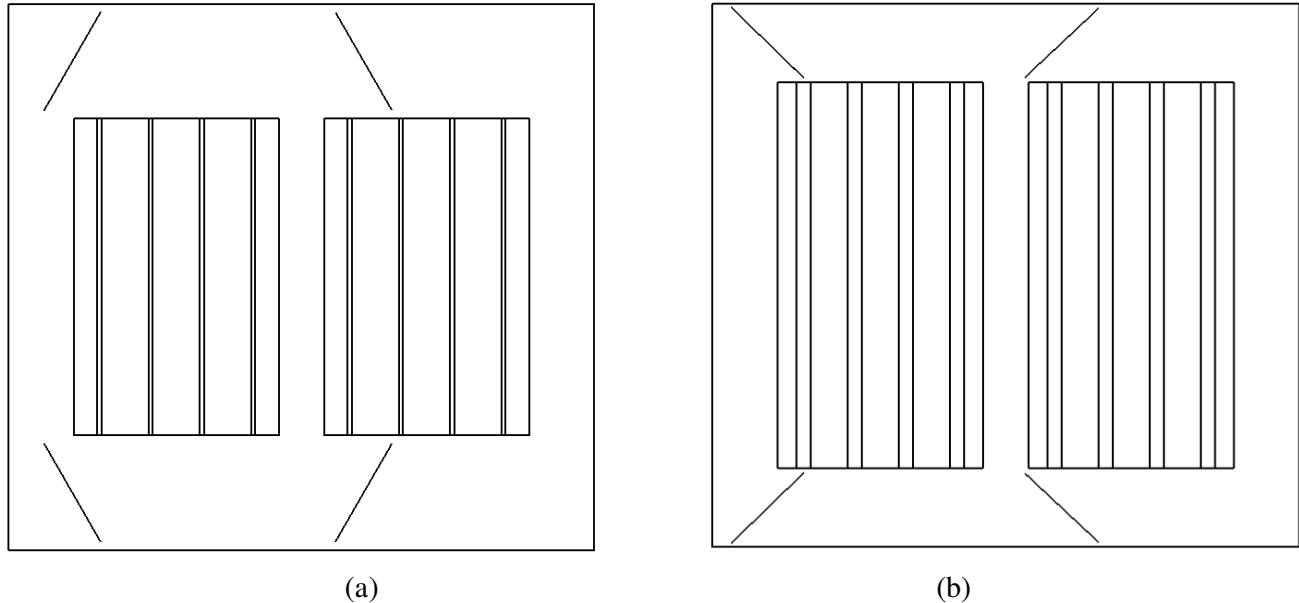
Figure 1-11 Top view of the (a) GEO$_1$ and (b) GEO$_2$.

1.4 Description of this research

The thesis comprises 7 chapters with complementary information to the main content, as described below:

- **Chapter 1**: gives an introduction about the main subject of this research and introduces the concept of heat transfer enhancement from multilouvered fins and vortex generators. The last issue presents motivation, objective of and scope of this research.

- **Chapter 2**: presents the state of art for heat transfer enhancement in multilouvered fin and vortex generators, with a deep survey on references containing both experimental and numerical researches. Moreover, a

bibliographic review of the application of parametric studies and optimization procedure applied to compact heat exchangers on heat transfer enhancement is presented.

• **Chapter 3**: is dedicated to the basic statistical definitions and concepts of optimization processes. Concepts of design of experiments (DoE) and analysis of variance (ANOVA), especially the theory of Smoothing Spline ANOVA for variable screening, are discussed. Recent advances in surrogate-based models are shown. The surrogate-based subject is basically focused in artificial neural networks and the optimization procedure by genetic algorithm is pointed out.

• **Chapter 4**: presents a general explanation of the problem discription focused on computational domain, numerical methodologies (CFD and optimization procedure), numerical set up and mathematical formulation.

• **Chapter 5**: is devoted to validation of the numerical model and discussion of the results from screening analysis of the input parameters on heat transfer and pressure drop and from the optimization procedure. The most important results are analysed and discussed, especially focused on the flow patterns and heat transfer characteristics.

• **Chapter 6**: gives conclusions of the current research and suggestions for continuation of this research.

• **Chapter 7**: provides all the references used in this research.

2 Literature review

The subsequent sections present a synthesis of experimental and numerical researches related to heat transfer enhancement on compact heat exchangers which use louvered fins and longitudinal vortex generators. Also, it is presented a review of statistical analysis, surrogate models and optimization applied to compact heat exchangers.

Both experimental and numerical parts are constituted by a review of selected papers, which bring the background theory of heat transfer enhancement. The experimental and numerical sections are separated and divided on: (*i*). Louvered fins and; (*ii*). Longitudinal vortex generators (LVGs). The numerical part is devoted to review works done with CFD methodology applied to louvered fins and LVGs.

2.1 Experimental research focused on louvered fins

The first experimental research involving louvered fin array that appears in the litetarure was performed by Beauvais (1965). In his study, a smoke flow visualization technique was used with 10:1 scale models. The results were only of qualitative value, since the actual geometric dimensions and velocities were not documented in that paper. From inspection of the photographs included in the paper, it appears that the louver angle (θ) was approximately 30º and the louver-to-fin pitch ratio (L_P/F_P) was approximately 0.80. His figures showed that the main flow was nearly parallel to the louvers for the velocities tested. Prior to this work, it was speculated that louvers acted as a surface roughness that enhanced the performance characteristics of the fin by promoting turbulence.

Davenport (1983) performed flow visualization experiments identical to those of Beauvais (1965) and demonstrated that the flow structure within the louvered array was a function of Reynolds number (Re_{LP}). At low values of Re_{LP}, the louvers had

only a slight influence on the flow structure. Thus, the main flow stream did not pass through the louvers. However, at high values of Re_{LP} the flow became nearly parallel to the louvers. He speculated that at low air velocities the developing boundary layers on adjacent louvers became thick enough to effectively block the passage, resulting in nearly axial flow through the array.

Achaichia and Cowell (1988) studied the heat transfer for three louver fin geometries used on plate fins with 11 mm tube pitch. As can be observed in Figure 2-1, at the highest Re_{LP}, the data are parallel to (but lower than) that for laminar boundary flow over a flat plate (the "flat plate" line). At low Re_{LP}, the data showed characteristics similar to those of laminar duct flow. The "duct flow" line was for fully developed laminar flow in a rectangular channel with a 3:3:1 aspect ratio. This behavior was consistent with Davenport's flow observations.
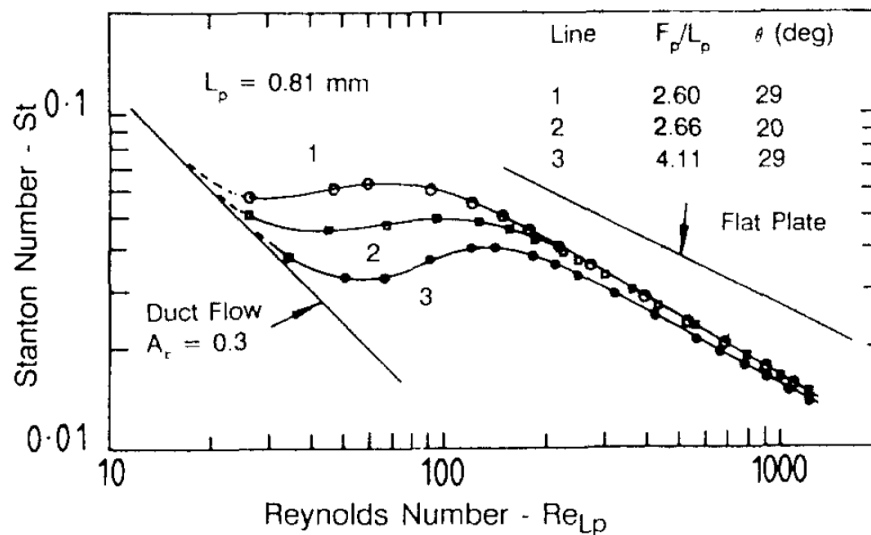
Figure 2-1 Heat transfer behavior for different louvered plate fin geometries (Achaichia and Cowell, 1988).

Webb and Trauger (1991) performed a flow visualization study of the louvered fin geometry commonly used in automotive heat exchangers by using a dye injection technique with 10:1 scale models. The Reynolds number, which was based on louver pitch, ranged from 400 to 4000. Data were taken for six louver-to-fin pitch ratios

(0.49, 0.56, 0.66, 0.79, 0.98 and 1.31) and two louver angles (20º and 30º). Figure 2-2 (a) and (b) present flow efficiency plotted against Reynolds number for louver angles of 20º and 30º, respectively. Inspection of these figures revealed that the flow efficiency increased with increasing Re_{LP}. This occurred up to a particular Reynolds number and above this Reynolds number, the flow efficiency became independent of Reynolds number for fixed L_P/F_P. Also based on Figure 2-2 (a) and (b), it appeared that the critical Reynolds number was independent of L_P/F_P for a fixed louver angle. Comparison of these figures revealed that the critical Reynolds number decreased slightly with increasing louver angle. For louver angles of 20º and 30º, the critical Reynolds number was approximately 1380 and 1200, respectively. The effect of louver-to-fin pitch ratio on flow efficiency was also shown in Figure 2-2 (a) and (b). It was evident that the flow efficiency increased with increasing L_P/F_P. The flow was parallel to louvers ($\eta = 1$) only if $L_P/F_P > 1.31$. Comparisons showed that increasing the louver angle (for a fixed L_P/F_P) increases the flow efficiency. This holds true up to the critical Reynolds number, after which the flow efficiency was independent of louver angle. As L_P/F_P increased, the effect of louver angle on flow efficiency decreased.

Cowell et. al. (1995) presented a performance study of louvered fin surfaces and some comparisons with other compact enhanced surfaces, and it was shown that louvered fins have the potential to compete in applications where overall size, weight and pumping power are important. The most obvious conclusion on their research was that the flow-directing properties of louver array effectively increased the velocity of working fluid relative to elemental flat-plate surfaces. However, this effect alone was insufficient to explain fully the degree of improvement shown by a real louvered fin surfaces. Boundary layer growth on both surfaces of adjacent louver resulted in a favorable pressure gradient, which in turn produced thinner boundary layers.

Kim and Bullard (2002) experimentally studied the air-side heat transfer and pressure drop characteristics for multi-louvered fin and flat tube heat exchangers. 45 heat exchangers with different louver angles (15-29º), fin pitches (1.0, 1.2 and 1.4 mm) and flow depths (16, 20 and 24 mm) were used. The Reynolds numbers ranged from 100 to 600, based on louver pitch. According of them, the heat transfer coefficients

decreased with flow depth and increased exponentially with face air velocity. The effect of louver angle on heat transfer was different according to the flow depth, fin spacing and Reynolds number, but the effect of fin spacing was relatively small. Pressure drops increased with louver angle and flow depth and decreased with fin pitch increasing. They commented that heat exchangers with a smaller non-louvered portion had relatively higher heat transfer coefficients. Also, the authors suggested correlation for j and f, for $F_P/L_P < 1$. The authors compared their proposed equations with correlations from literature and it was observed some discrepancy between the data.
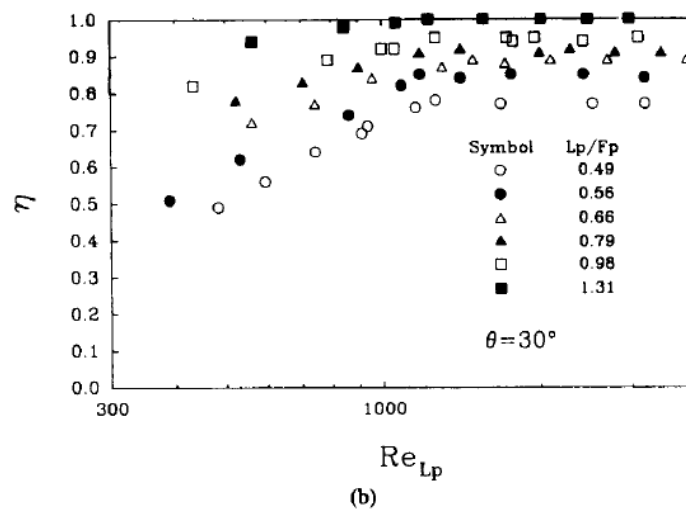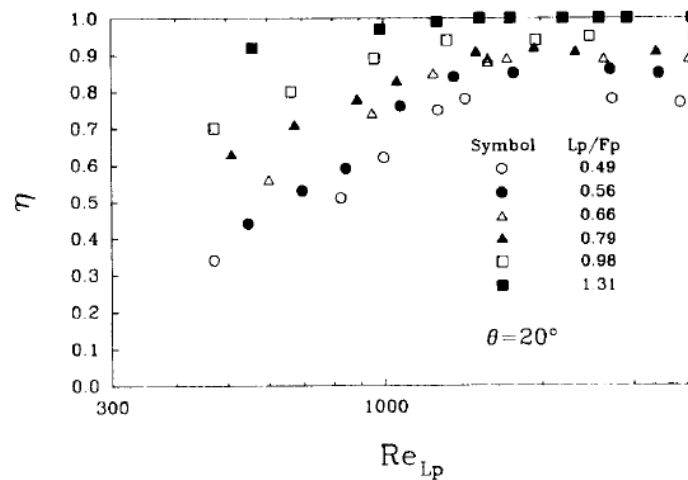
Figure 2-2 Flow efficiency versus Reynolds number for (a) $\theta = 20^{\circ}$ **and (b)** $\theta = 30^{\circ}$
(Webb and Trauger, 1991)

Lyman et al. (2002) experimentally investigated the scaling of heat transfer coefficients along louvered fins. Nine louver geometries were used on their studies and in all of those models the number of streamwise louvers was remained constant with 17 louvers. Three Reynolds numbers, based on louver pitch, were studied (230, 370 and 1016) for louver angles of 20º, 27º and 39º. At higher Reynolds numbers the heated wakes were more concentrated and convected further downstream while at lower Reynolds numbers the heated wakes were more diffuse.

A detailed study of flow, heat transfer and pressure drop for louvered fins was presented by DeJong and Jacobi (2003A) for Reynolds number from 130 to 1400 (based on louver pitch). They varied the louver angles (18º, 22º and 28º), fin-to-louver pitch ratio ($F_P/L_P = 1.09, 1.20$) and number of fins (12 and 15). The louver pitch was set constant for all samples and equal to 11.9 mm. The authors showed that as louver angle increased (from 18º to 28º) the flow became more louver-directed (Figure 2-3). The duct diameter effectively decreased with an increase in louver angle and then the friction drag for flow through the duct increases. Also, as the louver angle increased, there was a greater pressure-drop penalty due to form drag associated with duct-directed flow, and the path of least resistance became more and more louver-directed. Figure 2-4 shows the Euler number as function of Reynolds number, louver angle and fin pitch to louver pitch ratio. Moreover, flow through geometry with a larger louver angle became louver-directed at a lower Reynolds number. The flow visualization results for $\theta = 18º$ and $F_P/L_P = 1.09$ showed that as the Reynolds number increases, in the case from 260 to 670, the flow efficiency increases. Additional increases in Reynolds number, while not affecting the flow efficiency, cause the flow to become unsteady. When $Re = 1130$, the flow in the downstream half of the array has become unsteady. The Reynolds number at which a given row of louvers begins to shed vortices from their leading edges can be seen in Figure 2-5. At low Reynolds number, the flow was steady and laminar. As the Reynolds number was increased, small-scale periodic transverse velocity fluctuations generated upstream propagated downstream, and louvers downstream of the turnaround louver started to shed small spanwise vortices. Figure 2-5 has also indicated that downstream of the turnaround louver, the onset of votex shedding had little spatial dependence within the array. A streakline passing by a louver in the

downstream half of the louver array did not necessarily pass by every upstream louver on that fin. Thus, the number of upstream interruptions, and then the extent of perturbation, depends on the flow efficiency, which in turn depends on the geometry and Reynolds number. Louvers in the first two rows of the array (upstream of the turnaround louver) were not noted to shed vortices from their leading edges in the Reynolds number range of operation. Finally, the authors commented that vortex shedding in the louvered-fin geometry causes only small increases in heat transfer and pressure drop over the Reynolds number studied. Furthermore, since vortex shedding has much less impact on the thermal-hydraulic performance of louvered-fin arrays, steady-state computational models of louver arrays may be expected provide accurate predictions of flow and heat transfer over a wider Reynolds number range.

DeJong and Jacobi (2003B) experimentally studied the effects of bouding walls on flow and heat transfer in louvered-fin arrays and the results for spatially periodic flow far from the walls were compared to results for the near-wall flow, where the impact of the bounding surface is important. The fin height was 7.06 cm, and the louver pitch was 1.19 cm for all samples. They varied the louver angles (18º, 22º and 28º), fin-to-louver pitch ratio ($F_P/L_P = 1.09,\ 1.20$) and Reynolds number of 130-1400. The flow behavior near the bounding walls was significantly different than the flow behavior far from the walls in the periodic region. The flow efficiency in the near-wall region was significantly lower than the flow efficiency in the fully periodic region of the array. Also, the flow in the near-wall region was characterized by large separation and recirculation zones. At the lowest Reynolds numbers, flow far from the bounding wall was louver-directed. Flow near the walls had much lower flow efficiency, and thus the flow angle of incidence to the louvers was much higher. Another characteristic of the flow in the near wall region was a transition to unsteady flow at lower Reynolds numbers relative to flow in the fully periodic region of the array. As the Reynolds number increased – and with it the amplitude of the flow oscilations – the vortices begin to be ejected into the flow, causing a rapid diffusion of momentum and energy. As the Reynolds number increased further, the flow takes on a turbulent appearance. Finally, the authors concluded that large separation zones cause a heat transfer decreasing, compared to louvers far from the walls, at low Reynolds numbers, but at higher Reynolds numbers vigorous flow unsteadiness causes an increase in heat transfer.
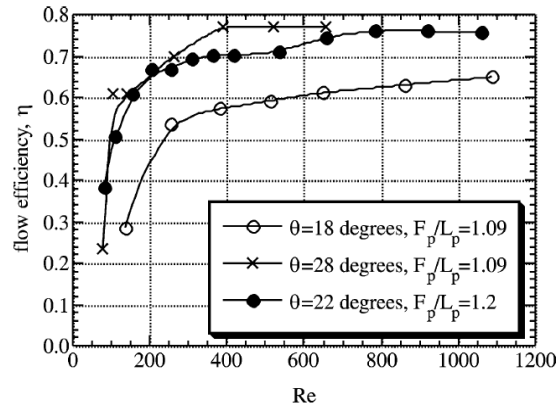
Figure 2-3 Flow efficiency versus Reynolds number for three different arrays (DeJong and Jacobi, 2003A).
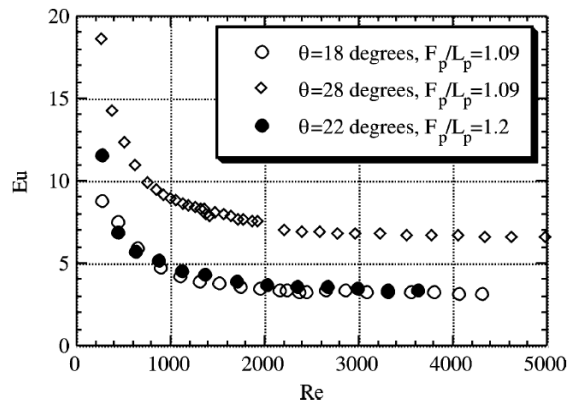
Figure 2-4 Effect of louver angle on pressure drop (DeJong and Jacobi, 2003A).
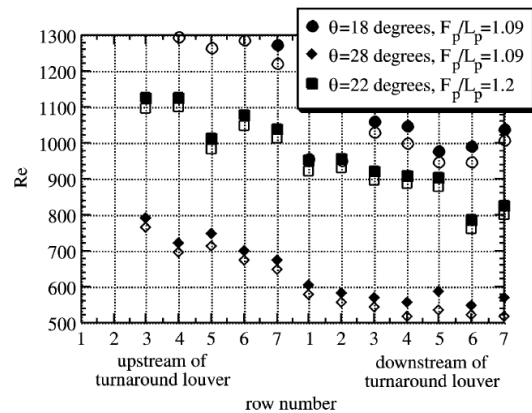
Figure 2-5 The Reynolds number at which a given row of louvers in an array begins to shed vortices from their leading edges. The clear symbols indicate the Reynolds number at which very weak, small vortices are noted. The dark symbols indicate the Reynolds number at which larger vortices are clearly shed (DeJong and Jacobi, 2003A).

Dong et. al. (2007) performed experimental studies on the air side heat transfer and pressure drop characteristics for 20 types of multi-louvered fin and flat tube heat exchangers. A series of tests were conducted for air Reynods numbers of 200-2500, based on louver pitch, with different fin pitch, fin height, fin thickness, angle louver and flow length. The effects of fin pitch (2.0, 2.25 and 2.5 mm) on the performance of the multi-louvered having fin height of 8.0 mm, louver angle of 28º and fin lengths of 65 mm and 53 mm were analysed (Figure 2-6). The heat transfer coefficients and pressure drop increased with fin pitch decreasing at the same frontal air velocity. The cause is that, when the fin pitch decreased, the air flow inside the interrupted flow channel can be mixed better, and the direction of flow tends more to being louver directed. The Figure 2-7 shows the effects of fin height (7.0, 8.0 and 10.0 mm) on the performance of the multi-louvered fin having fin pitch of 2.0 mm, fin length of 36.6 mm and louver angle of 28º. It can be seen that the fin height has a smaller influence on the heat transfer coefficients at low frontal air velocity, and the heat transfer increases with fin height decreasing at high frontal air velocity. In addition, the pressure drop increased with fin height decreasing at the same frontal air velocity in the test range. The influence of fin length (36.6, 53.0 and 65.0 mm) on multi-louvered performance was also studied (Figure 2-8) for fin height of 8.9 mm, fin pitch of 2.0 mm and louver angle of 22º. The fin length had a more obvious influence on heat transfer coefficients and pressure drop as a function of frontal air velocity. The heat transfer coefficients increased with the fin length decreasing at the same frontal air velocity, while the pressure drop decreased. The authors also suggested correlations for calculation of Colburn factor and friction factor, *f*.

Li and Wang (2010) experimentally studied the air-side heat transfer and pressure drop characteristics for heat exchangers with multi-region louver fins with flat tubes. The range of Reynolds numbers was from 400 to 1600, based on louver pitch. Combined with interrelated test data in Dong et. al. (2007), the authors provided correlations for *j* and *f* factors to cover a wide range of geometry parameters, including number of louver regions, louver angle, fin pitch, fin height, louver height, flow depth, and fin thickness, fitted using the regression method.

Dogan et al. (2015) experimentally performed comparisons of two multilouvered fin heat exchangers with different numbers of fin rows. The models under consideration

had either double or triple fin rows between the flat-tubes. Transient and quasi-steady state conditions were considered. The results were compared with the correlations in the literature, and it was observed that the friction factor values of both methods were in agreement with the values found in the literature.
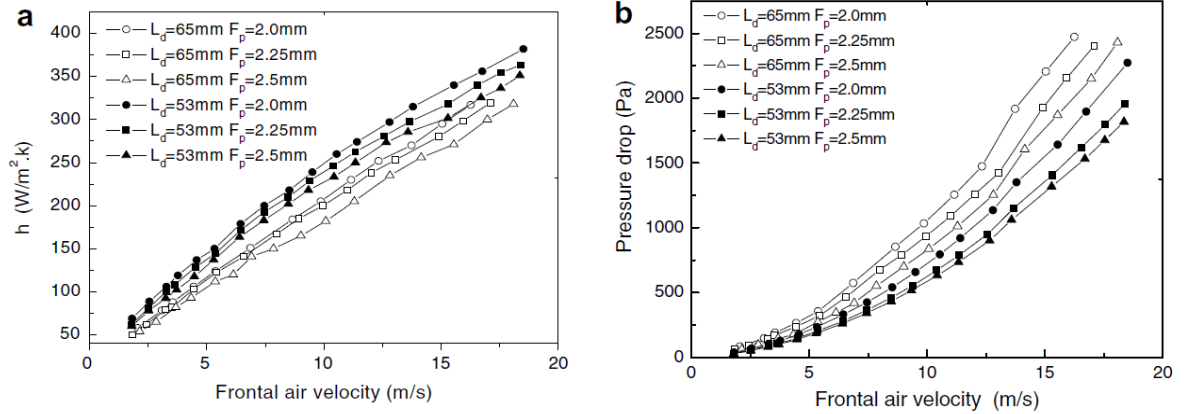
Figure 2-6 Effects of fin pitch on heat transfer coefficients and pressure drop (Dong et al., 2007).
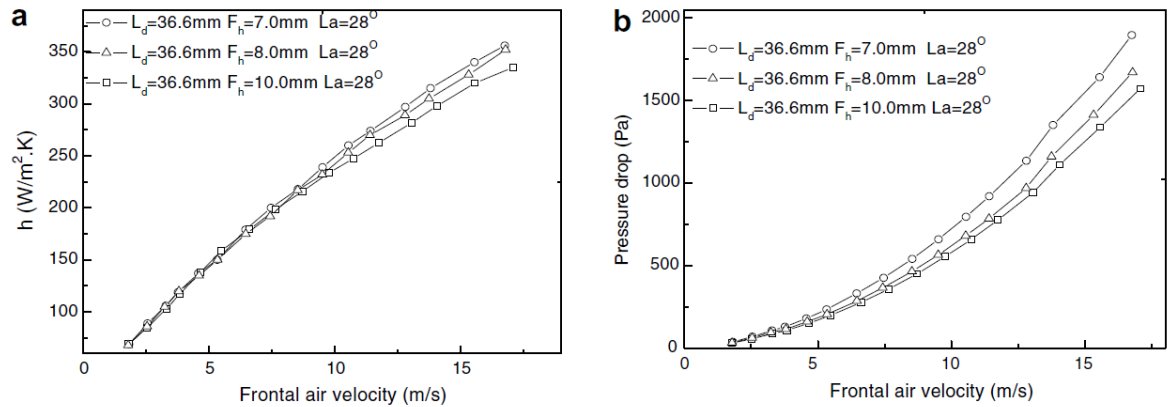
Figure 2-7 Effects of fin height on heat transfer coefficients and pressure drop (Dong et al., 2007).

Figure 2-8 Effects of fin length on heat transfer coefficients and pressure drop (Dong et al., 2007)
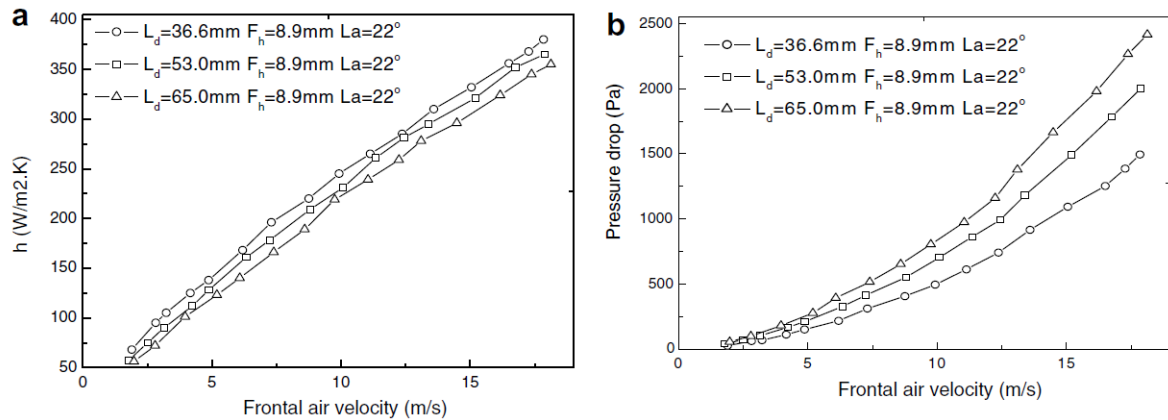
Vaisi et. al. (2011) studied the heat transfer and pressure drop characteristics for two types of louvered fin configurations: Asymmetric and Symmetric patterns (Figure 2-9 and Figure 2-10). The inlet air velocity ranged from 5.58 to 12.66 m/s. The results indicated that, at same velocity, the symmetrical pattern had the higher heat transfer rate than the asymmetrical one. Also, the symmetrical pattern louvered fin behave better in pressure drop performance.

Figure 2-9 Dimensions of the louvered fin with asymmetric pattern (Vaisi et al., 2011).
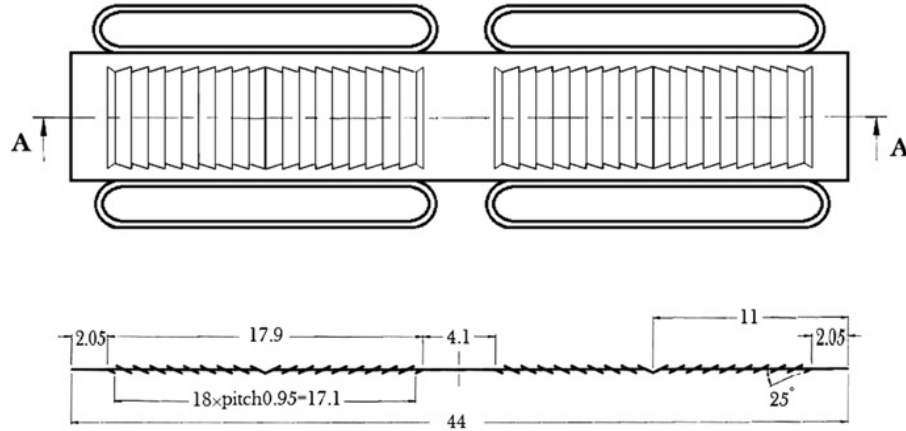
Figure 2-10 Dimensions of the louvered fin with symmetric pattern (Vaisi et al., 2011).

2.2 Experimental research focused on longitudinal vortex generators

Torii and Yanagihara (1989) experimentally investigated the isolated influence of longitudinal vortices "far enough" from a delta-winglet vortex generator on heat transfer of laminar boundary layer. The inlet velocity varied from 2.61 and 2.96 m/s, with free-stream turbulence intensity lower than 0.3%. The longitudinal vortex was generated by six different types of DWL whose heights were 3, 4.5, 6, 10, 15 and 30 mm. The generators were positioned 300 mm from the leading edge, where the boundary layer thickness was about 6 mm, depending on the velocity. The attack angle (α) was varied from 4º to 25º. A single vortex was generated at the centerline of the laminar boundary layer by means of a DWL and then passed over a constant heat-flux heat transfer surface (Figure 2-11). The Stanton number ratio (St/St_0) for attack angles from 5º to 25º, with a step of 5º, was investigated for a nearly constant free-stream velocity of 2.92 to 2.98 m/s. The peak Stanton number ratio for $10º < \alpha < 25º$ increased from 1.1 in the first row ($x = 0.658\,\text{m}$) to 2.4 in the fourth row ($x = 1.708\,\text{m}$), which means a considerable improvement of the heat transfer coefficient. The enhanced region spread as the flow moved downstream and the point of the peak Stanton number shifted slightly in its spanwise position to the upwash side of the vortex (corresponding to negative z-axis) – Figure 2-12. On another section of the paper, the free-stream velocity was slightly varied from 2.61 to

2.96 m/s. The same vortex generator was used for the four measurements ($H = 6\,\text{mm}$ and $\alpha = 5^\circ$). The results revealed the remarkable influence of the free-stream velocity and, consequently, of a slight variation of H/δ. The heat transfer augmentation rate was found to grow with increasing the velocity. The influence of vortex size was studied by varying the generator height. The basic attack angle was 15° and the height ranged from 3 to 30 mm, corresponding to $0.5 < H/\delta < 5$. The internal ($H/\delta \leq 1$) and external ($H/\delta > 1$) vortices affected heat transfer in different ways. Internal longitudinal vortices influenced only the position of transition so that the symmetrical spreading of turbulent wedge occurrs independent of the vortical motion. On the other hand, external vortices determined not only the transition position but also the development pattern of the transition to a turbulent boundary layer.
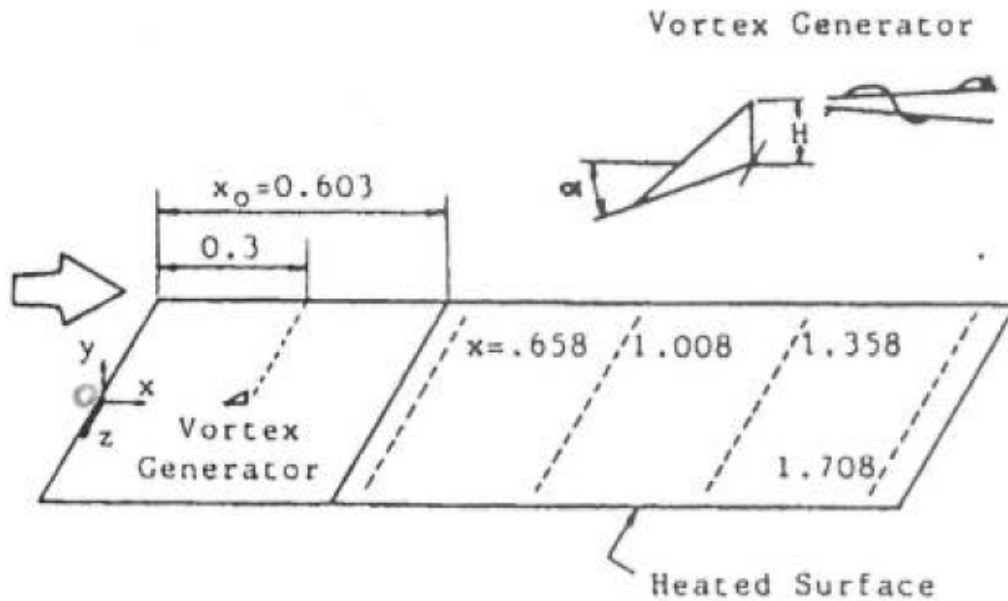
Figure 2-11 Test surface with thermocouple positions (Torii and Yanagihara, 1989).
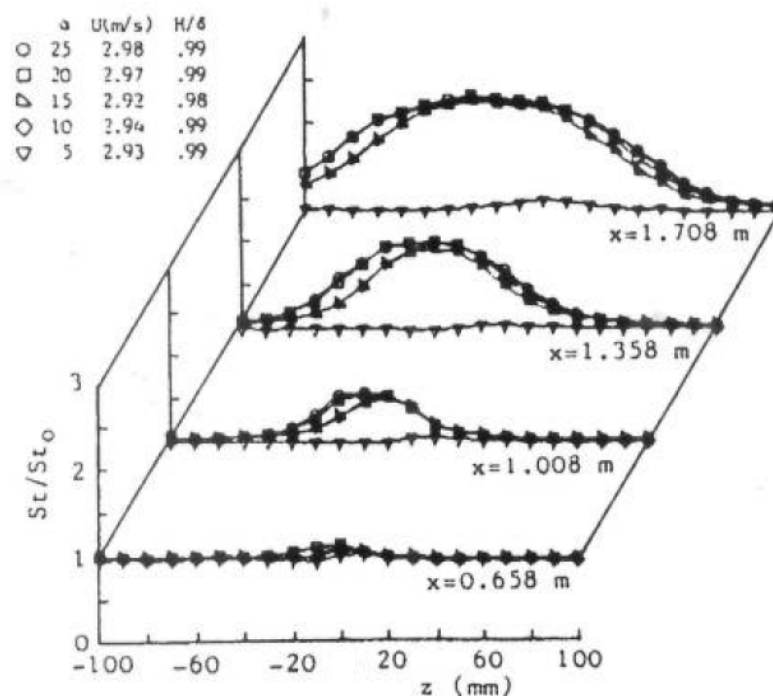
Figure 2-12 Axial development of spanwise Stanton number ratio for different angles of attack (Torii and Yanagihara, 1989).

Yanagihara and Torii (1992) investigated the enhancement of heat transfer caused by the presence of a single vortex generator in a laminar boundary layer. The local heat transfer coefficients just downstream of the vortex generator and the mean and fluctuation components of velocity were measured. The longitudinal vortices were generated by DWL of various heights ($H = 6/10/15/25$ mm) and attack angles ($\alpha = 5^\circ/10^\circ/15^\circ/20^\circ/25^\circ$). The nominal free-stream velocity was 4 m/s, with the free-stream turbulence intensity around 0.3%. The generators were positioned just upstream of the heating starting point (Figure 2-13).

The velocity boundary layer thickness (δ) at the generator's location was 4.8 mm. The authors noted that the longitudinal vortex, although suffering from the influence of viscous dissipation, persisted well downstream, modifying the entire velocity field. Because of the interaction between the vortex and the wall, the vortex shifts its position to the upwash region. In the first streamwise section ($x = 0.08$ m), there were indications of three vortices (main, corner and induced vortices). These vortices

modified the flow structure near the wall. The corner and the induced secondary vortices declined more rapidly because they were located near the wall (see Figure 2-14). The heat transfer enhancement downstream from the vortex generator could be attributed to the boundary layer thinning due to the vortical motion, or to the local growth of turbulence intensity. The size of the vortices was varied by modifying the generator's height. The main and corner vortices appear clearly for $H \geq 10\,mm$ and $\alpha = 15^{\circ}$. For $H = 25\,mm$, a second corner vortex appeared especially in vortex generators with large frontal areas. For $H = 6\,mm$, the corner vortex was apparently weak with slight influence on heat transfer. Also, the heat transfer enhancement level was around 50% in the region near the generator and 80% well downstream. It was established that the strength of the vortices generated by DWL was proportional to the attack angle. The heat transfer results, for $H = 15\,mm$, showed that the heat transfer enhancement for both the downwash region (heat transfer dominated by the main vortex) and the upwash region (heat transfer dominated by the corner vortex) became larger for larger attack angles. Well downstream, the region of heat transfer enhancement became broader for generators with larger attack angles.
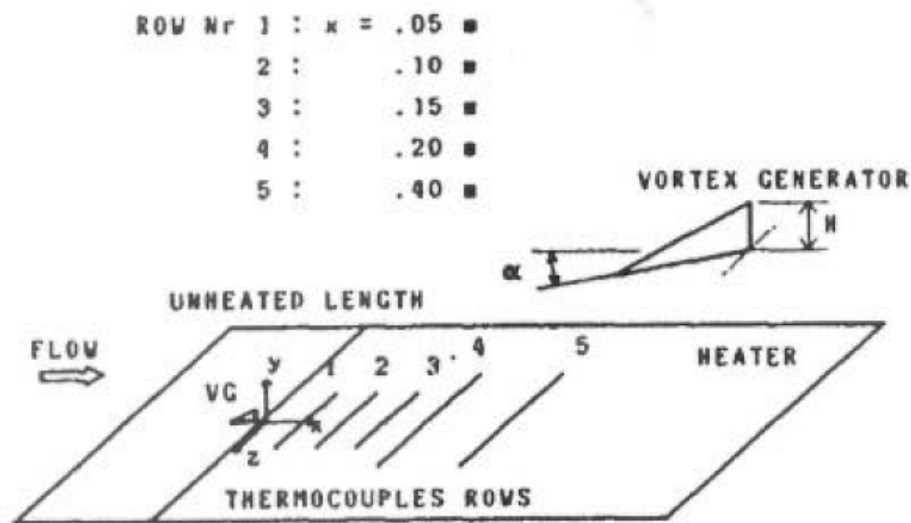
Figure 2-13 Sketch of heated test surface with thermocouple rows (Torii and Yanagihara, 1992).
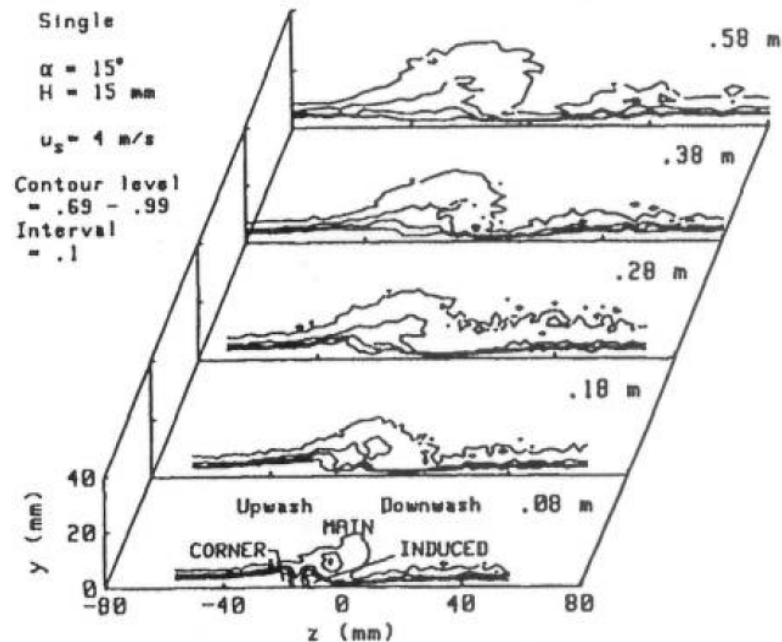
Figure 2-14 Streamwise velocity pattern for a vortex generator - $H = 15$ **mm and attack angle of 15º (Torii and Yanagihara, 1992).**

Tiggelbeck et. al. (1992) investigated experimentally the flow structure and heat transfer enhancement by longitudinal vortices in plane channel. The longitudinal vortices were generated by single and double rows of delta winglet vortex generators (puched out of the channel wall) with inline arrangement. The mean flow velocity varied from 0.4 to 4 m/s, the aspect ratio was of 2.0 and angle of attack of 45º. The investigations showed that flow visualization in the wake or vortex generators can be made only for low Reynolds numbers, based on hydraulic diameter, less than 1700. At higher Reynolds numbers the flow in the vortex became unsteady, and no distinct vortex pattern can be observed. For $\text{Re} = 1350$, at the rear edge of the winglets, a primary longitudinal vortex of elliptical shape, whose major axis forms an angle about 45º with the channel wall, could be seen. Further downstream, the shape of this vortex changed from elliptical to approximately circular. The distance between the cores of two primary longitudinal vortives of a winglet pair was nearly constant at all streamwise positions. Two secondary longitudinal vortices (called base vortex and stagnation vortex) were generated at the regions between the two neighboring counter-rotating primary vortices. The base vortex was resulted from the interaction of the flow through the stamping and the main flow; stagnation vortex was due to the interaction of the counter-rotating primary vortices and the channel wall (the

entrainment effect). Also, the shapes, diameters, and positions of the secondary vortices were strongly linked with their streamwise position. They were not as large and stable as the primary vortex. Maximum global heat transfer enhancement of 83% (compared to plane duct) was obtained at downstream position to channel height ratio of 22. The increasing of Reynolds number from 2000 to 8000, the global Nusselt number with two rows of vortex generators increased faster than for either the plane duct. This showed that multiple rows of vortex generators were more benefitial at higher Reynolds numbers than lower Re.

Tiggelbeck et. al. (1993) experimentally studied the flow structure, heat transfer, and drag by longitudinal vortices generated by doulble rows of delta-winglets (both in common-flow-up configuration) in transition channel flow. The aspect ratio of the DWL was 2.0 and the streamwise and spanwise distance between DWL was maintained constant. Two different attack angles were studied (45º and 60º). The flow structure at the wake of the vortex generators was strongly dependent on angle of attack and Reynolds number. It was observed that for single rows of vortex generators only at small Reynolds numbers less than 1300 a laminar longitudinal vortex appears. For higher Reynolds numbers the vortex grew turbulent with turbulence levels of the main flow component of more than 10 times the turbulence level of the homogeneous oncoming flow. It was also shown that for high angles of attack (greater than 70º), there was no longitudinal vortex downstream of the delta-winglets, the separating flow forms a recirculation zone. Investigations for second row delta-winglets have shown similar behavior. Moreover, it was observed light sheets perpendicular to the main flow direction behind one delta winglet of the symmetrical pair for those two angles of attack for aligned and staggered rows of vortex generators. The flow was observed parallel to the main flow direction from the back side of the channel. The visualization for $Re = 1300$ and attack angle of 45º, in aligned and staggered arrays, showed that downstream of a delta winglet for the second row the dominating primary vortex small secondary vortices resulting from entrainment effects and flow through the stamping of the vortex generator appear. For angles of 65º, the flow did not form a longitudinal vortex downstream of the second delta winglet row, even for aligned arrangement. The critical angle of attack for the second row was about 55º. This was in contrast to the first row, where that angle was 70º. The inhomogeneties and the higher turbulence level of incoming flow

of the second row probably were the reasons for this. The flow structures behind the second row for staggered or aligned arrangement of the two rows were qualitatively similar, no distinct influence of the row configuration can be found. Behind the second row was slightly more unsteady than behind the first row. For $Re = 4600$ and attack angle of 45º, the local heat transfer increasing can be seen especially at the rear edges of the winglet stamping where new boundary layers started to grow, and behind the winglets showing the effect of the formation of longitudinal vortices. The distribution was qualitative similar for the first and second row. The structures of the heat transfer for staggered and aligned configurations were similar with regard to the number and position of the heat transfer peaks. For greater flow lengths the aligned arrangement was advantageous, the heat transfer was up to 10% higher than for the staggered winglets. The span averaged enhancement over the plane duct heat transfer was sufficiently higher at the second row since the plane duct value decreased rapidly downstream of the channel entrance. The peak enhancement value at the first winglet row was 150%, at the second was 250%. This indicates that for a double row arrangement of vortex generators the vortices of the oncoming flow can be benefitial for the vortex formation by the generators of the following row. The streamwise decrease of the heat transfer enhancement was, however, stronger for the winglets in the second row than for the first row. At the channel exit the heat transfer was still increased by 50%. The global Nusselt number for the complete channel wall for the aligned configuration was 60% higher than for the plane channel; it was 5% higher than for the staggered arrangement.

Jacobi and Shah (1995) provided a broad review of the studies related to vortex-induced heat transfer which deliberate generation of large-scale longitudinal vortices in the flow. On that review, the theoretical basis for the method was discussed and both active and passive implementations were reviewed. For these flows, there were several important length scales and geometrical effects. The channel height was a relevant length scale and it was useful to consider the ratio of the area of the vortex generator to the enhanced fin area. Normally, the vortex generator area was less than a few percent of the fin area. A summary of passive vortex enhancement results was presented by the authors. It can be seen that for parallel plates with a delta winglet pair, at $1000 < Re < 4000$, the observed overall heat transfer enhancement

was about 84% and for rectangular channel with winglet pair, at $\mathrm{Re} = 5600$, this value is 77%.

Fiebig (1995) provided a broad review of heat transfer and pressure enhancement for embedded vortices in internal flow. Comparisons between rectangular and triangular winglets show that the difference in terms of heat transfer enhancement and pressure penalty between them is small and winglets gave higher heat transfer enhancement and lower pressure loss penalty than wings. Fiebig (1995) also explained the three heat transfer enhancement mechanisms (developing boundary layers, swirl flow and flow destabilization) and concluded that longitudinal vortices enhance heat transfer in steady flow. Moreover, it is shown that the flow is still steady at $\mathrm{Re} = 350$. Finnaly, he commented that when the angle of attack is small, mainly longitudinal vortices are generated; in turn, when the angle of attack is 90º, mainly transverse vortices are generated.

Fiebig (1998) explained the main differences between longitudinal and transverse vortices in terms of heat transfer and pressure drop and concluded that the longitudinal vortices are more efficient for heat transfer enhancement than transverse vortices. The author also showed that in laminar flow the heat transfer enhancement from DWLs and delta-wings increase with Reynolds number.

Yang et. al. (2010) examined the air side performance of heat sinks having fin patterns of plate fin, interrupted fin geometry (louver and slit fins), dense vortex generator, and loose vortex generator. The results indicated that the heat transfer performance was strongly related to arrangement of enhancements. The interrupted and dense vortex generator configurations normally contributed more pressure drop penalty than improvements of heat transfer. This was especially pronounced when operated at lower frontal velocity. It was found that the friction factor for interrupted fin geometry was significantly higher than other fin types, and the louvered fins showed the highest friction factor among all fin pattern, followed by the dense vortex generator and loose vortex generator. The heat transfer performance for the vortex generators exceeded all other fin geometry. Also, the results indicated that the vortex generators operated at a higher frontal velocity was more benefitial than that of plain fin geometry. However, it was observed that the formation of longitudinal vortex was constrained when the fin spacing was reduced.

Aliabadi et al. (2015) experimentally investigated the heat transfer enhancement in a tube using vortex generators insert with different arrangements of delta-winglets. The authors observed that under similar conditions the heat transfer rate, pressure drop was consistenly higher than those in the plain tube. The maximum performance was found at Reynolds number, based on hydraulic diameter, of 8715.

2.3 Numerical research focused on louvered fins

Since the early 1980s, numerous attempts have been made to develop 2D and 3D numerical models of louvered fin surfaces. Finite fin thickness models were analysed in a number of numerical studies on flow through louver arrays for a few isolated configurations and/or flow rates. Baldwin et. al. (1987) used a Cartesian grid and solid cells with zero porosity to define the fin. The louver surface was therefore respresented by a series of staircase-type steps with the grid spacing selected to make the solid cells approximate the geometry. A finite-volume solution of the flow equations was carried out using commercial software PHOENICS code. Results were presented for only two louver configurations, each at a single Reynolds number, and compared with the LDA measurements of Button et al. (1984). The numerical results displayed the same basic phenomena as the experimental studies, showing flow separation after the first louver and almost complete alignement after the third. As the flow entered the second bank of louvers, it took longer to become aligned relative to the first bank.

Ha et al. (1995) performed 2-D numerical study of the fluid flow and heat transfer characteristics in multi-louvered fin heat exchanger. The numerical solutions of the laminar governing equations, in steady state conditions, were obtained using the Fluent computer code. The Reynolds number ranged from 176 to 1006, which inlet velocity corresponding from 1.4 to 8.0 m/s. Two louver angles were tested: 23º and 31º. The temperature distribution was affected by the complex flow structures. With increasing Reynolds number, decreasing proportion of the flow passing through the channel between the fins and increasing proportion of the flow was diverted through the louvers, directing the flow downwards in the first bank of louvered fin array and

upwards in the second bank. Pressure drop and heat transfer rate increased with increasing Reynolds number and louver angle.

Tafti et al. (2000) numerically investigated the detailed transition mechanism from steady to unsteady flow in multilouvered fin geometry. The configuration used on their calculations consisted of an entrance and exit louver with four louvers on either side of the center and redirection louver. The louver angle and louver thickness were set with 30º and 0.1 mm, respectively. The Reynolds numbers, based on hydraulic diameter, ranged from 100 to 1300 in increments of 100. The governing equations for momentum and energy conservation were discretized with a conservative finite-volume formulation. Both, convection and viscous terms were approximated by second-order central-difference schemes. Periodic boundary conditions were applied in the transverse direction while Dirichlet boundary conditions were specified at the entrance of the array. The entrance and exit domains extended approximately 5.5 non-dimensional units upstream and downstream of the array, respectively. At the fin surface, no slip, no penetration boundary conditions for the velocity field, and the constant temperature were applied at fin. Convective boundary conditions were used at outflow boundary nodes. The initial instability appeared in the wake of the exit louver at Reynolds number of 400. It was found that the initial wake instability propagated inside the array as the Reynolds number increased. By Reynolds number of 900, free shear layer or Kelvin-Helmhotz type instabilities had developed on the leading edge of the louvers near the exit. The authors concluded that more studies are needed to study the effect of geometrical parameters, particularly the ratio of fin pitch to louver pitch and louver angle on flow transition.

Studies aiming at classifying and isolating the effects of thermal wake intereference that occurs in multilouvered fins were presented by Zhang and Tafti (2001). The computational domain and Reynolds numbers range are the same of presented by Tafti et al. (2000). Their study classifies two types of thermal wake interferences that occur in multilouvered fins. Inter-fin interference occurs between adjacent rows of louvers and is dominant at high flow efficiencies when the flow is louver directed. Intra-fin interference occurs on subsequent louvers of the same row or fin and is dominant at low flow efficiencies or when the flow is predominantly duct directed. While the heat transfer transfer capacity of multilouvered fins increases

unconditionally when thermal wakes were eliminated, the heat transfer coefficient either increased or decreased depending on the location of thermal wakes in the vicinity of the louver. The increase in heat flux or heat transfer capacity was larger for small pitch ratios. On the other hand, the heat transfer coefficient decreased on elimination of the inter-fin thermal wake and increased with the elimination of all thermal wakes. The increase was much larger as the fin pitch increased.

Tafti and Zhang (2001) investigated the effect of fin pitch, louver angle and thickness, and flow depth on the onset and propagation of the instabilities in multilouvered fins. The computational domain and Reynolds numbers range are the same of presented by Tafti et al. (2000). The instabilities were always found to develop first in the wake of the exit louver, which the spread upstream into the louver bank. In spite of this, it was shown through numerical simulations that the interior louver bank instabilities were completely independent of the exit wake instability. Conversely, the exit wake instability was not only dependent on the exit louver geometry, but also on the upstream geometry of the louver bank. Louver angle and louver thickness had the largest effect on the onset of the exit wake and internal louver bank instabilities – large angles and thicker fins exhibit an earlier onset of instabilities. The effect of fin pitch on the onset was weak. However, the rate of propagation of instabilities into the louver bank was much higher for large fin pitches and large louver angles.

Zhang and Tafti (2003) studied the effect of Reynolds number, fin pitch, louver thickness, and louver angle on flow efficiency in multilouvered fins. The computational domain was the same that presented on Tafti et al. (2000). Two fin pitch ratios (1.0 and 1.5) were studied with variations in louver angle (15º, 20º, 25º and 30º), and three thickness ratios (0.05, 0.1 and 0.15) were chosen. Reynolds number, based on louver pitch, varied from 50 to 1200. It was observed that the flow efficiency has strongly effect on the heat transfer capacity in multilouvered fins. Results showed that the flow efficiency was strongly dependent on geometrical parameters, especially at low Reynolds numbers. Flow efficiency increases with Reynolds number and louver angle, while decreasing with fin pitch and thickness ratio. Compared to fin pitch, louver angle has a strong effect. Louver thickness effect on flow efficiency was also significant for small louver angles. At the end, the authors proposed a correlation to predict the flow efficiency based on those input parameters.

Perrotin and Clodic (2004) studied the heat transfer performance by CFD codes. The flow was assumed to be laminar and according of the authors, this assumption seems to be reasonable at the Reynolds numbers (based on louver pitch) ranging from 40 to 1200. However, five 2D simulations were performed with the low Reynolds $k - \varepsilon$ turbulence model in order to estimate the effect on heat transfer and pressure drop characteristics and to see where the flow field becomes locally turbulent. The heat transfer results in this case were 5.8% higher than without turbulence model, and the turbulent kinetic energy was localized in very small regions. Moreover, low Reynolds turbulence model requires a cell size leading to a y^+ value near the unity, which was obtained with intermediate mesh size. For the 3D steady model, conjugate heat transfer was taken into account and the solid was assumed isotropic. The computational domain was composed of a complete louvered fin cross-section with entry region, first set of five louvers, turn-around fin, second set of five reversed louvers and outlet region. The height of the computational domain was equal to fin pitch and matching cyclic boundary conditions were applied at the top and the bottom of the domain. Constant wall temperature condition was applied on the inner surface of the microchannel tube. The average cell size was roughly equal to the fin thickness in all directions and the total number of cells was 305066. Equations were discretized with finite volume technique. Second-order spatial discretization scheme MARS (Monotone Advection and Reconstruction Scheme) was used for steady simulations for the convection terms. For the pressure field calculations, the used algorithm in steady state was the SIMPLE. The heat transfer coefficient calculated with 3D models was much closer to the experimental data. At $Re_{LP} = 78.6$ the boundary layers over the louvers were very thick. The air flow between the louvers was blocked by those boundary layers. The global motion of the fluid was fin directed and the flow was predominantly ducted. Also, the thermal wake of each upstream louver surrounded the downstream louver of the same fin. The mean temperature increased rapidly in the first half of the array, near the fin temperature. Consenquently heat transfer saturation was reached and the fin performance was poor. At higher Reynolds numbers ($Re_{LP} = 604.8$), the boundary layers around the louvers were thinner and the flow was nearly aligned with the louvers. In this case, the predominant thermal wake effect was inter-fin effect, when the thermal wake of the upstream louver impinges the downstream louvers of adjacent fins. A local

maximum of the bulk temperature was observed between the first louvers. This was due to the presence of a stationary vortex which develops between the first louvers when the Reynolds number was increased. High heat transfer rates were observed where the thermal boundary layer re-grew. The heat transfer coefficient increased also at the trailing edge of each louver due to the acceleration of the fluid. This penhomenon was much more visible at high Reynolds numbers ($Re_{LP} = 604.8$). At low Reynolds number ($Re_{LP} = 78.6$), it was noticed that, for the first part of the louvered array, the heat transfer coefficient over the top surface was always higher than over the bottom surface. The contrary was observed for the second set of louvers. At high Reynolds number, it was shown that the heat transfer coefficient over the bottom surface was higher than over the top surface, except for the second louver (due to the presence of stationary vortex).

Tafti et. al. (2004) studied the effect of large louver angles on the performance of large pitch fins at low Reynolds numbers. The Reynolds number based on face velocity and louver pitch was varied between 50 and 300. Louver angles were varied from 20º to 60º for fin pitch ratios of 1.5 and 2.0. The governing equations for *momentum* and energy conservation in generalized coordinates were discretized with a conservative finite-volume formulation. Both, convection and viscous terms were approximated by second-order central-difference schemes. Periodic boundary conditions were applied in the transverse direction while Direchlet boundary conditions were specified at the entrance to the louver bank. For all the calculations, the louver thickness was fixed. The exit domain extended approximately 55 fin thicknesses downstream the array where outflow boundary conditions were applied. At the fin surface, no slip and no penetration boundary conditions for the velocity field and for temperature field were applied. The numerical results showed that when the louver angle was increased, both the heat transfer coefficient and friction coefficient increased. The flow efficiency had an optimal value near 50º when the Reynolds number was less than 100, and then decreased with a further increase in louver angle. As the Reynolds number increased further, the flow efficiency started decreasing at lower louver angles. The decrease was primarily a result of recirculation zones forming in the wake of louvers, which behave as blockages. Contrary to expectations, in spite of the flow efficiency decreasing, both heat transfer and friction coefficients increased monotonically with an increase in louver angle. The

increase in the heat transfer coefficients in spite of a drop in flow efficiency was found to be a result of enhancement provided by flow impingement, both direct and that induced by recirculation fluid, on the leading surface. As the louver angle increased impingement heat transfer became a dominant mode of heat transfer augmentation. Hence, they concluded that large louver angles can be used to augment heat transfer at low Reynolds numbers and large fin pitches at the price of a larger system pressure drop.

3-D numerical analysis on heat and fluid flow were carried out by Hsieh and Jang (2006). On that research, successively increased or decreased louver angle patterns were proposed (Figure 2-15). The Reynolds number was maintained constant and equal to 1075 (based on fin pitch). The governing equations were solved numerically using a control volume based finite difference formulation. A third-order upwind TVD (total variation diminishing) scheme was used to model the convective terms of governing equations. Second-order central difference schemes were used for the viscous and source terms. The turbulence model used to perform analysis was the extended $k - \varepsilon$ model proposed by Chen and Kim (1987). The fluid was considered incompressible with constant properties and the flow was assumed to be turbulent, steady, three-dimensional and with no viscous dissipation. There was a local maximum of span-averaged Nusselt number at the upstream of each louver, because of the repeated growth and destruction of the boundary layer. The upper surface span-average Nusselt number was 6-20% higher than the lower surface. Both the span-averaged Nusselt number and pressure drop coefficient for successively variable louver angles (cases A-D) were higher than those for the uniform louver angle (case E). For the case A, B, C and D the maximum heat transfer improvement interpreted by j/j_E were 115%, 118%, 109% and 107%, and the corresponding friction factor ratio f/f_E were 116%, 119%, 110% and 108%, respectively.
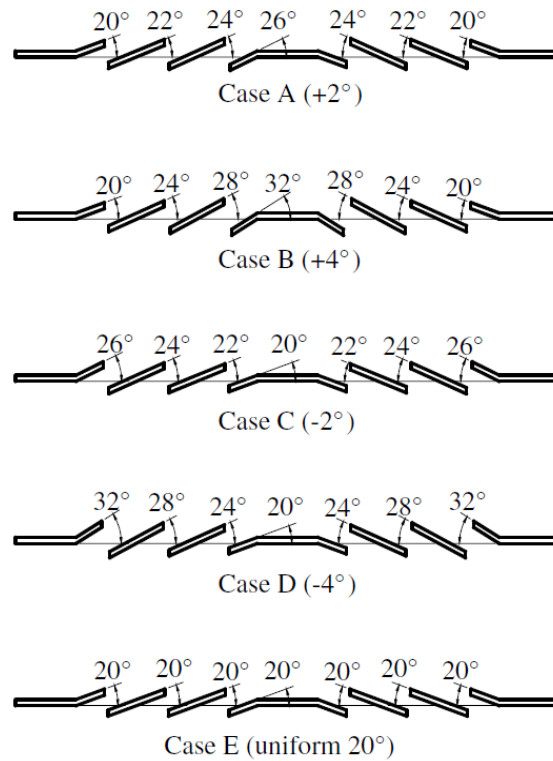
Figure 2-15 Five different cases studied by Hsieh and Jang (2006).

Malapure et. al. (2006) numerically investigated the fluid flow and heat transfer characteristics over louvered fins and flat tube in compact heat exchangers. Three-dimensional simulations of single and double row tubes with louvered fins were conducted. The simulations were performed for different geometries with varying louver pitch, louver angle, fin pitch and tube pitch and for different Reynolds number. The Reynolds numbers, based on hydraulic diameter, ranged from 400 to 4000 (this was equivalent to Reynolds number range based on louver pitch of 60 to 1800). The 3-D simulations were performed with the RNG $k - \varepsilon$ turbulence model in order to estimate the heat transfer and pressure drop characteristics and to verify the local turbulence behavior of the flow field. The commercial code Fluent 6.1 was used for the numerical solution of the Navier-Stokes and energy equations by using finite-volume methodology. A second-order spatial interpolation method was employed to obtain the velocity components, pressure and temperature on the control volume faces. SIMPLE algorithm was used to couple pressure and velocity. A second-order upwind scheme was used for the space discretization of the *momentum,* turbulence

and energy equations. Due to symmetry of the flow domain, calculations were performed for half fin height and periodic boundary conditions were imposed on the top and bottom of the domain. At the inlet, velocity boundary was imposed. The pressure-outlet boundary was used to outlet plane, where static gauge pressure and temperature were given. Tubes walls were defined as constant wall temperature. On the fin and tube surfaces, no slip boundary condition was assumed. The numerical setup was compared with experimental data and close agreement was found between the computational results and experimental data at intermediate and high Reynolds numbers. It was shown that the heat transfer coefficient increases with louver angle (from 22º to 32º) and reaches maximum value at 28º-29º and the again decreases with the louver angle increasing. High heat transfer coefficient was obtained at smaller louver pitch ($L_P = 0.81$ mm). Decreasing on louver pitch caused the formation of a thin boundary layer which in turn interrupts the air flow. Decreasing the fin pitch from 3.33 mm to 2.11 mm, heat transfer rate increased. However further reduction in fin pitch from 2.11 mm to 1.72 mm, did not result in any additional improvement on heat transfer. Also, the pressure drop increased with fin pitch decreasing from 3.33 mm to 1.72 mm. This was because as the fin pitch was reduced, air flowing smoothly between the louvers could no longer pass easily and hence the full effect of louver was not obtained due to development of boundary layer and vortex formation.

Junjanna et. al. (2012) studied the performance improvement of a louver-finned automotive radiator. The Fluent 13.0 software was employed for simulations. The assumptions made during their research were: (1) flow was steady, (2) flow was incompressible, (3) there was no viscous dissipation, (4) constant material properties and (5) there were no buoyancy effects. The inlet air velocity was constant (9.71 m/s), the louver angle was 25º, the fin pitch was 2.7 mm and the tube pitch was 10.5 mm. The turbulence model adopted to run the simulations was the $k - \omega$ model. Simulations were carried out for heat exchanger models with different louver pitches, air and water flow rates and at different fin and louver thicknesses. About the boundary conditions, at the inlet, velocity was imposed; at outlet, it was assumed 'zero' static pressure; walls were assumed smooth and without slip; tube uniform temperature was specified. The coupling between pressure and velocity was made by SIMPLE algorithm. Second-order upwind scheme was used to have higher

accuracy. According to authors, the results from the computations were found to be in good agreement with that of the experiments of Vaisi et al. (2011). The effect of five louver pitches was studied (from 1.43 mm to 2.85 mm). Higher values of heat transfer coefficient were observed in the fin facing the air (ahead of the first tube). Louver immediate downstream showed lower values of heat transfer since the heat transferred from the fins to the louvers were small due to lower contact area. Louver in the second row showed higher heat transfer values than the louvers in the first tube row area.

Gunnasegaran et. al. (2012) numerically investigated the effects of geometrical parameters such as louver angle and fin pitch on airflow and heat transfer characteristics on compact heat exchangers. The 3-D numerical simulations were performed using five different cases with increased and decreased louver angle (Hsieh and Jang, 2006). Reynolds number between 100 and 1000, which was based on fin pitch. The standard SIMPLE algorithm was used. The iterations were continued until the sum of residuals for all computational cells reached 10^{-7}. The flow was considered laminar. At the entrance of the domain, the uniform inlet air temperature and the uniform inlet velocity was imposed. At the domain wall, non-slip conditions were applied, and it was assumed to be an adiabatic surface. At the outlet surface, it was set outflow boundary condition. The validation of the computational model was done by comparison with the data available from Hsieh and Jang (2006), for inlet velocity of 5 m/s; the CFD results agreed well. According to results, there was a maximum and minimum value of Nusselt number at each louver along the flow direction because of the repeated growth and destruction of the boundary layer. The Nusselt number was all higher for successively increased or decreased louver angle compared to uniform louver angle. Both the Nusselt number and pressure drop coefficient increased with the decrease of fin pitch and increase of Reynolds number. The heat transfer enhancement for smallest fin pitch was more apparent at high Reynolds number.

Saad et. al. (2013) numerically studied via Computational Fluid Dynamics (CFD) the interactions between the air flow and louvered fin. 3D numerical simulation results were obtained by using the ANSYS Fluent 13.0 code and compared to experimental data. The paper studied the effect of louver angle, fin pitch and louver pitch

geometrical parameters on overall thermal- hydraulic performance. Symmetry conditions were assumed on both sides of the domain. Periodic boundary conditions were applied at the left and right of the domain. Thetrahedral mesh was used and the total number of cells for 3D model was 10 millions. At the entrance, the velocity of the air was applied. For the fin, non slip boundary conditions were applied, as well as a constant temperature boundary condition. Laminar and different steady state turbulence models ($k - \varepsilon$ enhanced wall treatment and $k - \omega$ SST) were used. Laminar steady and both turbulence models gave the same friction and Colburn factors. Based on this, the authors chose the laminar steady model. Close agreement was found between the computational results and experimental data at intermediate and high Reynolds number. However, at low Reynolds number there was some deviation. The authors also investigated the effect of increasing or decreasing the louver pitch of the three first louvers of the fin. It was observed that there were geometries which decreased pressure drop up to 11% and heat transfer up to 6%, compared to constant louver angle of 28º. Moreover, according to results, the temperature gradient for successively variable louver angle was higher than that for the uniform louver angle. In addition, since the temperature difference between the air and the fin (driving potential for heat transfer) decreased along the fin, the heat rate in the second panel was lower than the one in the first panel. This heat rate degradation was more pronounced as the air velocity decreased. At low Reynolds number, second half of the louvers array only accounts for pressure losses without any significant heat transfer. This means that is not necessary to keep a relatively high louver angle in the second panel to maintain a high heat transfer coefficient.

Ferrero et al. (2013) studied the effects of fin pitch, louver pitch and louver angle on louvered-fin compact heat exchangers performance by means of the commercial CFD solver CD adapco STAR-CCM+. Two extended rectangular regions at inlet and outlet were coupled to the main domain. Both extensions were of 6 mm (almost 3.4 hydraulic diameters). Uniform airflow velocity of 3 m/s and constant air temperature were imposed. A constant pressure boundary was set at outlet and periodic boundary conditions were applied at the airflow transverse direction. The temperature of the tubes was set as constant. The prime assumptions to run the numerical simulations were: (1) steady state condition; (2) laminar model flow; (3) incompressible ideal gas flow; (4) temperature dependent air properties. Flow equations were solved in an

uncoupled manner, while the linkage between *momentum* and continuity equations was achieved with a predictor-corrector approach. The increase of the fin pitch from 100% to 108.33% caused pressure drop decreasing by 11% on average for all louver angles, with a corresponding reduction of about 3% in the thermal performance. High F_P means more duct-directed flow and thus the air particles were prone to prosecute along the axial direction bypassing the louvers. Among the three variables investigated, the louver angle showed the highest influence on pressure losses without significantly affecting the heat transfer performance. By diminishing the louver angle from 31º to 26º, it was possible to reduce the pressure drop up to 13% against an almost negligible reduction of 1.2% in the heat transfer. Moreover, the benefits of louver angle reduction were higher for geometries with many louvers. High values of louver pitch played a role in the growth of the air particles dwell time inside the louver array. High louver lengths and, most of all, high louver gaps, modified indeed the balance of aerodynamics resistances toward the louver direction. Thus, the increase in louver pitch also diminished the number of louver per row and reduced also the number of the leading edges, which can mitigate the heat transfer for louver-directed flows.

Jaiboon et al. (2013) numerically studied the effects of geometric parameters for a plate-fin. Simulations were performed for different geometries with various fin pitches, louver pitches, tube pitches and louver angles. A three-dimensional model was constructed with the smallest fluid cell size next to wall being smaller than or equal to the fin thickness. The numerical solution of the Navier-Stokes and energy equations was performed by using finite-volume method. RNG $k - \varepsilon$ turbulence model, with enhanced wall treatment was used. One-half of the tube pitch was considered with symmetry plane at one side and constant wall temperature at the other. The top and bottom surfaces of the domain were defined as periodic boundaries. The numerical simulations were performed for different Reynolds number within the range of 100 to 4000 (based on hydraulic diameter). All thermo-physical properties of the tube and fin surfaces were assumed constant. The SIMPLE algorithm was used to couple fluid pressure and velocities. The discretizations of the *momentum*, turbulence kinect energy, turbulence dissipation rate, and energy equations were set to second-order upwind. Good agreement was observed as far as Stanton number was concerned but large deviation was found for friction factors. The most important conclusion was

that the heat transfer coefficients and pressure drop increased with decreasing of fin pitch.

Ryu et al. (2014) performed numerical analysis for a corrugated louvered fin. They selected the fin pitch, louver pitch, and louver angle as the parameters to be investigated. 2-D steady state models were compared with experimental results from Kim and Bullard (2002). The turbulence models used to run the simulations were: Standard $k-\varepsilon$ model, RNG $k-\varepsilon$ model, Realizable $k-\varepsilon$ model, Standard $k-\omega$ model and SST $k-\omega$ model. The Reynolds numbers of 50, 250 and 450 were chosen for comparison. The Realizable $k-\varepsilon$ model produced the smallest deviations in terms of performance equation, $\dfrac{j/j_{ref}}{(f/f_{ref})^{1/3}}$. Also, they compared a steady stated 2-D model with a steady state 3-D model, with Realizable $k-\varepsilon$ model. The 3-D model generated errors less than 2% with respect to reference model and the 2-D model generated errors less than 5%. In addition, they compared steady and unsteady 2-D model to determine the effect of flow around a louvered fin. The results for both were practically the same.

Carija et al (2014) numerically evaluated the heat analysis of fin-and-tube heat exchangers with flat and louvered fin geometries. The flow over the louvers was assumed laminar and steady. The inlet air flow velocity ranged from 0.5 and 2.5 m/s. The numerical results agreed well with experimental data. The greatest heat transfer performance of 58%, compared with flat fins.

Ryu and Lee (2015) experimentally and numerically investigated the thermal-hydraulic performance of louvered fins. They proposed generalized heat transfer and pressure drop correlations for flat-tube louvered fins. The Reynolds number, based on louver pitch, ranged from 100 to 3000. About the numerical procedure, it was used SIMPLE algorithm to couple pressure and flow fields and QUICK scheme to discretize the governing equations. The flow was considered unsteady and several types of turbulence models were used. The comparison between numerical and experimental data from Kim and Bullard (2002) showed that the maximum deviation for both heat transfer and pressure drop was 17%.

2.4 Numerical research focused on longitudinal vortex generators

Kim and Patel (1994) numerically studied the influence of streamwise curvature on longitudinal vortices imbedded in turbulent boundary layers, in common-flow-down and common-flow-up arrangements. They compared the numerical results with experimental data. The flow near wall was resolved by the two-layer $k - \varepsilon$ turbulence model. About the common-flow down vortices, the two vortices moved apart as they grew in size and produced region of boundary layer thinning between them. Convection of each vortex by the flow field of the other holds the vortices close to the wall, while the effect of the wall is to force them move apart. The boundary layer between the two vortices was thinned by the strong downward flow and the lateral outflow of the boundary-layer fluid. In the upwash region, the boundary layer was thickened because the vortex sweeps low-*momentum* fluid away from the wall. Also, for this case, the computational study reproduced most of features of the mean-velocity field except near the vortex center, where the calculations appear to diffuse the velocity deficit more rapidly than was observed in the experiment. There was good agreement between the calculations and data with respect to the shape of the spanwise distributions of the resultant friction coefficient. The downwash between the vortices thins the boundary layer and led to higher friction factor there. The region of upwash, where low-*momentum* fluid was lifted by the vortex, showed a low friction factor coefficient. Vortices in a common-flow-up pair interacted more strongly with each other rather than with the boundary layer. Common-flow-up vortices produced strong upward flow in the plane of symmetry and lift low-*momentum* fluid from the boundary layer, resulting in a thickening of the boundary layer between the vortices.

Biswas et al. (1996) numerically and experimentally investigated the flow structure and heat transfer effects of longitudinal vortices in a channel with single delta winglet. The main obejctives of their studies were perform comparison of the predicted flow structure with the experimentally, and prediction of heat transfer and pressure drop characteristics for different geometrical parameters. The maximum discrepancy of combined spanwise average Nusselt number for fine and intermediate grids was 1.4%. For Reynolds number of 1580 (based on average axial velocity at the inlet and characteristic dimension of the channel), aspect ratio of the channel (ratio of channel

width, B, and channel height, H) of 3.0 and angle of attack of 15º, the maximum cross-flow velocity was nearly equal to the mean axial velocity. The elliptic deformation of the vortical structure due to the channel walls became obvious when the cross-flow at any two stations downstream of the winglet were compared. The same analysis, but on cross-section position $x/H = 2.5$ (behind of the trailing edge of the DWL), the maximum velocity was found to be 1.659 times the average axial velocity at the inlet. Also, the vortex axis lied at about the mid-plane of the channel height and the axial velocity had a low value at the axis. When the value of $B/H = 5.0$, angle of attack was 30º, the axial velocity contours on the bottom plate behind the winglet, indicated that the vortices led to a thinning of the velocity boundary layer in the downwash region. In this particular case, the maximum velocity was equal to 1.683 times the average axial velocity at the inlet. Behind the winglet, it was observed that smaller velocity in the boundary layer on the flat bottom wall which is attached to the side of the winglet leads to a smaller pressure increase. Thus, the induced pressure gradient causes a flow towards the bottom wall which interacts with the main-stream. The fluid rolls up forming vortices which are finally swept around the obstacle base and are carried downstream. These vortices were the corner vortices. The induced vortices had their rotate axis opposite (counterclockwise) to the main and corner vortices. Moreover, it can be seen that the main vortex axis lied at about the mid-plane in the vertical direction and it was shifted to the right side of the cross-stream plane.

Yanagihara and Rodrigues (1998) conducted a numerical study of the effects of longitudinal vortices on flow structure and heat transfer in a fin-tube channel with a pair of delta winglets in the laminar flow regime. They obtained a combined effect of augmented heat transfer and reduced pressure drop for winglets with attack angle of 45º in a certain position with respect to the tube.

Chen et al. (1998) performed numerical investigations of conjugated heat transfer of a finned oval tube with a punched delta winglet vortex generator, varying parameters like angles of attack (20º, 30º and 45º) and two aspect ratios (1.5 and 2.0), for a fixed Reynolds number of 300. Unsteady three-dimensional flow and conjugate heat transfer were calculated for a thermally and hydrodynamically developing laminar flow by using finite volume method. Based on flow field analysis, the authors

concluded that the form drag of the winglet dominated the flow loss penalty and the longitudinal vortices hardly caused any additional pressure drop. The core of the primary longitudinal vortices stemmed from fluid on the lower part of the leading edge of the winglet. Also, the body and outer layer of the primary longitudinal vortices were formed by the fluid near the leading edge and near the upper part of the trailing edge of the winglet. About the thermal-hydraulic performance, winglet with angle of attack equals 30º and aspect ratio of 2.0 were the best of the investigated configurations.

Yang et al. (2001) numerically analysed the flow field and heat transfer by interaction between a pair of vortices in rectangular channel flow. They used a pseudo-compressibility method to solve the incompressible Navier-Stokes equations. This methodology is similar to the case in which the steady, incompressible Navier-Stokes equation is used for compressible flow. They used the same two-layer $k - \varepsilon$ turbulence model of the Kim and Patel (1994), for common-flow-down and common-flow-up configurations. The aspect ratio and angle of attack were 2.5 and 18º, respectively. The inlet velocity was fixed at 16 m/s. As the vortices moved downstream, no interaction occurred between them, but strong interactions between the vortices and boundary layers occurred. The movement of the secondary vortex toward the upwash region was not predicted well because of the isotropic assumption of the eddy viscosity model. However, the numerical analysis can well predict the Reynolds stress and the phenomenon in which the boundary layers become thin in the downwash region and thick in the upwash region of the vortices. It was also observed that the turbulent energy of the vortices diffused rapidly and the turbulent kinectic energy was high near the wall but it became weaker as it became more distant from the wall. The average temperature distribution and the heat transfer coefficients for the whole wall closely agreed with the experimental data by Pauley and Eaton (1988). The skin friction coefficients and heat transfer coefficients were also the same as those of the experimental data.

Tiwari et al. (2003) numerically evaluated the heat transfer enhancement in cross-flow heat exchangers using oval tubes and multiple delta-winglets. The Reynolds number was set constant and equal to 1000 (based on channel height). The flow was considered laminar, unsteady and incompressible. The mean span-average Nusselt number for the case of four DWL pairs, each two in sequence having a staggered

configuration was about 100% higher as compared to no-winglet case. The authors concluded that two or three DWL pairs caused further enhancement of heat transfer.

Zhu et al. (2006) performed a numerical study of interactions of vortices generated by LVGs and the effects of such interactions on heat transfer enhancement of flat tube bank in staggered array. The flow and heat transfer were assumed to be laminar, incompressible and in steady state, with constant Reynolds number of 1810 (based on hydraulic diameter). The discretization was done by using finite-volume method. The maximum difference of Nusselt number for numerical and experimental data was 9.6%; for friction factor, the maximum difference was 32.4%. The numerical results showed that because of the convergence of the core of vortices induced by the flat tube, a real staggered ratio is related to the interactions between vortices generated by upstream VGLs and vortices generated by downstream LVGs, which had counter-rotating direction. The reason for weakening heat transfer enhancement was that the interaction of counter-rotating vortices decreased the intensity of vortices and hence the heat transfer enhancement. The insight that came from these results was that the relative position of VGs in the channel was a very important parameter that should be carefully considered in design of such heat transfer enhancement surfaces.

Ferrouillat et al. (2006) numerically studied the heat transfer enhancement and mixing by artificially generated streamwise vorticity in a rectangular channel using delta winglet pair and rectangular winglet pair. The authors showed that the predominance of longitudinal and transverse vortices depends on DWL angle of attack (for angles of attack less than 65º the predominance is for longitudinal vortices while angles higher than 70º, the transversal vortices is dominant). Several turbulence models were used on their study. The $k - \varepsilon$ model and the large eddy simulation (LES) were tested with different model laws: standard, RNG and Realizable for the $k - \varepsilon$ model and Smagorinsky and RNG for the LES model. The software Fluent was used. The RNG and Realizable $k - \varepsilon$ turbulence models seem to give the best results when compared with experimental data. A comparison of the LES computations led to the conclusion that the generation of longitudinal vortices was actually a quasi-steady phenomenon. Indeed, there was no significant difference between these two simulations in terms of heat transfer and drag enhancement. Also, both RNG and Realizable $k - \varepsilon$ models and LES simulations described a pair of

counter-rotating vortices in the wake of the winglets, but the standard $k - \varepsilon$ model did not correctly predict counter-rotating vortices. The influence of the attack angle was also studied with the best turbulence models, using rectangular delta winglet pair. Using LES model with RNG subgrid scale model and RNG $k - \varepsilon$ model, computations for Reynolds number 4600 and angle of attack 65º were performed. The LES simulations provided good predictions in term of heat transfer (5.88% of error) and pressure drop (3% of error). The RNG $k - \varepsilon$ model predicted heat transfer with 5.88% of error and strongly overestimates the pressure drop (15% of error). The authors concluded that the RNG $k - \varepsilon$ model, even with swirl and pressure gradient effect, can no longer predict strong anisotropic flow patterns. Also, when the LES model was used for Reynolds number of 2000, the computations overestimate the heat transfer about 36%.

Hiravennavar et al. (2007) focused their studies on analysis of the heat transfer enhancement in a channel with delta winglet pair. Computations were done by solving the unsteady, three dimensional, incompressible Navier-Stokes equations and energy equation using a modified Marker-and-Cell (MAC) method. The comparison between numerical predictions and experimental data showed that the results were very close. Effects of thickness of the winglets on the heat transfer enhancement were presented. The Reynolds number ranged from 790 to 2000 (based on average velocity at the channel inlet and channel height). The length of the channel was equals 11.4 times the height of the channel, the aspect ratio of the channel equals 3.0 and the aspect ratio of the DWL was 2.46. The winglets were positioned such their trailing edges were at downstream position of 2.856 times the channel height from the inlet. The angle of attack was 15º. The arrangement of the DWL pair was in common-flow-down configuration. The maximum cross-flow velocity at a plane was seen to be nearly equal to the mean axial velocity on that plane. Two counter-rotating main vortices behind the winglets caused the fluid churn. This churning motion caused the fluid near wall to flow in the central region and vice versa. Also, it can be seen that the axes of the main vortices moved downward and away from each other as they move downstream. The heat transfer was obtained by calculation of the Nusselt number at top and bottom plates for DWL with zero thickness and finite thickness. The results indicated that a winglet with finite thickness was marginally superior to the idealized zero thickness winglet. Moreover, it was

observed an enhancement of heat transfer due to pair winglets of twice that due to a single winglet.

Wu and Tao (2007) numerically investigated the heat transfer in fin-and-tube heat exchanger in aligned arrangement with longitudinal vortex generator under laminar flow condition. The Reynolds numbers, based on inlet average velocity and 2 times of net fin were below to 2000. The flow was considered steady and incompressible. The results from the numerical procedure agreed well with experimental data. The average Nusselt number increased 16-20% by DWLs with attack angle of 30º and is increased 20-25% with angle of attack of 45º.

Wu and Tao (2008) numerically investigated the laminar convection heat transfer in a rectangular channel with rectangular longitudinal vortex generator. The effects of Reynolds number (from 800 to 3000), the attack angle of the vortex generator (15º, 30º, 45º, 60º and 90º) were examined. Fluent commercial code was used to simulate the flow field. Second order upwind scheme was used to discretize the convective term of the governing equations, and central difference scheme was employed for the diffusion term. SIMPLEC algorithm was adopted for coupling between pressure and velocity. The relative error between theoretical solutions and numerical data for Nu and f was 0.8% and 1.9%, respectively. The pressure drop of the channel with the LVG increased rapidly with the increase of the attack angle of the LVG. Moreover, the vortex generator with attack angle of 45º always provides the better effectiveness of heat transfer enhancement. The thickness of LVG mainly influenced the flow and heat transfer near the LVG. The average Nusselt number of whole channel at the condition of considering the thickness of LVG was lower than that of the case neglecting the thickness of LVG. The thickness of LVG had little influence on the average friction factor of the channel for those conditions.

Effects of the common-flow-up pair produced by delta winglet vortex generators in a rectangular channel flow on fluid flow and heat transfer were numerically investigated by Yang et al. (2008). The numerical approach and geometrical parameters were the same those presented in Yang et al. (2001). In comparison with the experiment of Pauley and Eaton (1988), although some discrepancies were observed near the center of the vortex core, the overall performance of the numerical analysis was found to be satisfactory. In the case of flow field, they identified that the boundary

layer was thinned in the region where the secondary flow was directed toward the wall and thickened where it was directed away from the wall. The interaction between the vortices became very strong while the interaction between the vortices and the boundary layer became very weak. As the common-flow-up pair developed, their lifting effect from the bottom wall increased more and more. About the heat transfer, the distortion of the thermal boundary layer was not as strong as the distortion of the hydraulic boundary layer. The influence of the common-flow-up pair on heat transfer enhancement was maintained at the downstream location 30 times the chord length of the vortex generators.

Numerical study of the relationship between heat transfer enhancement and absolute vorticity flux along main flow direction in a channel with delta-winglet vortex generator pairs was performed by Chang et al. (2009). The flow and heat transfer were assumed to be incompressible and in steady state. According to mathematic formulation, the flow was considered laminar. The aspect ratio and attack angle of the VG was, respectively, equal to 2.0 and 35º. Also, three types of fin spacing were selected. The numerical method used was the finite volume method with structure grid system. The power scheme was used to discretize the convective terms. SIMPLE algorithm was used to handle the coupling between pressure and velocity. The Reynolds number was fixed at 1136, based on hydraulic diameter. Good agreement between numerical and experimental results was obtained, with maximum relative error for Nusselt of 9.8%, and for friction factor of 7.9%. In the most cases, the secondary flow could not change greatly the boundary layer characteristics, especially for the internal flow at the beginning region of boundary layer. The averaged absolute vorticity flux could account for only the secondary flow effects on convective heat transfer but could not quantify the effects of developing boundary layer on convective heat transfer. The streamwise averaged absolute vorticity flux normal to the cross-section had the same trend with the Nusselt number.

Tian et al. (2009) numerically studied of fluid flow and heat transfer in a flat-plate channel with longitudinal vortex generators. The flow was considered laminar. The effects of rectangular winglet pair (RWP) and delta winglet pair (DWP) with two different configurations, common-flow-down (CFD) and common-flow-up (CFU) were studied. The attack angle was set to 30º. The Reynolds number based on the

channel height varied from 470 to 1700, which corresponding to air velocity in the channel inlet ranging from 0.246 to 0.9. According to authors, the comparison of numerical and experimental data for heat transfer coefficient agreed well with the experiments. However, the validation for that range of velocity, showed that all values of heat transfer coefficient were out of accuracy range of the experiment. Also, no comparison for friction factor was done. The friction factor of the channel with RWP was higher than that of DWP, and the friction factor of the channel with common-flow-up configuration was larger than that of common-flow-down configuration. For the channel with DWP, the difference between the common-flow-down and common-flow-up configurations was very small.

Chu et al. (2009) numerically studied the fin-and-oval-tube heat exchanger with longitudinal vortex generators. The Reynolds number, based on hydraulic diameter) ranged from 500 to 2500. The flow was assumed laminar and steady. The coupling between velocity and pressure was performed with SIMPLEC algorithm. The convective terms were discretized with second-order upwind scheme. It was verified a good agreement between numerical model and experimental data. The LVGs located in downstream of oval tubes were more effective than those located in upstream of oval tubes for heat transfer enhancement. Moreover, both average Nusselt number and friction factor decreased with the increase of the tube row number. The less was the tube row number, the better the heat transfer rate.

Lei et al. (2010) numerically investigated hydrodynamics and heat transfer characteristics of a novel heat exchanger with delta-winglet vortex generators. The Reynolds numbers ranger from 600 to 2600 (corresponding to the frontal air velocity that ranges from 0.53 2.30 m/s), the angle of attack of DWLs from 10º to 50º and the aspect ratio from 1.0 to 4.0. The fluid was assumed to be incompressible and the flow was laminar in steady state condition. SIMPLE algorithm was used as pressure-velocity coupling. The convective terms in governing equations were discretized by QUICK scheme. According to the results of Colburn factor and friction factor, the numerical predictions agreed well with experimental data.

Min et al. (2012) numerically investigated the turbulent flow and heat transfer in a channel with rectangular delta winglet. The Reynolds number ranged from 2000 to 16000. The influences of six main parameters of the combined rectangular winglet

pair (CRWP) in a rectangular channel were examined. Those six parameters included the location of the CRWP and geometric sizes. The main attack angle of the CRWP ranged from 15º to 75º. The numerical simulations were conducted using finite-volume methodology (software Fluent 6.3.26). The turbulence model was RNG $k - \varepsilon$, with SIMPLE algorithm and QUICK scheme for the discretization of the convective terms, whereas the diffusion terms were discretized by the central difference scheme. The deviation of the heat transfer between the numerical and experimental data was less than 10%. The major findings of their work were that the application of LVGs can obviously increase the heat transfer and pressure drop of the channel. Also, in comparison with rectangular winglet pair, the CRWP generates vortices that have larger area and lower core.

Wu and Tao (2012) numerically investigated the effect of delta winglet vortex generator on heat transfer in rectangular channels at attack angles of 15º, 30º, 45º and 60º. The numerical set up was the same adopted in Wu and Tao (2008), with Reynolds number ranging from 400 to 1700, which was based on channel height. The deviations between tested and simulated results of the average Nu for all cases were less than 10%, and it was observed that the numerical results were underestimated compared to the experiment results for every tested cases. The average heat transfer of both surface of the plate with delta winglet pair increased with the increase of Reynolds number and attack angle. Strong and persistent longitudinal vortices were visualized in the upper channels. Moreover, it was observed that the transverse flow through the punched holes under the delta winglets disturbed the flow field of the lower channel. The computed velocity and temperature fields indicated that the generated strong longitudinal vortices made the temperature distribution more uniform in the upper channel; the transverse flow of the air stream through the punched holes led to a pair of weaker vortices in the lower channel, benefiting to enhance the heat transfer on the under surface of plate.

He et al. (2012) numerically analysed the thermal-hydraulic performance of heat exchangers with rectangular vortex generators. The fluid was considered incompressible and the flow was assumed laminar and steady. The convective terms were discretized with the second order upwind scheme. SIMPLE was used as the pressure-velocity algorithm. Compared with the baseline case, the heat transfer

coefficient was improved by 28.8-34%, 54.6-61.5% and 83.3-89.7% for angles of attack of 10º, 20º and 30º, respectively. However, the associated pressure drop penalty was also enlarged.

He et al (2012) numerically studied the heat transfer enhancement by punched winglet-type vortex generator arrays in fin-and-tube heat exchangers. The Reynolds numbers ranged from 600 to 2600, corresponding to inlet velocities from 0.54 and 2.3 m/s. The flow was considered laminar, steady and incompressible. Excellent agreement between numerical and experimental data was observed. For punched VGs, the corner vortex showed the characteristcs of the main vortex, and played a more important role on the fluid flow behavior and heat transfer characteristics in the channel of fin-and-tube heat exchanger than that of the main vortex.

Unsteady numerical investigations pertaining to heat transfer enhancement of a plate-fin heat exchanger using two rows of winglet type vortex generators (VG) were performed by Sinha et al. (2013). On that work, five different strategic placements of the VG, namely, common-flow-up in series, common-flow-down in series, combined (common-flow-down and common-flow-up), inline rows of winglet and staggered rows of winglet, were considered. The Reynolds number was varied from 250-1580, which was defined on the basis of average axial velocity at the inlet and the characteristic dimension of the channel. The angle of attack was fixed at 15º. Figure 2-16 shows those arrangements. The authors concluded that in terms of heat transfer, common-flow-up in series performed best followed by common-flow-down in series and combined. The performance of common-flow-up in series in terms of quality factor was comparable to common-flow-down in series and combined arrangements. In the far downstream the effect of staggered rows of winglet and inline rows of winglet was very close to that of common-flow-up in series. Basically, common-flow-up in series, common-flow-down in series and combined arrangements were various combinations of counter rotating vortex pairs with common flow character at the central longitudinal mid-plane. The staggered rows of winglet and inline rows of winglet arrangements of the winglets generate co-rotating vortex pairs without a common flow character at the central longitudinal mid-plane. The symmetric nature of the vortex-pairs in the cases of common-flow-up in series, common-flow-down in series and combined dictated the heat transfer rate.

Numerical simulations were performed by Saha et al. (2014) in a rectangular channel containing built-in longitudinal vortex generators on the bottom wall arranged periodically both in the streamwise and spanwise directions. Two types of vortex generators, rectangular winglet pair and delta-winglet pair with two different flow arrangements, common-flow-up and common-flow-down were explored to assess the influence of shape and flow arrangements on heat transfer enhancement. The flow was considered to be three-dimensional, unsteady and laminar, for Reynolds ranging from 50 to 200 (based on average axial velocity and channel height), keeping the angle of attack of the vortex generators fixed at 45º for all configurations. The solution procedure was done using a modified version of Marker and Cell algorithm. Compared to delta winglet pair, rectangular winglet pair produced more heat transfer enhancement and the difference increased with increase the Reynolds number. The common-flow-down configurations provided better heat transfer enhancement as compared to common-flow-up configurations. For all combinations, the RWP developed slightly higher pressure than delta winglet pair.

Salviano et al (2014) numerically optimized the thermal-hydraulic performance of the vortex generators positions and angles of attack on fin-tube compact heat exchangers. The aspect ratio was set constant and equal 2.0. Numerical analyses based on finite-volume methodology were performed to analyze the heat transfer and pressure drop of fin-tube heat exchanger with two round-tubes in staggered arrangement. Turbulent flow simulations (SST k-ω method) were performed at Reynolds number 1400, which was based on fin pitch. The results indicated that the position and angles of the VGs close to tube 1 and tube 2 were not necessarily symmetrical.

Lin et al (2015) numerically studied the flow and heat transfer enhancement of circular tube bank fin heat exchanger with curved delta-winglet vortex generators. The flow was considered laminar and steady. The authors concluded that the curved delta-winglets guide the flow to reduce the area of wake region and generate secondary flow to enhance the heat transfer. The average Nussel numbers increased by 16.1% to 28.7% while the friction factor increased by 7.6% to 15.2% for Reynolds number ranging from 1100 to 3000.
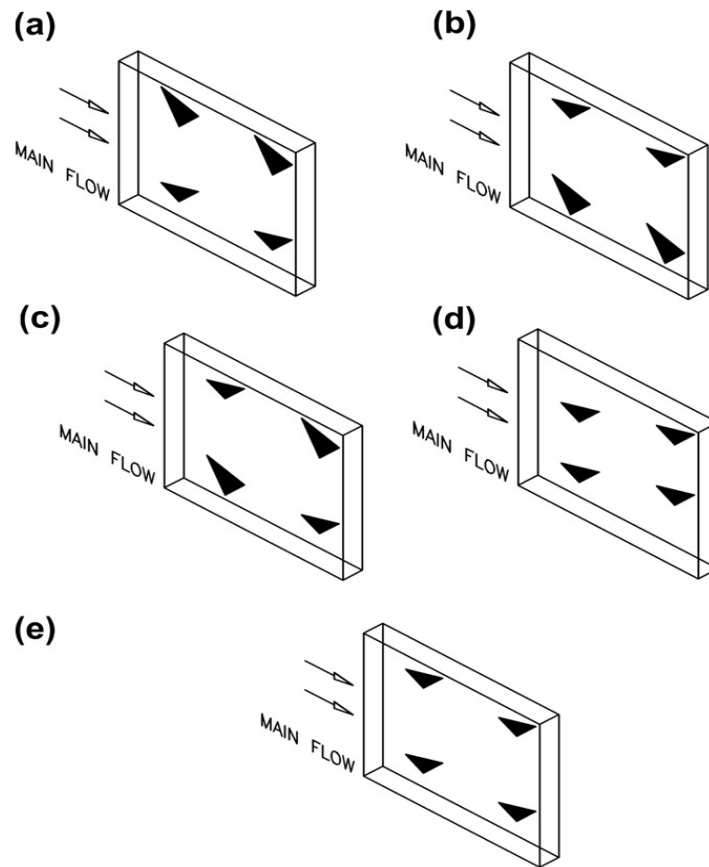
Figure 2-16 Different winglet array configurations: (a) Common-flow-up in series, (b) Common-flow-down in series, (c) Combined, (d) Staggered rows of winglet and (e) Inline rows of winglet (Sinha et al., 2013).

2.5 Literature review focused on multilouvered fins combined with delta winglet vortex generators

The first attempt to the combine louver fins and delta winglets vortex generators was described in a patent by Diemer-Lopes and Yanagihara (1999) in which both enhancement techniques were applied to fin-tube heat exchangers for air-conditioning application. Several experimental studies connected to this work showed that the introduction of delta-winglet vortex generators produced an enhancement of heat transfer of more than 13% above the louvered fin only results.

Sanders and Thole (2006) studied the effects of winglets to augment tube wall heat transfer in louvered fin heat exchangers. The experiments were completed on a 20 times scaled model an idealized louvered fin exchanger with a fin pitch to louver pitch ratio of 0.76 and a louver angle of 27º. A number of geometrical winglet parameters, including angle of attack, aspect ratio, direction and shape were evaluated based on heat transfer augmentation. The Reynolds numbers, based on louver pitch, ranged from 230 to 1016. Figure 2-17 shows a schematic of such winglet placed on a louver as well as definitions of delta winglet geometry. The experiments were perfomed by placing the winglets on symmetric conditions on both tube wall sides for each louver. Values of aspect ratio used on their study were 1.5, 2.0 and 3.0, where the value of 1.5 was the largest winglet. The winglet angle of attack was chosen as 20º, 30º and 40º. The thickness of the winglet was maintained constant and equals 3% of the louver thickness. The winglets were affixed to the louver surfaces and the heat transfer benefits to the tube wall were measured. Therefore, the parameter distance from the wall (Z) was defined as the distance from the tube wall to the nearest part of the winglet. Values of Z tested were $0.15L_P$, $0.22L_P$ and $0.29L_P$. Two orientations of the winglets were tested: Forward Vortex Generator (VG-F) and Backward Vortex Generator (VG-B) – Figure 2-18. Several experiments were conducted for both VG-B winglets and rectangular winglets. Regarding Reynolds number, at $Re = 230$ none of the winglet setups produced augmentations greater than 4%. Augmentations at Reynolds numbers of 615 and 1016 were much higher than those at 230. Friction factor augmentation also increased with Reynolds number. In general, the heat transfer augmentation increased with increasing of angle of attack, increasing of winglet size, and with decreasing winglet distance from the wall. The best heat transfer augmentation was found with rectangular winglets giving 38%, 36% and 3% at Reynolds numbers of 1016, 615 and 230, respectively. In the configuration where all of the winglets were aimed towards the wall in the VG-F configuration, the average heat transfer augmentations were typically very low. When the winglet direction and orientation were alternated on every other louver, results were significantly improved with maximum augmentation of 25%. For winglets placed in the VG-B orientation with alternating direction, results improved yielding augmentations of up to 33%.
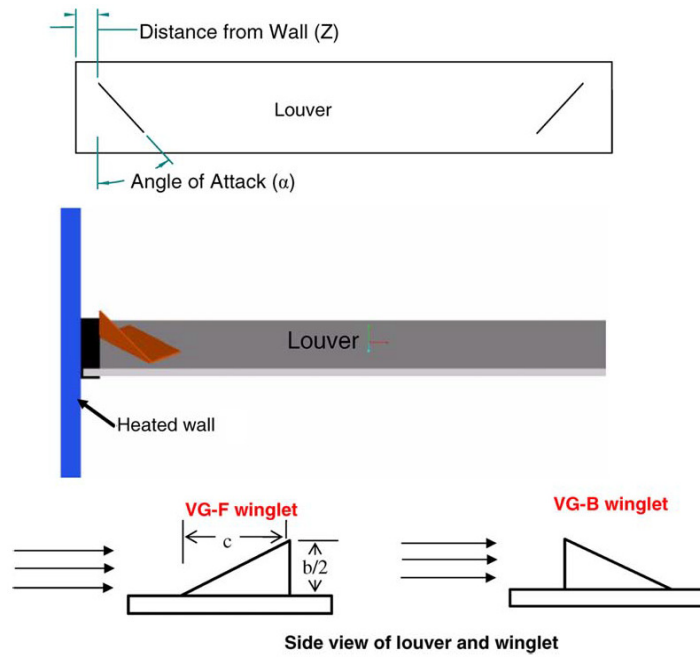
Figure 2-17 Geometric parameters of the winglets (Sanders and Thole, 2006).
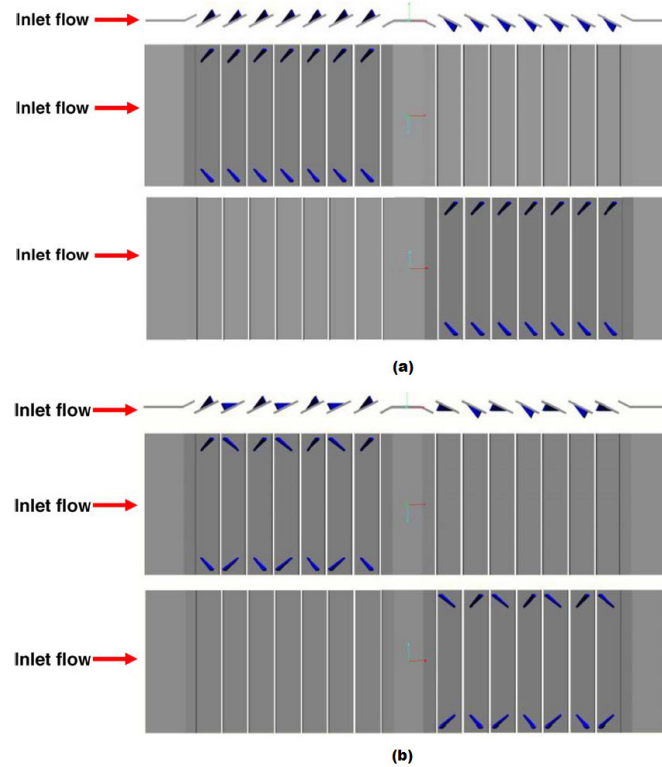
Figure 2-18 (a) VG-F winglets all aimed towards the wall; (b) VG-F/B alternating winglets (Sanders and Thole, 2006).

Numerical and experimental investigations of heat transfer augmentation along the tube wall of a multilouvered fin using delta winglet were made by Lawson and Thole (2008). The Reynolds numbers ranged from 216 to 955, which was based on louver pitch. All louvers had a louver angle of 27º, a louver pitch of 27.9 mm, a fin pitch of $0.76L_P$, a louver thickness of $0.079L_P$, a fin depth of $20L_P$, and a fin height of $5.3L_P$. Winglet aspect ratios were varied between 1.5 and 3.0. For all tests, the winglet height was maintained at $0.35F_P$. Moreover, distances from the tube wall of $0.15L_P$, $0.22L_P$ and $0.29L_P$ were tested. Two different winglet thicknesses were tested that included thin winglets having a thickness of 3% of the louver thickness, as well as thick winglets having the same louver thickness. The computational predictions were made using the three-dimensional, steady flow solver Fluent. The flow was considered to be laminar and periodic in the pitchwise direction. The louvered fins were placed in a two different orientations by those assembling the core. Figure 2-19 ilustrates the difference between both (mirrored and non-mirrored winglet configurations). The analyses also took into account the influence of the percings. For the most tests with no piercings, the winglets had attack angle of 40º; on the other hand, to allow for piercings fitting onto the flat landing, tests incorporating piercings had attack angle of 30º. Piercings in the louvered fins (Figure 2-20) decreased the benefits of winglets on augmenting heat transfer. Piercings disrupted the vortex formation by allowing flow pass through the piercings and follow the louver-directed flow path. While piercings were shown to negatively affect heat transfer performance along the tube wall relative to winglets placed on solid louvered fins, they have the desirable effect of lowering pressure losses. Another effect of incorporating winglets and piercings into louvered fin designs in a decrease in the area available for heat conduction from the tube wall through the louvered fins. This area reduction could possibly cause a decrease in louver heat transfer. It was shown that delta winglets placed on louvered fins produce augmentations in heat transfer along the tube wall as high as 47% with a corresponding increase of 19% in pressure losses.
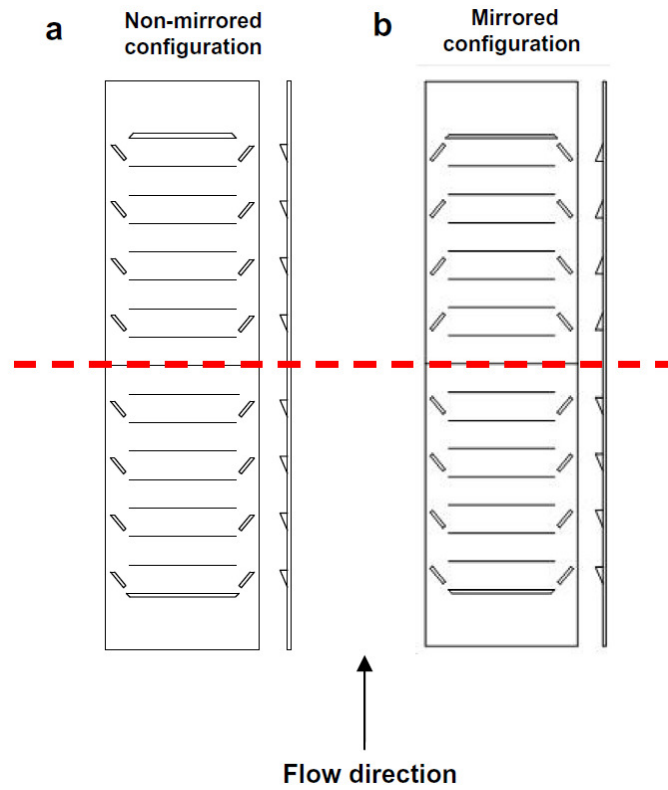
Figure 2-19 (a) Non-mirrored and (b) mirrored winglet configurations (Lawson and Thole, 2008).
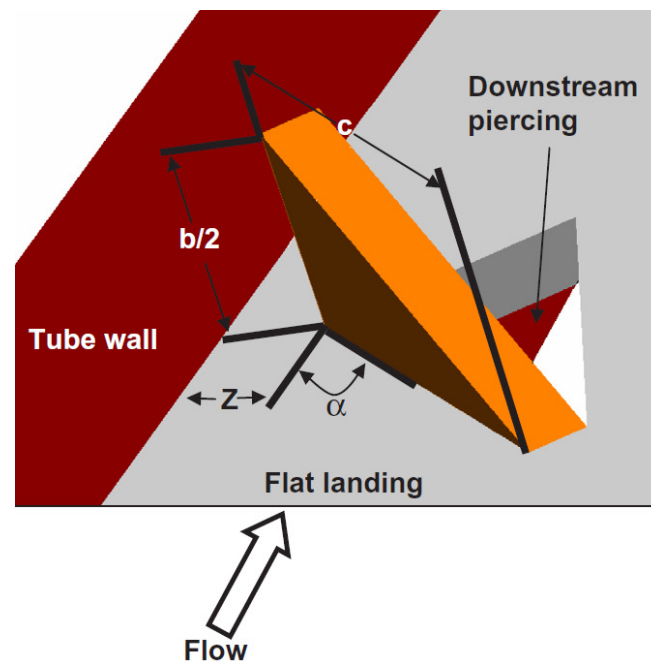
Figure 2-20 Sketch of a delta winglet located on the flat landing (Lawson and Thole, 2008).

Huisseune et al. (2013A) numerically investigated the performance of a compound heat exchanger by screening its design parameters. Three tube rows in a staggered arrangement were considered. Delta winglet vortex generators were punched out of the fin surface in a common-flow-down arrangement behind each tube. The mass, *momentum* and energy balance equations were solved using Fluent 12.0.16 for steady state condition. The flow was assumed laminar and the Reynolds numbers ranging from 100 to 1400, which was based on the hydraulic diameter and the minimum cross sectional flow area. Periodic conditions were applied on both sides of the domain as well as on the top and bottom. The height of the computational domain was equal to the fin pitch and the width was equal to transversal tube pitch. SIMPLE algorithm was applied for the pressure-velocity coupling. The discretization of the convective terms in the governing equations was done via a second order upwind scheme, while a second order central difference was applied for the diffusive terms. Figure 2-21 shows the three-dimensional computational domain. According to authors, comparing the numerical results to the measurements showed that there was an acceptable match between the simulations and experiments. It can be seen that for low Reynolds numbers, the numerical results agreed well with experimental data; however, for Reynolds greater than 1000, discrepancies between the experimental data and numerical results was observed.
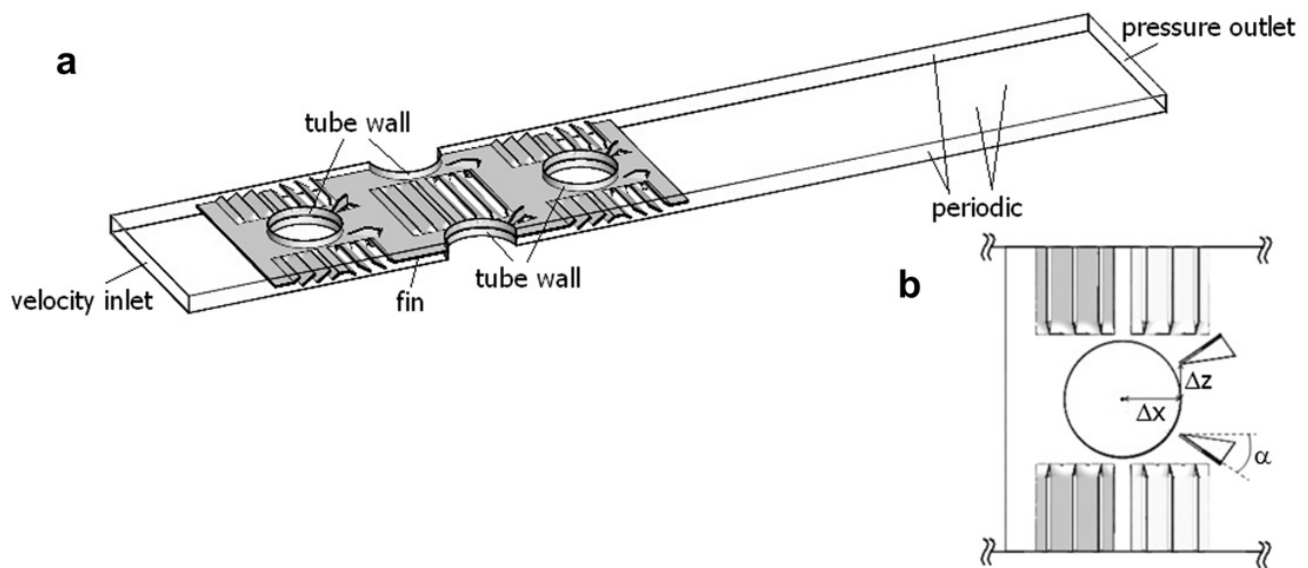
Figure 2-21 Computational domain and (b) top view the delta winglet position (Huisseune et al., 2013A)

The effect of punching delta winglet vortex generators into the louvered fin surface in the near wake region of each tube was numerically investigated by Huisseune et al. (2013B) by using CFD. The geometric information is the same that presented in Huisseune et al. (2013A). The Reynolds numbers ranged from 140 to 1220 (based on hydraulic diameter and minimum cross sectional flow area), which corresponded to inlet velocities of 0.63-5.25 m/s. The height of the punched delta winglets was equal to 90% of the fin spacing. The aspect ratio was 2.0 in the first and second row. In the third row, the aspect ratio was only 1.5 due to space restrictions. The louver angle was fixed at 35º. The commercial code Fluent 12.0.16 was used for the simulations. The boundary conditions were according to Huisseune et al. (2013A). The flow was considered 3-D and laminar. Only for the smallest Reynolds numbers, less than 200, steady simulations were found to converge. For higher Reynolds numbers, unsteady simulations were performed. Numerical results for Colburn factor agreed very well with experimental data, but the values for friction factor presented some discrepancies for Reynolds numbers greater than about 1000. For Colburn factor (Figure 2-22), the maximum increase was 16% compared to geometry without delta winglet. This enhancement of thermal performance was caused by the generated longitudinal vortices, which cause a better thermal mixing and modify the boundary layers downstream of the tubes. Also, it was observed that the delta winglets caused a penalty friction factor (about 35% at the largest Reynolds number) – Figure 2-23.

Huisseune et al. (2013C) numerically studied the influence of the louver and delta winglet geometry on the thermal-hydraulic performance of compound heat exchanger. The computational domain, boundary conditions numerical validation procedure were the same of Huisseune et al. (2013B). The investigated parameters were: delta winglet aspect ratio, variation of the delta winglet position, variation of the fin pitch, variation of the louver angle, variation of the delta winglet angle of attack and variation of the delta winglet height ratio. Two aspect ratios were considered for the analysis (1.5 and 2.0). The smallest aspect ratio resulted in highest Colburn factor and too large the aspect resulted in vortices too far from the tube wake. Consequently, their enhancement effect on the wake zone was smaller. The delta winglets were placed according to dimensionless position based on outer tube diameter, D_0. The results indicated that when the vortex generator are completely

located in the wake zone ($\Delta Z = \pm 0.3 D_0$), no longitudinal vortices are generated and thus the device do not cause any heat transfer enhancement. When the spanwise position is changed out of the wake ($\Delta Z = \pm 0.4 D_0$), the generated vortices reduce the wake zones and thus the local heat transfer is increased. To understand the influence of the fin pitch on thermal-hydraulic performance, three different fin pitches were used (1.20, 1.71 and 1.99 mm). On average, the boundary layers were thinner for small fin pitches and thus the overall Colburn factor were higher. From a thermal point of view, a smaller fin pitch was preferred as this results in a more louver directed flow; in turn, too small fin pitches is not good for delta winglet enhancement. The effect of louver angle on Colburn factor and friction factor was performed with three different louver angles: 22º, 28º and 35º. The highest Colburn factor was obtained for the largest louver angle. Also for small louver angles, the generated longitudinal vortices were stronger than for large louver angles.

Ameel et al. (2014) numerically studied the interaction effects between input parameters in round-tube multilouvered fin compact heat exchangers with delta-winglets. The Reynolds number ranged from 235 and 300, based on hydraulic diameter. Steady and laminar model was used during the simulations. Second-order upwind discretization scheme was used for the convective terms, whereas a central discretization scheme was used for the diffusion terms. Half of a periodic unit cell of the heat exchanger is analysed. Simmetric boundary conditions were used for the transversal boundaried of the domain and for top and bottom of the domain, periodic boundary conditions were applied.
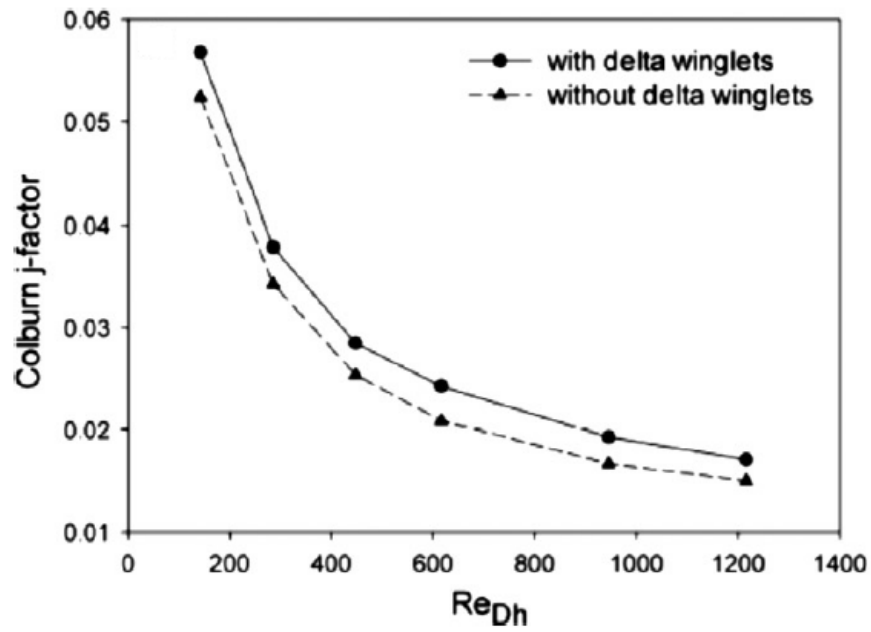
Figure 2-22 Comparison of Colburn factor in function of Reynolds numbers (Huisseune et al., 2013B).
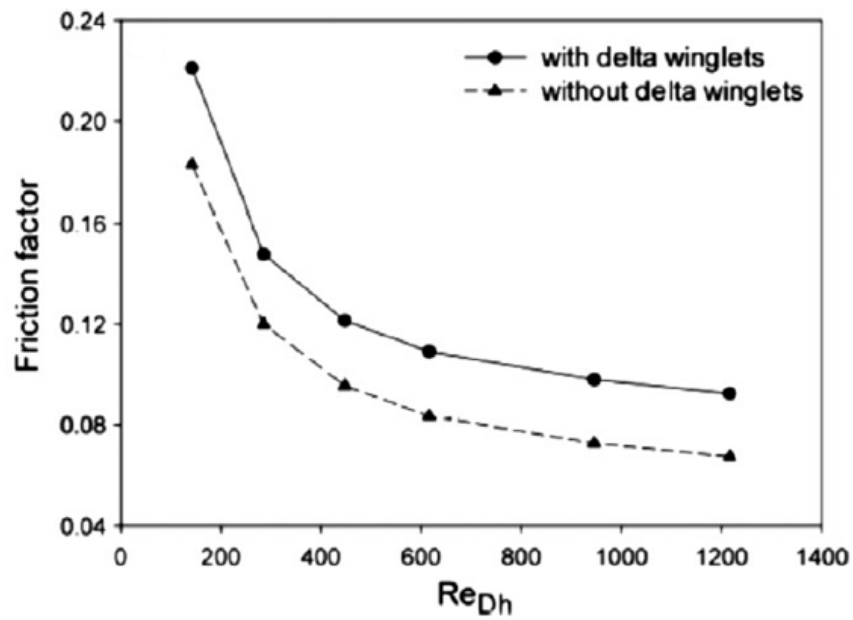
Figure 2-23 Comparison of friction factor in function of Reynolds numbers (Huisseune et al., 2013B).

2.6 Literature review focused *on* screening analysis, surrogate models and optimization applied to compact heat exchangers

Peng and Ling (2009) presented an application of artificial neural networks (ANNs), based on back propagation, to predict the pressure drop and heat transfer characteristics in the plate-fin heat exchangers (PFHEs). First, the thermal performances of five different PFHEs were evaluated experimentally. Different network configurations were also examined for searching a better network for prediction. In order to decide the configuration of neural network, the error convergence was checked by changing the number of hidden layers and also by adjusting the learning rate and momentum rate. Results indicated that the ANNs model can be trained to provide satisfactory estimations of both j and f factors in PFHEs. The Mean Square Error was 1.19% for *j* and 0.64% for *f*, respectively. Finally, they recommended that the ANNs prediction model has a high accuracy and reliability for simulating thermal systems.

Mishra et al. (2009) proposed a genetic algorithm (GA) based optimization technique for crossflow plate-fin heat exchangers using offset-strip fins. The objective was to find out the heat exchanger dimensions giving the required heat duty for minimum entropy generation. The following parametric valued were selected for GA: population size 40, crossover probability 0.4, mutation probability 0.01, and penalty parameter 500.

Husain and Kim (2010) selected two objective functions, thermal resistance and pumping power, to assess the performance of the microchannel heat sink. The design variables related to the width of the microchannel at the top and bottom, depth of the microchannel, and width of fin, which contribute to objective functions, were identified and a three-level full factorial design was selected to exploit the design space. The numerical solutions obtained at these design points were utilized to construct surrogate models (Kriging and Radial Basis Neural Network). A hybrid multi-objective evolutionary algorithm coupled with surrogate models was applied to find out global Pareto-optimal solutions. The design optimization of a microchannel heat sink was performed numerically to enhance the heat transfer performance by

coupling surrogate approximation with the hybrid MOEA. Based on the surrogated models, an analysis of variance (ANOVA) and a regression analysis, replete with *t*-statistics, were implemented to measure the uncertainty in the set of coefficients in the polynomial. The authors suggested, based on Giunta's work (Giunta, 1997), that the values of R^2_{adj} must vary between 0.9 and 1.0 for an accurate prediction of the surrogate model. A real-coded NSGA-II (Non-dominated Sorting Genetic Algorithm) was invoked to obtain weel-spread, approximate Pareto-optimal solutions with number of generations 250 and number of populations 100. The crossover and mutations probabilities were set to 0.95 and 0.25, respectively. The crossover and mutation parameters were decided as 20 and 200, respectively. Kriging was found to be more accurate for predicting Pareto-optimal solutions and the design space explored through the three-level full factorial design. Kriging also showed high fidelity at on-and-off Pareto-regimes in the design space.

Husseine et al. (2013B) numerically investigated the contribution of five important design parameters to the thermal-hydraulic performance of the compound heat exchanger. To reduce the required number of simulations, Taguchi method based on orthogonal parametric arrays was used (orthogonal arrays only identify the main effects and not the interactions between the geometrical parameters). Three levels of each control parameter (fin pitch, louver angle, delta winglet angle of attack, delta winglet height ratio and delta winglet aspect ratio) were investigated. At high inlet velocities the performance was mainly determined by the louvers: the louver angle and the fin pitch were the main parameters for optimization. At lower inlet velocities also the delta winglet geometry had a significant contribution to the performance and should thus be considered for design and optimization purposes.

Tan et al. (2009) reported the use of artificial neural network (ANN) models to simulate the thermal performance of a compact fin-tube heat exchanger. A Multi-Layer Feed-Forward ANN was used in their study. Also, a single hidden layer was found to be appropriate and the number of neurons in this layer was varied to optimize the performance of the neural network. For an un-biased assessment of the network performance, 359 sets of experimental measurements were randomly sampled into four equal-sized subsets of data. The first two subsets (training data) were used to train the network while the third subset of data (test data) was used to

monitor the likelihood of over-fitting the model during training. The resultant network was then independently validated using the remaining fourth subset of data (validation data). The authors presented the performance of the ANN model when all the data were used in the selection of the training, test and validation data. There was very good agreement between the predicted and measured overall heat transfer rates. In summary, the Mean Absolute Error of the ANN's predictions was 0.6%, 0.9% and 0.9%, respectively, for the training, test and validation data sets. Moreover, the authors comments that the application of artificial neural networks appears to have potential for monitoring the condition of an exchanger even for situations in which there are substantial variations in the composition, temperatures and flow rates of the individual fluid streams.

Xie et al. (2009) used an artificial neural network (ANN) to correlate experimentally determined and numerically computed Nusselt numbers and friction factors of three kinds of fin-and-tube heat exchangers having plain fins, slit fins and fins with longitudinal delta-winglet vortex generators with large tube diameter and large number of tube rows. The artificial neural network configuration had twelve inputs of geometrical parameters and two outputs (heat transfer Nusselt number and fluid flow friction factor). The commonly-implemented feed-forward back propagation algorithm was used to train the neural network and modify weights. Different networks with various numbers of hidden neurons and layers were assessed to find the best architecture for predicting heat transfer and flow friction. Also, the popular sigmoid function was adopted in hidden layers and output layer. The authors normalized, from 0.15 to 0.85, all the input–output data with the largest and smallest values of each of the data sets, since the variables of input–output data had different physical units and range sizes. The performance of the neural network was evaluated by calculating the RMSE values of the output error. Also, the ANN presented superior prediction of heat transfer and low friction compared to power-law or multiple correlations.

Sanaye and Dehghandokht (2011) proposed a modeling and multi-objective optimization of parallel flow condenser. The condenser heat transfer rate was maximized while its pressure drop was minimized applying genetic algorithm multi-objective optimization technique. Genetic algorithm optimization technique was applied to provide a set of Pareto multiple optimum solutions. Three design

parameters or decision variables for the optimization process were hydraulic diameter of multi-pass channels, the length of flat tube and the height of louvered fin. Uniform crossover and random uniform mutation were employed to obtain the offspring population.

Hsieh and Jang (2012) numerically performed parametric study and optimization of louver finned-tube heat exchangers by using Taguchi method. Eighteen kinds of models were made by compounding levels on each factor, and the heat transfer and flow characteristics of each model were analyzed. Through the calculation, the contribution ratio of every factor was evaluated as follows: 1.88% for number of longitudinal tube rows, 20.95% for fin pitch, 11.29% for fin collar outside diameter, 40.85% for transverse tube pitch, 4.13% for longitudinal tube pitch, 2.57% for louver angle, 9.20% for fin thickness, and 9.13% for louver pitch. The optimization process was done by using the SN (signal-to-noise) ratio, which was invented by Taguchi. According to authors, the SN ratio can help engineers to find out which levels of control factors are more efficient.

Jang and Tsai (2011) suggested a method for finding the optimal louver angle of a fin heat exchanger by use of a simplified conjugate-gradient method (SCGM) and a three-dimensional computational fluid dynamics model. The search for optimum louver angles ranged from 15º to 45º for Reynolds numbers ranging from 100 to 500 (based on fin spacing). The area reduction of using louver surface relative to the plain surface was the objective function to be maximized. Both the Colburn factor (j) and friction factor (f) increased firstly with the increase of louver angle for $\theta < 30°$. However, the variation of Colburn factor with greater louver angles was small, but the friction factor always increased for $\theta > 30°$. In the optimization searching process with the conditions of Reynolds number 300 and louver pitch of 1.0 mm, the range of louver angle for the optimum area reduction ratios were between 21.5º and 22.9°. When louver pitch was 0.7 mm, the louver angles for optimum area reduction ratios were 35.26º, 30.79º, 28.54º, 26.09º and 24.36° for Reynolds numbers from 100 to 500. When louver pitch was 1 mm, the louver angles for optimum area reduction ratios were 27.46º, 24.28º, 21.56º, 20.47º and 18.69°. Lastly, when louver pitch was 1.3 mm, the louver angles for optimum area reduction ratios were 22.37º, 18.80º, 18.28º, 16.37º and 16.05°, respectively.

Lemouedda et al. (2010) optimized the angle of attack of delta winglet vortex generators in a plate-fin-and-tube heat exchanger, in which the angle of attack mounted behind each tube was varied between -90º and +90º, by using CFD tool. The aspect ratio was fixed at 2.0. The authors used multi-objective genetic algorithm based on Pareto approach. The objective of that study was the maximization of heat transfer per unit volume with the minimization of the power input. The Reynolds number also was varied from 200 to 1200. On that research, the etilist multi-objective genetic algorithm NSGA-II (Non-dominated Sorting Genetic Algorithm) was used. The Kriging technique was found to be more suitable than ANNs and polynomials of second and fourth order, and thus, it was chosen as the surrogate model. Finally, the authors pointed out the benefit of using the optimization process for other kind of engineering applications with large design spaces. Furthermore, they commented that the combination of the CFD tool, genetic algorithms and surrogate model considerably decreases the number of CFD computations needed.

Fabbri (2000) studied the heat transfer in a channel composed of a smooth and a corrugated wall was studied under laminar flow conditions. A genetic algorithm was used to maximize the heat transfer by optimizing the corrugation profile, for given volume of the corrugated wall and pressure drop in the channel.

Ameel et al. (2012) performed numerical optimization of louvered fin heat exchanger with variable louver angles. A round tube and fin geometry with individually varying louver angles was analyzed, with zero thickness for the louvers. Any interactions between the optimal louver angles and the fin thickness were hence not captured. Response surface model (RSM) was fitted to the data by using an ordinary Kriging response surface model. For the initial sampling of the data, latin hypercube sampling (LHS) was used. An initial 10 designs were sampled according to the LHS sampling plan, and a Kriging RSM was fitted to the data. Two separate Kriging models were used, one for the pressure drop and one for the heat transfer. All data were normalized with the pressure drop and heat transfer of the reference design, which was the uniform louver angle at 15°. The authors found the best design by using Pareto frontier. The main conclusion of that research was that using variable louver angles did not offer a significant advantage over a constant louver angle. The

Colburn factor was increased by only 1.3% for the same friction factor as the usual constant louver angle fin.

Tayal et al. (1999) provided a widely research for optimal design of heat exchangers by using genetic algorithm framework. Also, that work demonstrated the first successful application of genetic algorithms to optimal heat exchangers design with a black-box model. The main conclusions were: (1) The optimal design obtained using combinatorial algorithms such as GAs significantly improves base-case designs; (2) these algorithms also result in considerable computational savings compared to an exhaustive research and; (3) GAs have an advantage over other methods in obtaining multiple solutions of the same quality, thus providing more flexibility to the designer.

Qi et al. (2007) analysed five experimental factors (flow depth, ratio of fin pitch and fin thickness, tube pitch, number of louvers and louver angles) affecting the heat transfer and pressure dropof a heat exchanger with louvered fins using the Taguchi method. Fifteen samples were made by a combination of 3 levels on the orthogonal array. The values of those factors are: flow depth (16, 20 and 24), Fin pitch and thickness ratio (0.33, 0.6 and 0.7), Tube pitch (11.15, 10.15 and 10.15), number of louvers (8, 10 and 12) and louver angles (23, 25 and 27). The louver pitch, louver length and fin height are 1.7, 6.4 and 8.15 mm, respectively. They concluded that among the five factors, flow depth, the ratio of fin pitch and fin thickness and the number of louvers are the main optimum parameters in the design process of the new heat exchangers.

Salviano et al (2014) optimized thermal-hydraulic performance of the vortex generators positions and angles of attack on fin-tube compact heat exchangers by using artificial neural networks combined with Genetic Algorithm. Four independent input parameters were considered for both two round-tubes. Based on the detailed investigations, it was concluded that is possible to find different optimal configurations depending on the PEC (Performance Evaluation Criteria) applied by heat exchanger designers. Finally, the combination of surrogate model and optimization procedure, including CFD methodology, showed to be a powerful tool in researches concerned on heat transfer enhancement using vortex generator.

Salviano et al. (2015) proposed a thermal-hydraulic optimization procedure for DWL angles of attack and positions on thermal-hydraulic performance of plate-fin compact heat exchanger by using surrogate-based optimization and direct optimization. Direct optimization reported better results than surrogate-based optimization for all objective functions. The optimized VG configurations led to heat transfer enhancement higher than those reported in the literature.

Ameel et al. (2014) investigated the interaction effects between parameters in round-tube multilouvered fin compact heat exchanger with DWLs by using a full factorial analysis. The authors concluded that there are important interactions between the height of the DWL, the aspect ratio of the DWL and the louver angle and these interactions were of the same order of magnitude as the main effects of these parameters.

Abdollahi and Shams (2015) optimized shape and angle of attack of winglet vortex generator in a rectangular channel for heat transfer enhancement. A combination of CFD, artificial neural networks and non-sorting genetic algorithm were applied in the optimization process. For low Reynolds numbers, the winglet angle of attack did not cause the significant changes in the Nusselt number. But at higher Reynolds number, this parameter was very important. Also, the results show that the pressure drop in the VG location increases with an increase in the angle of attack due to increasing the form drag.

Arora et al. (2015) optimized the location of common-flow-up delta winglets for inline alignment finned tube heat exchanger. The numerical results showed that the optimally located of delta-winglets improved the average thermal performance of both the fins and the tubes at the same Reynolds number (ranged from 1415 to 7075).

Jang and Chen (2015) combined a finite differential method code as an optimizer to determine the optimal louver angle of louvered-fin heat exchanger with variable louver angles. The authors showed that the maximum area reduction ratios reached 48.5% - 55.2% for an optimal design at inlet velocities from 1.0 to 9.0 m/s, corresponding to Reynolds numbers from 133-1199.

2.7 Important remarks from literature review

Researches involving multilouvered fins show that the heat transfer and pressure drop is strongly related to flow behavior. Louver-directed flows present much higher heat transfer enhancement and pressure drop than duct-directed flows. The most important parameters to become the flow louver-directed are louver angle, louver pitch and Reynolds number. Normally, the louver-directed flow is observed for small fin pitches, and higher Reynolds numbers and louver angles. For Reynolds numbers about 1000, wake instabilities develop on the leading edge of the exit louvers and the flow in the downstream half of the array becomes unsteady. For Reynolds about 1300, vortex shedding can be seen on the louvers downstream of the turnaround louver. However, the vortex shedding in the louvered fin array provides small heat transfer enhancement. Since the vortex shedding is not present in very low Reynolds numbers, the numerical researches with laminar and steady-state assumptions have presented good agreement with experimental data in terms of heat transfer and pressure drop.

The longitudinal vortex generators increase the heat transfer with small pressure losses when compared to other types of passive heat transfer enhancement techniques, especially the delta winglets. The strength of the longitudinal vortices depends on the DWL angles of attack, frontal area and the Reynolds number. DWL with aspect ratio of 2.0 is the most commom on the researches related to LVGs because it normally presents good results of thermal-hydraulic performance. It is well agreed that longitudinal vortices are predominant for angles of attack less than 65º, while the transverse vortices are the dominant vortex system for angles of attack higher than 70º. Moreover, the heat transfer enhancement due to longitudinal vortices is much higher than the transverse ones. Some researches for LVGs have shown that longitudinal vortices enhance heat transfer in steady flow and several numerical researches with LVGs under steady-state condition have presented good agreement with experimental data for low Reynolds numbers.

Multilouvered fin compact heat exchangers with LVGs have presented greater heat transfer enhancement and seem to be a promising compound enhancement

technique. For those types of compact heat exchangers at low Reynolds numbers, the flow can be considered laminar and steady. The unique analysis of the effects of louver and DWL parameters on heat transfer are presented for round-tube multilouvered fin with DWLs. Moreover, it was not observed any studies of heat transfer optimization procedure for flat-tube multilouvered fin heat exchangers with DWLs. Furthermore, no investigations of main and interaction effects of both louver and DWL parameters on thermal-hydraulic performance were found in the open literature.

3 Statistical analysis – design of experiments, screening analysis and surrogate-based optimization

For any design and modeling purpose, the ultimate aim is to gain sufficient insight into the system of interest so as to provide more accurate predictions and better designs. Therefore, computational optimization, modeling and simulation forms an integrated part of the modern design practice in engineering and industry. As resources are limited, cost and energy comsumption minimizations, and the performance, profits and efficiency maximizations can be crucially important in all design effort.

Despite the significant progress made in the last few decades, many challenging issues still remain unresolved. Challenges may be related to various aspects and depend on many intertwined factors. In the current context, such challenges are related to nonlinearity, scale of the problem, time constraint and the complexity of the system. Solutions have to be obtained within a reasonably time, ideally instantaneously in many applications, which poses additional challenges.

3.1 Design an experiment

The confrontation of theories (or model structures) to data collected on the system to be described is essencial to experimental sciences. This is necessary for selecting the model structure which explains the observations best, and for obtaining estimates of the unknown parameters involved in this structure. An experimental design is an organized method to determine the relationship between the different factors affecting the output process (Ramu and Prabhu, 2013). Moreover, experiment design for model discrimination has received considerable attention, and one can refer to the survey papers by Atkinson and Cox (1974) and Fedorov (1987) that clarify the strong connection existing between experiment designs for parameter estimation and for model discrimination.

While experimenters and mathematicians agree on the fact that the quality of the model to be obtained depends heavily on that of the data collected, it must be admitted that they often disagree on the best way for designing an experiment. At the risk of being slightly provocative, one might say that most experimenters think of experiment design as an art owing much to intuition and very little to mathematics, while mathematicians view it as an essencially statistical problem.

Before collecting the data, the experiment must be designed, i. e., it must be decided if, where and how one will act on the system (location of input ports, type of actuators, shape of inputs, etc) and, where, how and when one observe it (location of input ports, type of sensors, sampling schedule, etc)

There are at least two reasons so that the experimeters must take care on their analysis (Fang et al., 2006):

➢ First, a configuration of the input and output ports which seems reasonable intuitively, may nevertheless lead to the impossibility of obtaining a single optimal estimate for the parameters of interest, even for very simple methods. It is therefore necessary to select the input/output port configuration to avoid such defects as far as possible. This can be done using the notions of structural identifiability and structural distinguishability, which allow one to know whether the right model structure and true value of its parameters could be recovered from noise-free data.

➢ Second, one must take into account the fact that measurements are often scarce and far from noise free, so that the quality of the parameter estimates will depend heavily on the input shape and measurement schedule. A quantitative design, based on the optimization of a suitable criterion, is then essential so as to return the maximum information from that data to be collected. Such a criterion depends on prior assumptions on the noise statistics, and, in general, on the value of the parameters to be estimated. It is therefore of the

special importance to take into account a suitable characterization of prior knowledge (or prior uncertainty) on the process under study.

Nowadays, experiments are performed almost everywhere as a tool for studying and optimizing process and systems. A good experimental design should minimize the number of runs needed to acquire as much information as possible. Experimental design, a branch of statistics, has enjoyed a long history of theoretical development as well as applications. The experiments can be basically classified as: (*i*). physical experiments and; (*ii*). computer experiments.

Many physical experiments can be expensive and time consuming because physical processes are often difficult or even impossible to study by conventional experimental methods. As computing power rapidly increasing and accessible, it has become possible to model some of these processes by sophisticated computer code. In the past decades computer experiments or computer-based simulation have become topics in statistics and engineering that have received a lot of attention from both practitioners and the academic community

3.1.1 Design of experiments methodology (DoE) for computing experiments

The underlying model in a computer experiment is deterministic and given, but it is often too complicated to manage and to analyze. One of the goals of computer experiments is to find an approximate model that is much simpler than the true one. The true model is deterministic and given as in a computer experiment, but errors on the inputs are considered and assumed. The simulation of the random process is conducted by incorporating random inputs into the deterministic model (Fang et al., 2006)

Currently, there are different DoE methods which can be classified into two categories: "classic" DoE methods and "modern" DoE methods. The classic DoE methods, such as full-factorial design, central composite design (CCD), Box-Behnken

and D-optimal design (DOD), were developed for the arrangement of laboratory experiments, with the consideration of reducing the effect of random error. In contrast, the modern DoE methods such as Latin Hypercube Sampling (LHS), Orthogonal Array Design (OAD) and Uniform Design (UD) were developed for deterministic computer experiments without the random error as arises in laboratory experiments. An overview of the classic and modern DoE methods was presented by Giunta et al. (2001).

In the present research, Latin Hypercube Sampling (LHS) has been chosen as the DoE method to generate randomly sample from some prior probability distribution on parameter space. Detais about LHS is discussed below.

3.1.2 Latin hypercube sampling (LHS)

Latin hypercube designs have long been used as an alternative to grids of computer experiments. Like a regular grid, a Latin hypercube partitions each parameter range into equally spaced values. Unlike a grid, the number of partitions is equal to the size of ensemble. Latin hypercubes are constructed to avoid the collapsing property of grids: no two LH design points share the same value for any parameters. In the case of two-dimensional design (Latin square), this property is equivalent to each row and each column containing exactly one design point (Figure 3-1). Unlike grids, LH ensemble sizes need not grow exponentially with the dimensionality of the parameter space, permitting a LH design to explore more parameters than a grid using the same ensemble size.

This method is a stratified sampling approach with the restriction that each of input variables has all portions of its distribution represented by input values. A sample of size N_S can be constructed by dividing the range of each input variable into N_S strata of equal marginal probability $1/N_S$ and sampling once from each stratum.
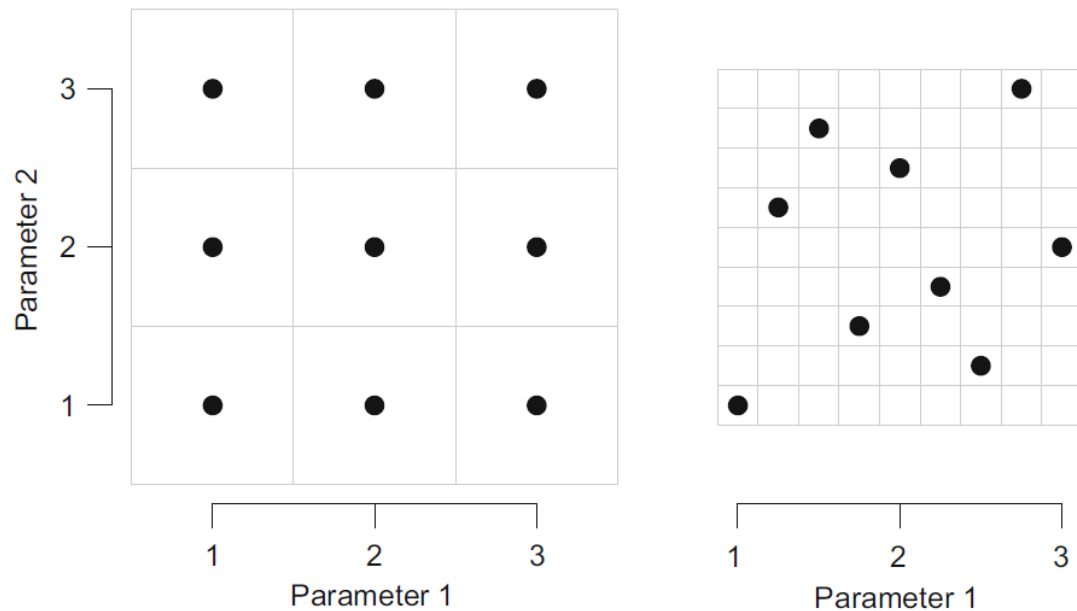
Figure 3-1 Example of regular grid (left) and Latin square (right) designs for two-dimensional with 9 members ensemble (Urban and Fricker, 2010).

While LHS represents an improvement over unrestricted stratified sampling, it can provide sampling plans with very different performance in terms of uniformity measured by, for example, maximum minimum-distance between design points, or by correlation between the sample data. Figure 3-2 illustrates this shortcoming; the LHS plan in Figure 3-2 (c) is significantly better than that in Figure 3-2 (a), for example.

One advantage of Latin hypercube sample appears when the output is dominated by only a few of the input variables. This method ensures that each of those components is represented in a fully stratified manner, no matter which components might turn out to be important. The N intervals on the range of each input component combine to form N^K cells which cover the sample space of input variables. These cells, which are labeled by coordinates corresponding to the intervals, are used when finding the properties of the sampling plan (McKay et al., 2000).

There are many different Latin Hypercube designs for a given parameter space, corresponding to different permutations of design points. A degenerate Latin square design puts all the points on the diagonal, which has obvious difficulty covering the

entire space. Intuitively, a maximum design spreads point as far away from each other as possible, to maximize their coverage of parameter space. This prevents design points from clustering too close together and over-representing some regions of parameter space. ESTECO Modefrontier commercial code uses an algorithm which maximizes the minimum distance between neighboring points. Also, this software uses a stochastic simulated annealing algorithm to generate a large number of candidate LH designs and chooses the one which best satisfies the maximum distance criterion.

(a)   (b)   (c)
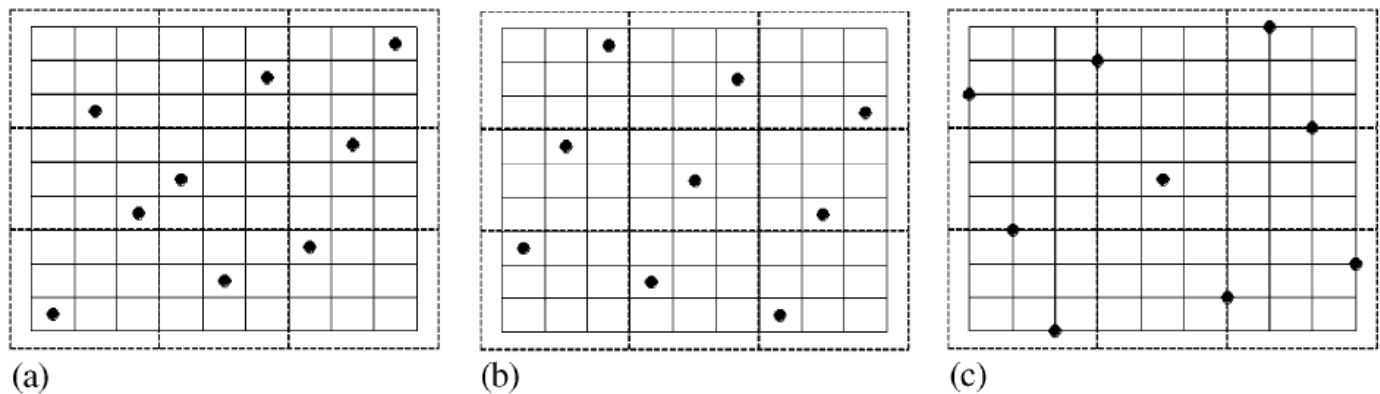
Figure 3-2 LHS designs with significant differences in terms of uniformity (Leary et al., 2003).

3.2 Smoothing spline anova method (SS-ANOVA)

ANOVA is probably the single most used analysis of variance method in many fields of science, ranging from biology to psychology. Historically, a balanced design was preferable since the formulae in this case are much easier and can be handled by hand, even with a large number of observations. By balanced, each cell has exactly the same number of observations. With the use of statistical packages, this is not a concern anymore, and in many fields a balanced design is almost impossible to obtain, either because of (missing at random) drop-outs or by design. It is therefore also useful to provide methods that also work for unbalanced designs (Pajouh and Renaud, 2010).

To test different effects or factors in ANOVA, i.e., main effects and interaction effects, some authors advocate a sequential approach: first allocate the part of the explained variance to the main effects (one after other), then to the two-way interactions (one after other) and then to increasingly higher-order interactions, if present. It is very likely that the assumption that the error terms are distributed according to a Gaussian distribution does not hold in many applied datasets. In this case, the required conditions for a parametric ANOVA test are not satisfied and a test that does not depend on parametric hypothesis is desirable, at least as a check for the parametric test. One famous class of so-called distribution-free tests is permutation or randomization tests. Also, analysis of variance is a method of portioning variability into identifiable sources of variation and the associated degree of freedom in an experiment. More details about ANOVA method can be seen on works from Siegel (2012) and Pajouh and Renaud (2010).

In the present research, the Smoothing Spline ANOVA (SS-ANOVA) has been chosen to run the analysis of variance. The SS-ANOVA models are a family of smoothing methods suitable for both univariate and multivariate regression problems. In this context, the term smoothing means nonparametric function estimation in presence of stochastic data. Following the pioneering work by Wahba (1978) in smoothing splines, Wahba et. al. (1995) decomposed the regression function based on tensor sum decomposition of inner product spaces into orthogonal subspaces, so the components of the estimated function from each subspace are identifiable and can be reviewed independently.

In the most common smoothing spline model, the measure of goodness-of-fit is the sum of square residuals, and the estimation is done by penalized least squares. Those measure and estimation methods are sensitive to outliers, which can lead to serious under-smoothing or over-smoothing. Robust smoothing spline models have been proposed and studied by Huber, Cox, Cantoni and Ronchetti (Liu et al, 2010). In these models, the goodness-of-fit measure is replaced by a robust loss function such as the commonly used Huber's loss function, and the robust spline estimate is defined as the minimizer of that loss plus a penalty to induce smoothing. These models are termed M-type smoothing spline models.

The SS-ANOVA is a statistical modeling algorithm based on function decomposition similar to the classical analysis of variance (ANOVA) decomposition and the associated notions of main and interaction effects. For this reason, it presents an important fringe benefit over standard parametric models: the interpretability of the results. In fact, each term (main effects and interactions) reveals an interesting measure: the percentage of its contribution to the global variance. For this reason, SS-ANOVA represents a suitable screening technique for detecting important variables (called variable screening) in a given dataset.

Indeed SS-ANOVA belongs to the family of nonparametric or semi-parametric models (more precisely it belongs to smoothing methods), which presents some peculiarities that distinguish them from the classical set of standard parametric models (polynomial models, for example). Usually the number of unknown parameters (the dimension of the model space) is much smaller than the sample size. Data are affected by noise but can be considered as unbiased, while parametric models help in reducing noise but are responsible for the (possible) introduction of biases in the analysis. On the other hand, nonparametric or semiparametric methods let the model vary in high dimensional (possible infinite) function space. In this case the so-called soft constraints are introduced, instead of the rigid constraints of parametric models: this leads to more flexible function estimation.

As outlined discussed, a key feature of SS-ANOVA is the interpretability of the results. In fact, after the model has been trained over the given sampling data, different heuristic diagnostics are available for assessing the model quality and the significance of terms in the built-in multiple-term ANOVA decomposition. Indeed statistical modeling has two phases: model fitting and model checking.

Usually in SS-ANOVA decomposition – compliantly with standard ANOVA models-only main effects and interaction effects are taken into account. In fact, higher-order interactions are tipically excluded from the analysis, mainly due to practical reasons: for limiting the model complexity, for improving the model interpreability and for reducing the required computational effort.

The framework for SS-ANOVA is a general multiple nonparametric regression model, with d independent variables $x_1, x_2, \ldots, x_d$ which can be either continuous or discrete, and response variable y_i (Cheng and Speckman, 2012)

$$y_i = f(x_{1i}, x_{2i}, \ldots, x_{di}) + \varepsilon_i, \quad i = 1, 2, \ldots, n \qquad \text{Eq. 3-1}$$

Through the SS-ANOVA decomposition, the unknown mean function is decomposed as a sum of main effects $(f_k(x_k))$ and interaction effects, for example $(f_{i,j}(x_i, x_j))$

$$E(x_1, x_2, \ldots, x_d) = f(x_1, x_2, \ldots, x_d) = \mu + \sum_{k=1}^{d} f_k(x_k) + \sum_{i<j} f_{ij}(x_i, x_j) + \ldots \qquad \text{Eq. 3-2}$$

This provides an extremely flexible class of additive models in which is possible to select a parsimonious model from a large class of semiparametric additive models. The SS-ANOVA model can include linear terms for discrete variables (equivalent to ordinary ANOVA), linear or smooth terms for continuous variables, and interaction terms between continuous and discrete variables. This flexibility makes SS-ANOVA a powerful tool in modeling.

One related practical aspect that should be always taken into account when dealing with multivariate curse (high dimensional) space is the so-called curse of dimensionality. This nasty reality affects all different aspects of multivariate analysis, and unfortunately it is an unavoidable evil. Its typical symptomatology involves the effects of sparsity of the space. This means that when the dimensionality (number of input variables) increases, the volume of the space increases so fast that the available data become sparse: in order to obtain a statistically significant and reliable result, the amount of needed sampling data grows exponentially with the dimensionality.

A major consequence of the curse of dimensionality on SS-ANOVA models is the explosive increase in the number of parameters (degrees of freedom) that would be required by the introduction in the model of higher-order effects in a high-dimensional space. So considering only main effects in building the model – or possibly adding at most only interaction effects – helps in tackling the curse of dimensionality. If N is the number of inputs variables, the number of main effects terms is clearly equal to N, while the number of interaction effects is equal to $N(N-1)/2$, so the growth rate of second order models goes as $O(N^2)$. For this reason, in practical data analysis in a high-dimensional space, usually only the main effects are included. Interaction effects are taken into account only if the relevant computational demand is affordable.

An useful diagnostics tool for assessing the model quality is represented by the collinearity indices, κ_k (Rigoni and Ricco, 2001). Defining the *pxp* cosines matrix C as

$$C_{ij} = \frac{\left(\Gamma_i^*, \Gamma_j^*\right)}{\left\|\Gamma_i^*\right\| \cdot \left\|\Gamma_j^*\right\|}$$ Eq. 3-3

Finally, the diagonal elements of C_{kk}^{-1}, κ_k, is

$$\kappa_k = \sqrt{C_{kk}^{-1}}$$ Eq. 3-4

The ideal situation of all $\kappa_k \approx 1$ holds only in case all the Γ_k^* are nearly orthogonal each other. In case of two or more Γ_k^* are highly (linearly) correlated – a phenomenon refered to as concurvity (or as identifiability problem) – can be detected since the relevant collinearity indices will be much greater than unity. This

unfortunate situation occurs when the chosen model decomposition is inadequately supported on the sampling points domain. There can be many causes to this patology: dependent input variables, bad sampling points, too low sample points, etc.

3.3 Surrogate-based optimization

For optimization problems, surrogate models can be regarded as approximation models for the cost functions and state functions. Surrogate modeling is referred to as a techinique that makes use of the sampled data (observed by running the computer code) to built surrogate models, which are efficient to predict the output of an expensive computer code at untried points in the design space. Thus, how to choose sample points, how to build surrogate models, and how to evaluate the accuracy of surrogate models are key issues for surrogate modelling. Once the surrogate models are built, an optimization algorithm such as Genetic Algorithm (GA) can be used to search the new design (based on the surrogate models) that is most likely to be optimum. Since the prediction with a surrogate model is generally more efficient than that with a numerical analysis code, the computational cost associated with the search based on the surrogate models is generally negligible.

Care must be taken that any assumptions are well founded. The first assumption we make with all the surrogate modelling techniques is that the engineering function is continuous. This is usually a well founded assumption, with some notable exceptions such as when dealing with aerodynamic quantities in the region of shocks, structural dynamics, and progressive failure analysis (e. g. crash simulation) (Forester and Keane, 2009). This can be accommodated by using multiple surrogates, patched together at discontinuities. Also, this is the only assumption in Kriging, making it versatile, but complicated method. Other methods may perform better if further assumptions prove to be valid.

A second assumption is that the function is smooth. Again, this is usually a perfectly valid assumption. Methods such as moving least-squares (MLS), radial basis functions (RBFs), support vector regression (SVR), and a simplified Kriging model

are based on this continuity assumption. Although the function may be smooth, several kind of analysis may not be.

Further assumptions can be made as to the actual shape of the function itself, e. g., by applying a polynomial regression. It is well known that many engineering quantities that obey such forms (within certain bounds). For example, stress/strain is often linear and drag/velocity is quadratic. Clearly, assumptions about shape of the function can be useful, but may be unfounded in many problems (Forester and Keane, 2009).

For an *m*-dimensional problem, suppose we are concerned with the prediction of the output of a high-fidelity, thus expensive computer code, which is correspondent to an unknown function $y : \Re^m \to \Re$. By running the computer code, y is observed at n sites (determined by DoE) (Han and Zhang, 2012)

$$S = \left[x^{(1)}, \ldots\ldots, x^{(n)} \right]^T \in \Re^{n \times m}, x = \left\{ x_1, \ldots\ldots, x_m \right\} \in \Re^m \qquad \text{Eq. 3-5}$$

with the corresponding responses

$$y_S = \left[y^{(1)}, \ldots\ldots, y^{(n)} \right]^T = \left[y\left(x^{(1)}\right), \ldots\ldots, y\left(x^{(n)}\right) \right]^T \in \Re^n \qquad \text{Eq. 3-6}$$

where the pair $\left(S, y_S\right)$ denotes the sampled data sets in the vector space.

With the above description and assumptions, the objective is to build a surrogate model for predicting the output of the computer code for any untried site x (that is, to estimate $y(x)$) based on the sampled data sets $\left(S, y_S\right)$, in an attempt to achieve the desire accuracy with the least possible number of sample points.

There are both parametric (e.g., polynomial regression, Kriging) and non-parametric (e.g., projection-pursuit regression, radial basis functions) alternatives for

constructing surrogate models. The parametric approaches presume the global functional form of the relationship between the response variable and the design variables is known, while the non-parametric ones use different types of simple, local models in different regions of the data to build up an overall model.

In summary, the metamodeling process involves basically four steps: (1) selecting a DoE method or the way to systematically conduct the experiments and generate data; (2) choosing a model to represent the data; (3) fitting the model and; (4) validating the model from the observed data obtained in the first step (PARK and DANG, 2010). In fact, there are several choices for each of these steps and they can be combined together in order to develop many metamodeling techniques. The most frequently used methods include response surface methodology (RSM), inductive learning, artificial neural network, and Kriging models (Park and Dang, 2010).

RSM, the most well-established metamodeling technique, is a popular and easy method for approximation. It is quite suitable and effective in engineering design applications due to its simplicity when the number of design variables is small and the response is not highly nonlinear. RSM are often in form of low order polynomials. Among these common models, the quadratic polynomial response function is the most popular. Radial Basis Function (RBF) is a kind of neural network metamodeling technique that is different from RSM because RBF interpolates data and the approximate response surface goes through all the data points. It is considered that this method is excellent to fit and interpolate the response of a deterministic process of computer simulation codes. Also, when the number of design variables increases and the response is highly nonlinear, the RSM becomes less attractive because the number of design points increases correspondingly. In this case, RBF would be one of the alternative options of metamodeling techniques. Kriging model is becoming popular in recent years, which was originally developed by South African engineer called Krige. Later on, the model was improved by Sacks et al. (1989).

This research is focused on a practical approach including surrogate model which is generated via artificial neural network. This method was choosen based on their maturity and simplicity as well as based on their characteristics in some particular circumstances such as that present in this work.

3.3.1 Artificial neural networks (ANN)

Artificial neural network (ANN) plays an important role in predicting the output of linear and non-linear problems in different fields of researches. The term neural network has evolved to encompass a large class of models and "learning" (i.e., parameter estimation) methods (Hassoun, 1995).

Generally, a neural network means a network of many simple processors (units) operating in parallel. Each processor has a small amount of local memory. The units are connected by communication channels (connections), which usually carry numeric data, encoded by one of various ways. One of the best-known examples of a biological neural network is the human brain. It has the most complex and powerful structure, which, by learining and training, controls human behavior towards responding to any problem encountered in every day life.

A single neuron or perceptron that consists of inputs, weights and output (Figure 3-3) performs a series of linear and non-linear mapping as follows:

$$v = \sum_{i=1}^{s} w_i x_i + w_0 \qquad\qquad \text{Eq. 3-7}$$

and

$$b(v) = \frac{1}{1 + e^{-\lambda v}} \qquad\qquad \text{Eq. 3-8}$$

where x_i are the inputs, w_i are the corresponding weights or parameters of the model, and $b(v)$ is the sigmoid activation function or transfer function usually chosen to have a logistic-type of function. The stepness of the logistic function, λ, is tipically set equal to 1.
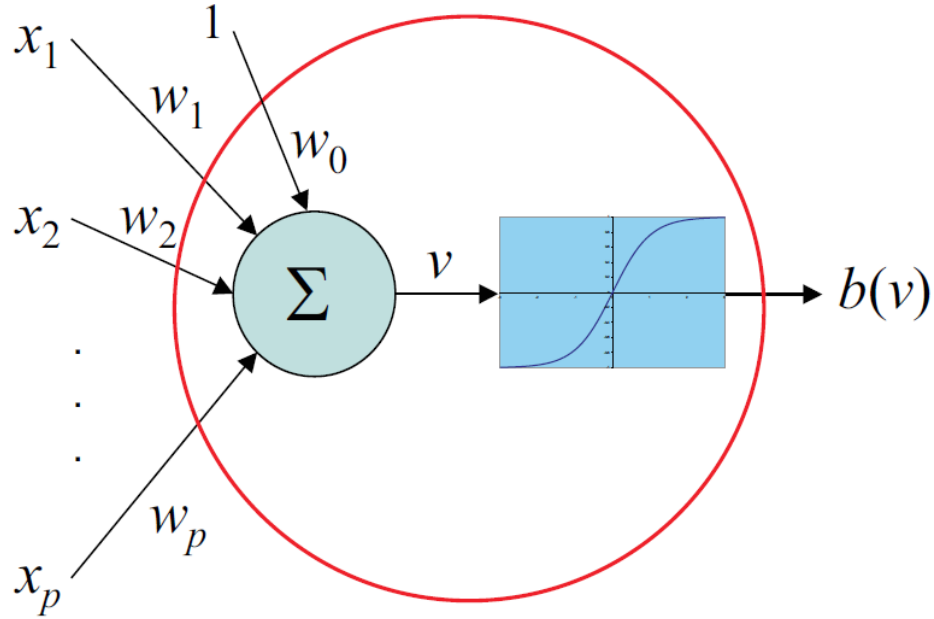
Figure 3-3 Sketch of a neural model with inputs, weights and the activation function output (Fang et al., 2006).

A multilayer-perceptron (MLP), Figure 3-4, that consists of input, hidden and output layers with nonlinear and linear activation functions in the hidden and output layers, respectively, approximates inputs and outputs as follows:

$$\hat{y} = \sum_{j=1}^{d} \beta_j b_j(v_j) + \beta_0$$

Eq. 3-9

where d is a pre-specified integer, β_j, is the weight connection between the output and the *jth* component in the hidden layer, and $b_j(v_j)$ is the output of the *jth* unity in the hidden layer,

$$b_j(v_j) = \frac{1}{1 + e^{-\lambda v_j}}$$

Eq. 3-10

and

$$V = \sum_{i=1}^{s} w_{ji} x_i + w_{j0}$$ Eq. 3-11

in which w_{ji} is the weight connection between *jth* component in the hidden layer and the *ith* component of the input.

Cybenko (1989) showed that a single hidden layer network employing a sigmoid type (as well as other types) activation function is a universal function approximator.

In the Modefrontier software, the multilayer perceptron uses the back propagation (BP) algorithm for training the network in a supervised manner. The (BP) algorithm is a steepest descent method, where weight values are adjusted in an iterative fashion while moving along the error surface to arrive at minimal range of error, when the input patterns are presented to the network for learning the network.
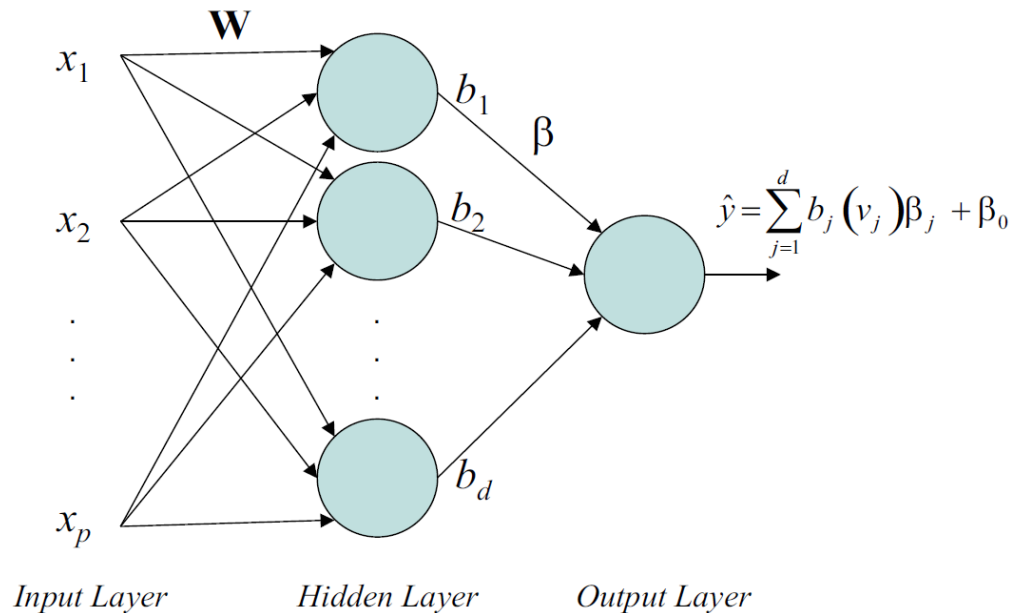
Figure 3-4 Sketch of a three-layer MLP network (Fang et al., 2006).

Modern second-order algorithm as conjugate gradient descent and Levenberg-Marquardt are substantially faster for many problems, but back propagation still has advantages in some circumstances, and it is the easiest algorithm to understand (Krose and Smagt, 2006). The generic approach of the BP is to minimize the errors by using a gradient descent and because of the compositional form of the model, the gradient can be derivated using the chain rule for differentiation (Krose and Smagt, 2006). This can be computed by a forward and backward sweep over the network, keeping track only of quantities to each unit (Friedman et al., 2008)

The learning process consists of two passes through different layers of the network, a forward pass and a backward pass. In the forward pass, the input pattern is applied to the nodes of the input layers and its effect propagates through the network, layer by layer. During the forward pass, synaptic weights are all fixed. The error, which is the difference between the actual output of the network and the desired output, is propagated as backward pass to update the synaptic weights. The weights are continuously updated every time the input patterns are presented to the network and the process continues until the actual output of the network comes closer to the desired output.

The steps for training MLP networks can be summarized as follows:

1. <u>Normalization</u>: Normalize the data set such that $N_i = \dfrac{\left(x_i - \bar{x}_i\right)}{s_i}$, where $\bar{x}_i$ and s_i are the sample mean and standard deviation of x_i, respectively. This normalization helps the training process to ensure that the inputs to the hidden units are comparable to one another and to avoid saturation (i.e., the sum products of the weights and the inputs resulting in values which are too large or too small for a logistic function) of the activation functions;

2. <u>Network architecture</u>: Select a single hidden layer. Select a proper number of units in the hidden layer. Too few or too many units can create under- or overfitting, respectively (over-fitting causes poor capability of prediction untried points). Select the sigmoid activation function.

3. <u>Select the learning rate</u>: Too large a value of learning rate may cause the learning process to fail to converge while too small a learnig rate may cause slow convergence. Many variations of learning algorithms to speed up the convergence rate employ different strategies of learning rate;

4. <u>Initialization</u>: Initialize the weights randomly within the small ranges. Because the network training employs gradient search, the training process may be trapped to a local minima. Therefore, several initial starting values of weights may be tried to get the best result;

5. <u>Training</u>: Train the network with back propagation algorithm until sufficient fitting error is achieved for the training data set. Many practices in neural networks suggest splitting the data sets into training and testing sets. The former is used for network training while the later is used to stop the training when prediction error on the testing data set achieves a minimum. When the size of the data set is small, however, this approach may be unjustified. Other practices include early stopping training. That is, the training iteration process is stopped after small number of iterations before the fitting errors are too small to avoid overfit.

All neural network training algorithms try to minimize the error of the set of the learning samples which are available for training the network. The average error per learning sample is defined as the learning error rate

$$
E_{learning} = \frac{1}{P_{learning}} \sum_{p=1}^{P_{learning}} E^{P}
$$

Eq. 3-12

in which P is the input pattern vector of the input data and E^{P} is the difference between the desired output value and the actual network output for the learning samples

$$E^P = \frac{1}{2} \sum_{o=1}^{N_o} \left(d_o^P - y_o^P \right)^2$$

Eq. 3-13

where this error is measured during the training process and the index *o* is referent to output unit.

The actual error of the network will differ from the error at the locations of the training samples. The difference between the desired output value and the actual network output should be integrated over the entire input domain to give a more realistic error measure. This integral can be estimated if we have a large set of samples: the test set. Thus, the test error rate is defined as the average error of the test set,

$$E_{test} = \frac{1}{P_{test}} \sum_{p=1}^{P_{test}} E^P$$

Eq. 3-14

These error measures depend on learning set size and number of hidden units. Figure 3-5 shows that a large number of hidden units leads to a small error on the training set but not necessarily leads to a small error on the test set. Adding hidden units will always lead to a reduction of the $E_{learning}$. However, adding hidden units will first lead to a reduction of E_{test}, but then lead to an increase of the E_{test}. This effect is called the *peaking effect*.

The model accuracy or the goodness-of-fit of the response surface model is often assessed by four error measures (Park and Dang, 2010):

1. Averages absolute error: averages differences between actual or observed and predicted or approximated values;

2. Maximum error: maximum differences between actual and predicted values;

3. <u>Root mean square error, RMSE</u>: the squrared difference between actual and predicted values

$$RMSE = \sqrt{\frac{\sum_{i=1}^{n}\left(y_i - \hat{y}_i\right)^2}{n}}$$ Eq. 3-15

4. <u>R-squared</u>, R^2: coefficient of determination, between 0 and 1, where $R^2 = 1$ means no error between observed and approximated values

$$R^2 = 1 - \frac{\sum_i \left(y_i - \hat{y}_i\right)^2}{\sum_i \left(y_i - \overline{y}_i\right)^2}$$ Eq. 3-16

where y_i, $\overline{y}_i$ and $\hat{y}_i$ are the observed values, mean of the observed value and approximated values, respectively. Forrester (2009) suggests that the surrogate model can be considered acceptable when $R^2 > 0.8$, maximum error less than 10% and $RMSE < 5\%$.

It is difficult to give a general rule on how to choose the ideal split of the data set. According to Friedman et al. (2008), the data set can be divided in 50% for training and 50% for testing; on the other hand, Kaastra and Boyd (1996) and Kreith et al. (2000) suggest training set ranging from 70% to 90% and testing set ranging from 30% to 10%.
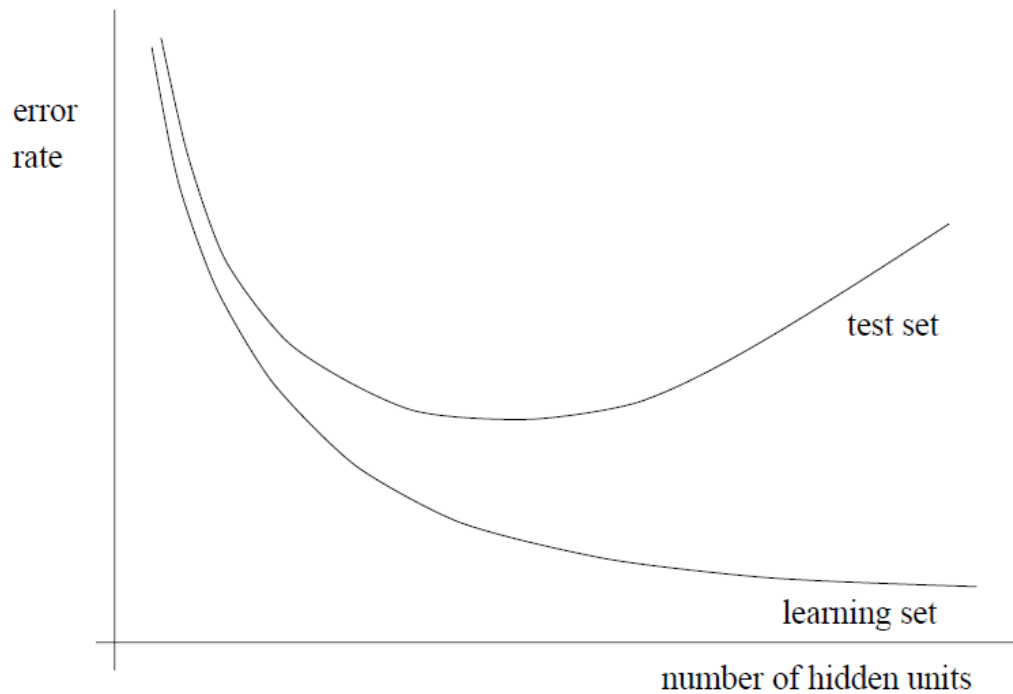
Figure 3-5 The average learning error rate and the average test error rate as a function of the number of hidden layers (Krose and Smagt, 2006).

For proper formulation of optimization problems, the design objectives and behaviors of a system to be reformulated in mathematical terms to define an objective function (or functions) so that the formal relationship between the values of the designable parameters and the system performance can be established. In some cases, this relationship can be represented in a form of a scalar function that can be minimized, while in many other cases, a set of competing objectives can be only formulated, leading to a complex, multi-objective optimization problem.

The recent trends in computational optimization move away from the traditional methods to contemporary nature-inspired metaheuristic algorithms (Yang and Gandomi, 2012), though traditional methods can still be an important part of the solution techniques. However, new studies and research tend to focus on the development of novel techniques that primarily based on swarm intelligence. New algorithms such as particle swarm optimization, cuckoo search and firely algorithm have become hugely popular (Yang et al., 2013).

Nature-inspired algorithms have the advantages of simplicity, flexibility, and ergodicity (Yang and Gandomi, 2012). These algorithms are typically very simple to understand and easy to implement, which requires little efforts for new users to learn. Therefore, researchers with diverse backgrounds can relatively use them in their own research. At the same, nature-inspired are quite flexible; that is, these seemingly simple algorithms can solve highly complex and high nonlinear optimization problems. In addition, nature-inspired metaheuristic algorithms can often find the global optimium solution within a relatively small number of iterations. Genetic Algorithm (GA), which is used in this research, is a type of nature-inspired algorithms.

3.3.2 Genetic algorithms – basic concepts and definitions

The Genetic Algorithms (GA) belong to the class of stochastic search optimization methods. These algorithms made the decisions based on random number generation. The GA use only the function values in the search process to make progress toward a solution without regard to how the functions are evaluated. Continuity or differentiability of the problem functions is neither required nor used in calculations of the algorithms. Therefore, the GA are very general and can be applied to all kinds of problems (discrete, continuous, and non-differentiable).

Genetic Algorithm have loosely parallel biological evolution and are based on Darwin´s theory of natural selection. The specific mechanics of the algorithm uses the language of microbiology, and its implementation mimics genetic operations. The basic idea of the approach is to start with a set of designs, randomly generated using the allowable values for each design variable. Each design is also assigned a fitness value, usually using the cost function for unconstrained problems or the penalty function for constrained problems. From the current set of designs, a subset is selected randomly with a bias allocated to more fit members of the set. Random processes are used to generate new designs using the selected subset of designs.

The size of the design set is kept fixed. Since more fit members of the set are used to create new designs, the successive sets of designs have a higher probability of

having designs with better fitness values. The process is continued until a stopping criterion is met. In the following paragraphs, some details of implementing these basic steps are presented and explained (Friedman et al., 2008):

- ➢ Population: the set of design points at the current iteration is called a population. It represents a group of designs as potential solution points.

- ➢ Generation: an iteration of the genetic algorithm is called a generation. A generation has a population of size that is manipulated in a genetic algorithm.

- ➢ Chromosome: this term is used to represent a design point. Thus, a chromosome represents a design of the system, whether feasible or infeasible. It contains values for all the design variables of the system.

- ➢ Gene: this term is used for a scalar component of the design vector; that is, it represents the value of a particular design variable.

With a method to represent a design point defined, the first population consisting of N_P designs needs to be created. This means that N_P *D*-strings need to be created. In some cases, the designer already knows some good usable designs for the system. These can be used as seed designs to generate the required number of designs for the population using some random process. Otherwise, the initial population can be generated randomly via the use of a random number generator.

The fitness function defines the relative importance of a design. Individuals with higher fitness values have a higher probability of being selected for mating and for subsequent genetic production of offsprings. This operator, which weakly mimics the Darwinian principal of survival of the fittest, is an artificial version of natural selection, where the selection is done stochastically (Mishra et al., 2009).

The fitness function may be defined in several different ways; it can be defined using the fitness function value as follows (Friedman et al., 2008)

$$F_i = (1 + z)f_{max} - f_i$$
                                                                                Eq. 3-17

where f_i is the cost function (penalty function value for a constrained problems) for the *ith* design, f_{max} is the largest recorded cost (penalty) function value, and z is a small value to prevent numerical difficulties when F_i becomes 0.

3.3.2.1 Fundamentals of genetic algorithm

The basic idea of a genetic algorithm is to generate a new set of designs (population) from the current set such that average fitness of the population is improved. The process is continued until a stopping criterion is satisfied or the number of iterations exceeds a specified limit. Three genetic operators are used to accomplish this task: *reproduction, crossover* and *mutation*. Reproduction, which constitutes a selection procedure whereby individual strings are selected for mating based on their fitness values relative to the fitness members.

After reproduction, the crossover operator alters the composition of the offspring by exchanging part of strings from the parents and hence creates new strings. Crossover is also achieved stochastically using suitable crossover probability. The need for mutation is to create point in the vicinity of the current point, thereby achieving a local search around the current solution, which sometimes is not possible by reproduction and crossover. Mutation increases the variability of the population. For a GA using binary alphabet to represent a chromosome, mutation provides variation to the population by changing a bit of the string from 0 to 1 or vice versa with small mutation probability (Mishra et al., 2009).

The main advantages of the Genetic Algorithms were discussed during this chapter. However, it is important comment the drawbacks about them, as follows (Friedman et al., 2008):

➢ They require a large amount of calculation for even reasonably sized problems or for problems where evaluation of functions itself requires massive calculation.

➢ There is no absolute guarantee that a global solution has been obtained.

The first drawback can be overcome to some extent by the use of massively parallel computers. The second one, can be overcome to some extent by execting the algorithm several times and allowing it to run longer.

3.3.2.2 Nondominated sorting genetic algorithm II (NSGA-II)

In NSGA-II, the first parent population and the offspring population created by parents using genetic operators, are combined together to form a new population. Then, the points of the new population are sorted in different non-dominated fronts according to their level of non-dominance. After that, the new parent population is created by points of the fronts. Slots in the new population are filled up starting with the first front, the second one and so on. If the number of points in the last allowed front is more than the remaining slots in the new population, a crowding distance sorting is applied to select the best points of the last allowed front. More details about how NSGA-II works as well as its algorithm can be seen on Deb et al. (2002).

4 Problem formulation

A brief review of the fluid mechanics and heat transfer theory is given in the next sections for fluid flow in steady state condition. The focus is to present the governing equations, hypothesis and models used in the fluid flow and heat transfer simulation. Moreover, a brief review of Computational Fluid Dynamics is presented. Geometrical information, operating ranges of the input variables and the computational domain used on the numerical simulations are shown. The subject related to screening analysis of the input parameters in terms of heat transfer and pressure drop by using Smoothing Spline ANOVA is also commented. Finally, details of the surrogate-based optimization procedure are exposed.

4.1 Governing equations and numerical method

The flow has been assumed fully three-dimensional steady-state and incompressible and laminar. The air is considered Newtonian fluid with constant properties. The mass, *momentum* and energy conservations equations can be written as follows

$$\frac{\partial}{\partial x_j}\left(\rho u_j\right) = 0 \qquad\qquad \text{Eq.4-1}$$

$$\frac{\partial}{\partial x_j}\left(\rho u_j u_i - \tau_{ij}\right) = -\frac{\partial p}{\partial x_i} \qquad\qquad \text{Eq.4-2}$$

where τ_{ij} is the viscous stress tensor defined as

$$\tau_{ij} = 2\mu S_{ij} - \frac{2}{3}\mu \frac{\partial u_k}{\partial x_k}\delta_{ij}$$

$$S_{ij} = \frac{1}{2}\left(\frac{\partial u_i}{\partial x_j} + \frac{\partial u_j}{\partial x_i}\right)$$

$$\frac{\partial}{\partial x_j}\left(\rho u_j h - k\frac{\partial T}{\partial x_j}\right) = -u_j \frac{\partial p}{\partial x_j} + \tau_{ij}\frac{\partial u_i}{\partial x_j} \qquad\qquad \text{Eq.4-3}$$

In this research, the commercial code ANSYS Fluent v.14.5 was used to solve the continuity, *momentum* and energy equations through the Finite Volume Method (FVM). A brief review of FVM will be presented on item 4.1.1.

4.1.1 Finite volume method – a brief review

Finite volume discretization is based on an integral form of the partial differential equations to be solved, with the values of the conserved variables averaged across the volume. The partial differential equations are written in a form that can be solved for a given finite volume (or cell). The computational domain is discretized into finite volumes, and then for every volume the governing equations are solved in an iterative manner (Ferziger and Peric, 2002). An example of structured mesh with control volume and respective cell center can be seen in Figure 4-1.

The generally used commercial code based on FVM, such as ANSYS Fluent, is widely used for simulating engineering fluid flow due to accuracy, robustness and convenience. This software uses cell-centered finite volumes (in cell centered schemes, the flow variables are stored at the centers of the mesh elements). Also, ANSYS Fluent offers several solution approaches (density-based as well as

segregated and coupled pressure-based methods). The algorithm used for the solution of the partial differencial equations is the pressure-based method because of the low Mach numbers in compact heat exchangers flows.
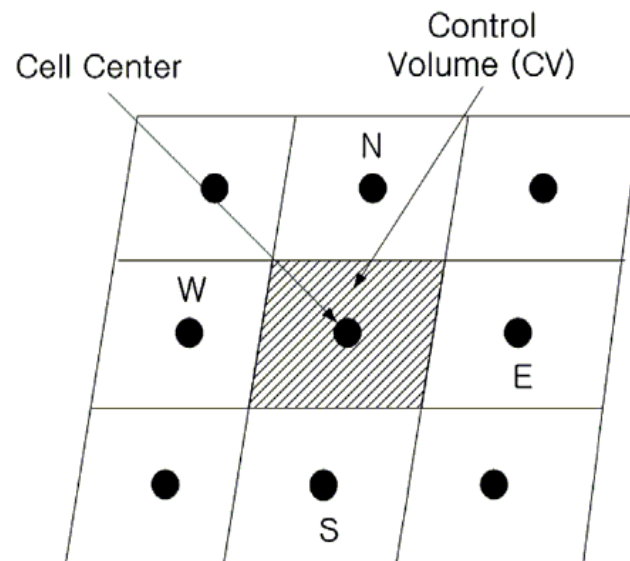
Figure 4-1 Structured mesh for FVM (Jeong and Seong, 2014)

The flow and heat transfer performances of compact heat exchanger surfaces are mainly dictated by boundary layer behavior over the interruptions or in complex flow passages, and flow separation, recirculation, reattachment, and vortices in the wake region. Therefore, careful consideration must be given to the grid used. Adequate grid refinement is needed to capture the boundary layer growth and separation, and this is not always possible with moderate computing resources. Moreover, the mesh density and structure have a significant influence on the accuracy and stability of the solution. Thus, the optimum mesh should be fine enough to reduce the discretization error and resolve flow and heat transfer details, especially in the areas of sharp gradients (Jeong and Seong, 2014).

The grid generation strategy is determined according to the size and location of flow features such as shear layers, separated regions, boundary layers, and mixing zones. For wall-bounded flows, the grid size at the wall can affect the accuracy of the

computed shear stress and heat transfer coefficient. One must address the specific requirements of the wall functions. Because of the strong interaction of the mean flow and turbulence, the numerical results for turbulent flows tend to be more susceptible to grid dependency than those for laminar flows.

The Figure 4-2 shows an example of how to calculate the equation of mass conservation in the volume, for 2D and incompressible flow, and for steady state condition. Based on that, the mass averaged in the volume is calculated as follows

$$\int\limits_{w}^{e}\int\limits_{s}^{n}\left[\frac{\partial}{\partial x}(\rho u) + \frac{\partial}{\partial y}(\rho v)\right]dxdy = 0 \qquad\qquad \text{Eq.4-4}$$

$$\int\limits_{s}^{n}\left[(\rho u)_e - (\rho u)_w\right]dy + \int\limits_{w}^{e}\left[(\rho v)_n - (\rho v)_s\right]dx = 0 \qquad\qquad \text{Eq.4-5}$$

$$(\rho u \Delta y)_e - (\rho u \Delta y)_w - (\rho v \Delta x)_n - (\rho v \Delta x)_n = 0 \qquad\qquad \text{Eq.4-6}$$

The calculation of *momentum* and energy equations is performed similarly to the outlined process.
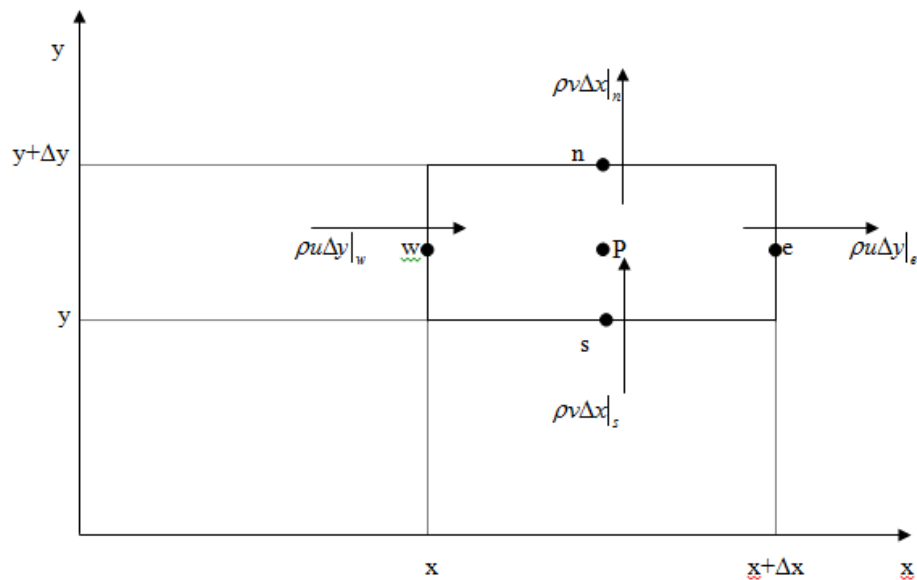
Figure 4-2 2D equation of mass conservation applied to finite volume

The variables are evaluated on the faces of volumes and they can vary according to the spatial discretization. The difference between the spatial discretization methods is how they calculate the value of the variable at point "*P*" based on the volume face's value. The most common spatial discretization methods applied to compact heat exchangers are: pressure (Linear, Second order and Presto), *momentum* (First order upwind, Second order upwind, QUICK and Power law), energy (First order upwind, Second order upwind, QUICK and Power law), turbulent kinect energy (First order upwind, Second order upwind, QUICK and Power law), specific dissipation rate (First order upwind, Second order upwind, QUICK and Power law) and turbulent dissipation rate (First order upwind, Second order upwind, QUICK and Power law).

When second-order upwind is desired, quantities at cell faces are computed using a multidimensional linear reconstruction approach. In this approach, higher order accuracy is achieved at cell faces through a Taylor series expansion of the cell-centered solution about the cell centroid (Fluent User's Guide, 2006).

The SIMPLE was the first pressure-correction algorithm (proposed by Patankar and Spalding (1972)). The acronym SIMPLE stands for semi-implicit method for the pressure-linked equation. It uses a relationship between velocity and pressure corrections to enforce mass conservation and to obtain the pressure field. The major approximations made in this algorithm are:

1) The initial pressure field and the initial velocity fields are independently assumed, hence the inherent interconnection between pressure and velocities is neglected, leading to some inconsistency between them;

2) The effects of the pressure corrections of the neighboring grids are arbitrarily dropped in order to simplify the solution procedure, thus make the algorithm semi-implicit. These assumptions will not affect the final solutions if the iterative process converges. However, they do affect the convergence rate. In summary, if the momentum equation is solved with a guessed pressure field, the resulting computed face flux does not satisfy the continuity equation. Consequently, a correction is added to face flux so that the corrected face flux satisfies the continuity equation.

The SIMPLER algorithm (Patankar, 1981) successfully overcomes the first approximation, and is widely used in the current CFD community. Even though there are more than ten variants of the SIMPLE-like algorithm, the second approximation, i.e., the dropping of the neighboring grid effects, have not been successfully resolved so far. These variants include SIMPLEC and SIMPLEX by Van Doormaal and Raithby (1984) and Van Doormaal and Raithby (1985), PISO by Issa (1985) and the revised versions by Connel and Stow (1986), Chatwani and Turan (1991), Lee and Tzong (1992), Yen and Liu (1993), Wen and Ingham (1993), SIMPLESSEC, SIMPLESSE by Gjesdal and Losius (1997), SIMPLET by Sheng et al. (1998), MSIMPLER by Yu et al. (2001). The character common to all these algorithms is that a pressure correction term is introduced to the segregated solution process.

An idea of improving velocity and pressure was proposed by Tao et al. (2004A) and Tao et al. (2004B): the improved velocity and pressure of each iteration level are not determined by adding a correction term to their temporary solution; instead, they are directly solved from the *momentum* and continuity equations, genuinely avoiding the introduction of pressure correction term and velocity correction term. Thus, the second approximation of the SIMPLE algorithm is totally discarded, making the algorithm fully implicit. This algorithm is named CLEAR, standing for Coupled & Linked Equations Algorithm Revised. Because of this key improvement, the convergence rate of the iterative procedure can be drastically increased. Details about this algorithm can be seen on Tao et al. (2005).

The boundary conditions are very important for CFD techniques as they govern the solutions. Usually, inlet conditions are uniform bulk velocity (based on the specified flow rate) and temperature or fixed velocity/temperature distribution. No-slip velocity conditions are used at the wall as a flow condition, whereas uniform temperature or heat flux at wall is specified as a thermal one. For the outlet, a zero spatial derivative in a direction normal to the boundary is commonly specified. As the pressure is obtained by the solution of the Navier-Stokes equations, uniform arbitrary pressure is usually fixed at the outlet of the computational domain. However, this condition is sometimes unsuitable when the reattachment point of the separated flow is near the outlet or when an eddy structure exists through it. For the lateral part, two conditions could be used: periodicity or symmetry (free slip condition). The former is based on a

direct pressure coupling between the two lateral sides and is well suited for deviated flows (louver fins, for example). The latter is usually used for spatially developed flows inside a symmetrical geometry (offset strip fins, for example). To simulate fully developed flows, it is common to adopt the outflow condition. However, a longer wake region downstream of the surface is required to get reasonable results, especially for unsteady flows. For example, to simulate flow past a cylinder at $Re = 300$, the flow becomes unsteady with vortices in the downstream region (Wang, 2010). If we set the length of the downstream wake region as smaller than 20 times cylinder diameter, the simulation may diverge or the results for flow performance may differ from what they should be by using the proceding outflow condition. This is because the actual flow cannot meet the outflow condition at the boundary. Thus, if we use the outflow conditions for the downstream boundary, the downstream wake region would be longer for more accurate results (and it is obvious that there is an increase of both number of grid cells and the computing time).

4.2 3-D computational domain and boundary conditions

The three-dimensional computational domain and DWLs and boundary conditions are shown in Figure 4-3. The thermal-hydraulic performance of two geometries, GEO_1 and GEO_2, are evaluated. The main differences between those two geometries are the louver height, which is greater for GEO_2, and delta-winglet frontal area, which is greater for GEO_1. The main differences between these two geometries can be seen in Table 4-1.

The computational domain is divided into three parts in the flow direction: the upstream-extended region, the core region and the downstream-extended region. The domain is discretized by non-uniform grids with meshes in the core region being very fine while those in the extension region were as coarse as possible to save computing resources. The upstream region is extended one time of core domain to ensure the inlet velocity uniformity and four times downstream so that the fully developed outflow boundary condition could be used. The constant geometric parameters of the core region are: fin pitch (F_P) of 1.10 mm, fin height (F_H) of 9.54

mm, flow depth (F_D) of 10.3 mm, louver pitch (L_P) of 0.9 mm and transverse tube pitch (T_P) of 11.04 mm. The aspect ratio of DWLs is kept constant and equal to 2.0 and the thicknesses of the multi-louvered fin and the delta winglets are assumed to be zero, for simplification.

The flow is described in a rectangular Cartesian coordinate system (x, y, z) in which x, y, z represent streamwise, spanwise and wall normal directions, respectively. Each louver array consists of an inlet louver, an exit louver and three louvers on either side of the turnaround louver. The spanwise directions of DWLs are kept constant for each geometry: (a) for GEO$_1$, $y_{DWL_1} = y_{DWL_2} = 1.00$ mm and $y_{DWL_3} = y_{DWL_4} = 8.54$ mm; (b) for GEO$_2$, $y_{DWL_1} = y_{DWL_2} = 0.69$ mm and $y_{DWL_3} = y_{DWL_4} = 8.85$ mm.
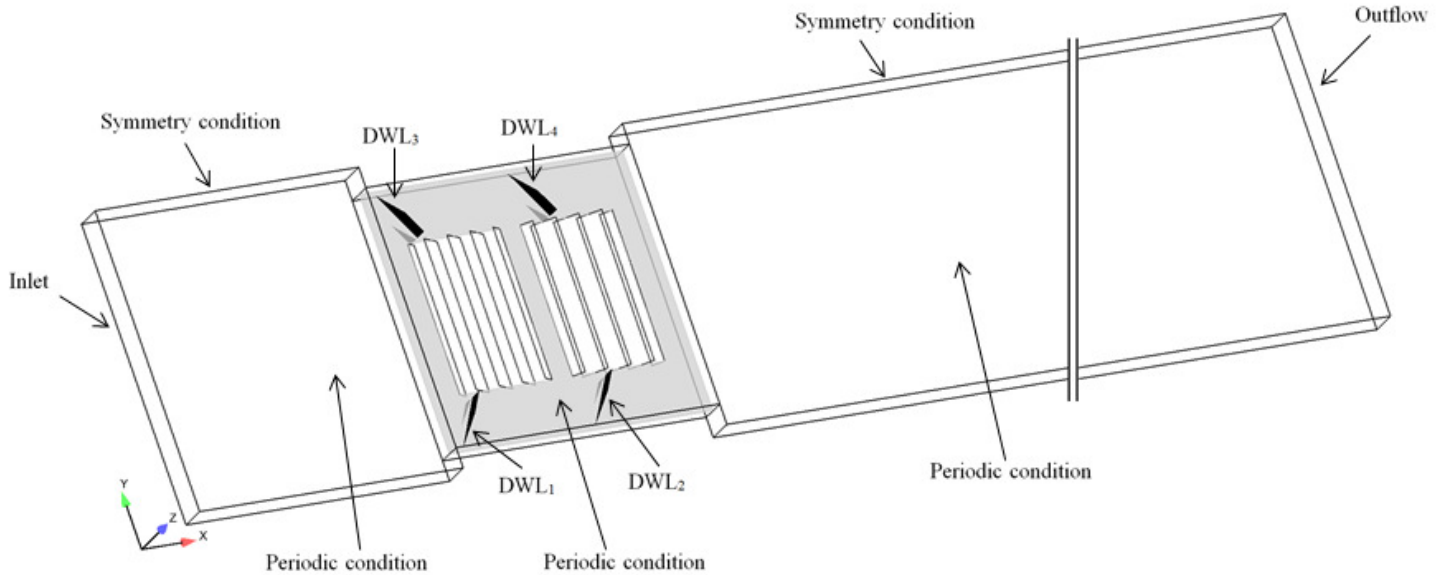
Figure 4-3 Three-dimensional computational domain and boundary conditions.

Figure 4-4 shows the input parameters placed at the computational domain as well as the reference point (0,0,0), which coincides with the point positioned exactly on the half chord of DWLs. It is considered that $x_1 = x_3$, $x_2 = x_4$, $\theta_3 = -\theta_1$ and $\theta_4 = -\theta_2$. The rotation axis of each DWL is positioned on its half chord and the rotation in the

clockwise direction is assumed to be negative. As observed in Table 4-2 and Table 4-3, the streamwise positions for GEO_1 and GEO_2 are slightly different in order to cover the larger design space as possible and to avoid interferences between DWLs, louvers and flat tubes.

Table 4-1
Louvers and DWLs geometrical parameters for both GEO1 and GEO_2.

Input parameter	GEO_1	GEO_2
Louver height	5.54 mm	8.00 mm
Total louver surface area	39.89 mm^2	48.75 mm^2
DWL height	$0.90F_P$	$0.80F_P$
DWL chord	1.98 mm	1.76 mm
Total DWL surface area	3.92 mm^2	3.10 mm^2
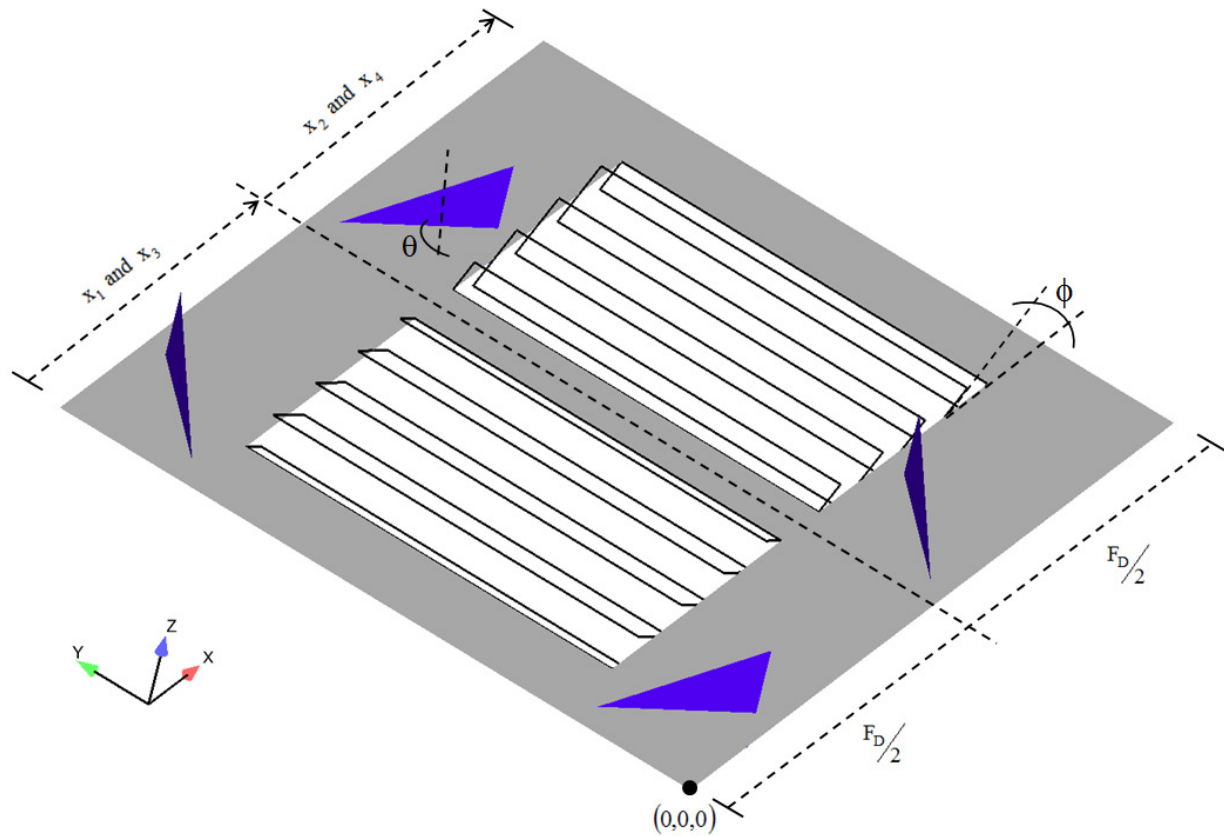
Figure 4-4 Schematics of the core region showing the input parameters to be investigated and the reference point (0,0,0).

Table 4-2
Input parameters for GEO$_1$

Input parameter	Symbol	Operating range
Louver angle	ϕ	$15^\circ \leq \phi \leq 45^\circ$
DWL$_1$ angle of attack	θ_1	$-45^\circ \leq \theta_1 \leq 45^\circ$
DWL$_2$ angle of attack	θ_2	$-45^\circ \leq \theta_2 \leq 45^\circ$
DWL$_1$ streamwise position	x_1	$1.109mm \leq x_1 \leq 4.060mm$
DWL$_2$ streamwise position	x_2	$6.240mm \leq x_2 \leq 9.210mm$

Table 4-3
Input parameters for GEO$_2$

Input parameter	Symbol	Operating range
Louver angle	ϕ	$15^\circ \leq \phi \leq 45^\circ$
DWL$_1$ angle of attack	θ_1	$-45^\circ \leq \theta_1 \leq 45^\circ$
DWL$_2$ angle of attack	θ_2	$-45^\circ \leq \theta_2 \leq 45^\circ$
DWL$_1$ streamwise position	x_1	$0.980mm \leq x_1 \leq 4.170mm$
DWL$_2$ streamwise position	x_2	$6.130mm \leq x_2 \leq 9.320mm$

The assumption of the laminar flow for louvered fin arrays is reasonable for the Reynolds numbers in the operating range for GEO$_1$ and GEO$_2$. This hypothesis was also considered in the studies by Antoniou et al. (1990), DeJong and Jacobi (2003), Ha et al. (1995), Ferrero et al. (2013) and Perrotin and Clodic (2004). Laminar assumption for the air flow is also acceptable for the vortex generators placed in a channel, which can be verified from previous works by He et al (2012), Lei et al. (2010), Wu and Tao (2007), Chu et al. (2009), Yanagihara and Rodrigues (1998) and Biswas and Mitra (1995). Moreover, the steady state condition for louvered fins and DWLs can also be considered suitable, as observed from researches by DeJong and Jacobi (2003), Tafti et al. (2000), Huisseune et al. (2013A), Ryu et al (2014), Fiebig (1995), Ferrouillat et al. (2006) and Zhu et al. (2008).

The boundary conditions in those three regions are described below:

> <u>At the inlet boundary</u>: $U = U_{in} = const,\ V = W = 0,\ T = T_{in} = 311\ K$

> <u>At the louvered fin and tube regions</u>: $T_{fin} = T_{tube} = 373\ K,\ U = V = W = 0$

> <u>At the DWLs</u>: $\dot{Q} = 0\ (\text{adiabatic})$

> <u>At the right and left sides of the domain</u>: $\dfrac{\partial U}{\partial y} = \dfrac{\partial W}{\partial y} = 0,\ V = 0,\ \dfrac{\partial T}{\partial y} = 0$

> <u>At the top and bottom sides of the domain</u>:

$U(x,y,0) = U(x,y,F_P),\ V(x,y,0) = V(x,y,F_P),\ W(x,y,0) = W(x,y,F_P),\ T(x,y,0) = T(x,y,F_P)$

> <u>At the outlet boundary</u>: $\dfrac{\partial U}{\partial x} = \dfrac{\partial V}{\partial x} = \dfrac{\partial W}{\partial x} = \dfrac{\partial T}{\partial x} = 0$

Finally, the convergence criteria of 10^{-7} for velocity components, 10^{-8} for energy and 10^{-6} for continuity, are imposed. The convection and diffusion terms of the governing equations are discretized by second-order upwind discretization. The SIMPLE algorithm is used for pressure-velocity coupling.

4.3 Important parameters

The parameters to calculate the heat transfer and pressure drop in heat exchangers depend on the geometry and flow conditions. The flow condition can be characterized by the Reynolds number (generally based on hydraulic diameter). Colburn factor, j, and friction factor, *f*, are used to describe the heat transfer and pressure drop of heat exchangers, respectively. In order to improve the model to be easily understood, Reynolds number, Colburn factor and friction factor are defined by

$$Re_{Dh} = \frac{\rho U_C D_h}{\mu}$$

Eq.4-7

where U_C is the maximum air velocity, which is calculated as

$$U_C = \frac{UA_{fr}}{A_C}$$

Eq.4-8

A_{fr} is fin frontal area and A_C is the minimum free-flow area for air side.

D_h is the hydraulic diameter,

$$D_h = \frac{4A_{fr}}{E}$$

Eq.4-9

where E is the wet perimeter.

The Colburn factor is defined by

$$j = \frac{h}{\rho U_C c_P} Pr^{\frac{2}{3}}$$

Eq.4-10

where Pr is the Prandtl number for the air side.

The Fiction factor is calculated as

$$f = \frac{A_C}{A_0}\left[\frac{2\Delta P}{\rho U_C^2}\right]$$

Eq.4-11

where

A_0 is the total air side surface area

ΔP is the pressure drop

The mean pressure and temperature are defined as

$$\overline{p} = \frac{\iint_A p \, dA}{\iint_A dA}$$

Eq.4-12

$$\overline{T} = \frac{\iint_A UT \, dA}{\iint_A U \, dA}$$

Eq.4-13

The total heat transfer, pressure loss and log-mean temperature difference are defined as

$$Q = \dot{m} c_p \Delta T_{ln}$$

Eq.4-14

$$\Delta P = \overline{p}_{in} - \overline{p}_{out}$$

Eq.4-15

$$\Delta T_{ln} = \frac{\left(T_W - \overline{T}_{in}\right) - \left(T_W - \overline{T}_{out}\right)}{\ln\left[\dfrac{T_W - \overline{T}_{in}}{T_W - \overline{T}_{out}}\right]}$$

Eq.4-16

where T_W is the wall temperature.

Finally, the average convective heat transfer coefficient is determined by Eq. 4-17

$$h = \frac{Q}{A_0 \Delta T_{ln}}$$

Eq.4-17

4.4 Screening analysis

The thermal-hydraulic performance of multilouvered fin compact heat exchangers with DWLs can be affected by several geometric parameters. Some of these parameters have small impact, others have large impact. As shown outlined, 5 input parameters were chosen to run the screening analysis in order to understand the contribution of main and interaction effects on heat transfer and pressure. The analysis of variance is performed by using Smoothing Spline ANOVA (SS-ANOVA). The SS-ANOVA models are a family of smoothing methods suitable to both univariate and multivariate regression problems.

A useful diagnosis tool for assessing the model quality is represented by the collinearity indices (Rigoni and Ricco, 2011). In the ideal situation, all collinearity indices are close to the unity in order to ensure that the column vectors are nearly orthogonal to each other. When the vectors are highly correlated, a phenomenon referred to as concurvity can be detected, since the relevant collinearity indices will be much higher than unity. There can be many causes to this pathology, such as dependent input variables, bad sampling points, too low sample points, etc. Ricco (2013) performed benchmark tests with SS-ANOVA and the validation of this procedure is presented.

In order to avoid bad sampling points, Latin hypercubes designs (LHD) have been used as the method to generate randomly sample from some prior probability distribution on parameter space. How the sampling points are distributed on the design space can be seen in details on Chapter 5.

In a few words, the strategy to perform the screening analyses is:

➢ Step 1: Generate the initial distribution of the sampling points on the design space;

➢ Step 2: Run the numerical simulations for those geometry configurations;

➢ Step 3: Calculate the collinearity indices;

➢ Step 4: If the coolinearity indices are very close to unity, then stop the process.

➢ Step 5: If the Step 4 is not satisfied, generate more sampling points and go to Step 2. Follow the steps until the collinearity indices are very close to the unity.

4.5 Surrogate-based optimization

For any design and modeling purpose, the ultimate aim is to gain sufficient insight into the system of interest so as to provide more accurate predictions and better designs. As computing power rapidly increasing and accessible, it has become possible to model some of these processes by sophisticated computer code. In the past decades computer experiments or computer-based simulation have become topics in statistics and engineering that have received a lot of attention from both practitioners and the academic community.

Here, a surrogate model known as Artificial Neural Networks (ANN), by using back propagation method, was chosen. It is trained by a steepest descent method called by Back Propagation. In this method, weight values are adjusted in an iterative fashion while moving along the error surface to arrive at a minimal range error, when inputs are presented to the network for learning the pattern of the data.

The model accuracy or the goodness-of-fit of the ANN is assessed by three error measures (as shown on item 3.3.1):

1.   Maximum absolute error

2.   Root mean square error, RMSE

3.   R-squared, R^2

As discussed before, Forrester and Keane (2009) suggest that the surrogate model can be considered acceptable when $R^2 > 0.8$, maximum error is smaller than 10% and $RMSE < 5\%$. Giunta (1997) indicated that the value of R^2 should vary between 0.9 and 1.0 for an accurate prediction of the surrogate model.

Another important step regarding surrogate model training is to define the ratio size between training and testing data set. Overall, for the purposed research, the data set is randomly split into 80% for training and 20% for testing. Obviously, the data set used on training process was completely different of the data set used on testing. Thus, the ANN was trained to extrapolate the conditions which fell outside the region of the traing data. The steps for the proposed surrogated model selection are shown in Figure 4-5.

Once the surrogate models are built, an optimization algorithm, herein based on the Genetic Algorithm approach, can be used to search the new design (based on the surrogate models) that is most likely to be optimum. Since the prediction with a surrogate model is generally faster than numerical analysis code, the computational cost associated with the search based on the surrogate models is generally negligible. The basic idea of this approach is to start with a set of designs, randomly generated using the allowable values for each design variable, which are assigned to a fitness function. From the current set of designs, a subset is selected randomly with a bias allocated to the most fit members of the set. Random processes are used to generate new designs using the selected subset of designs and two GA basic operators: mutation and crossover. GA performance is strongly linked with these operators. NSGA-II is invoked here to maximize the Colburn factor with $N_{gen} = 5000$ and $N_{pop} = 100$. The crossover and mutation operators are set to 0.90 and 1.00, respectively, which allow a broad capability of exploration and exploitation of the solution space. The method is schematically illustrated in Figure 4-6. The following optimization routine shows the steps to achieve the maximization of Colburn factor.
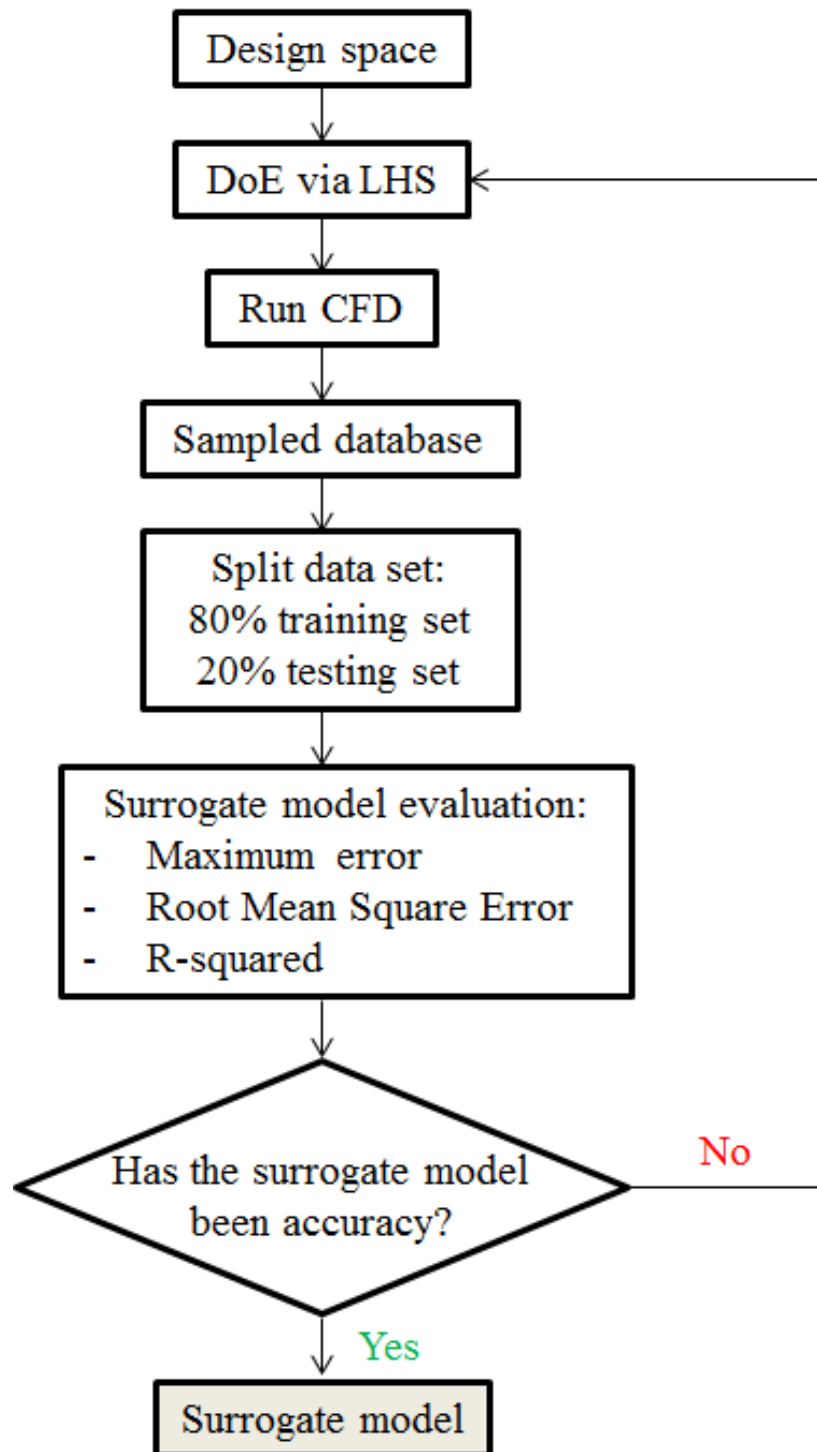
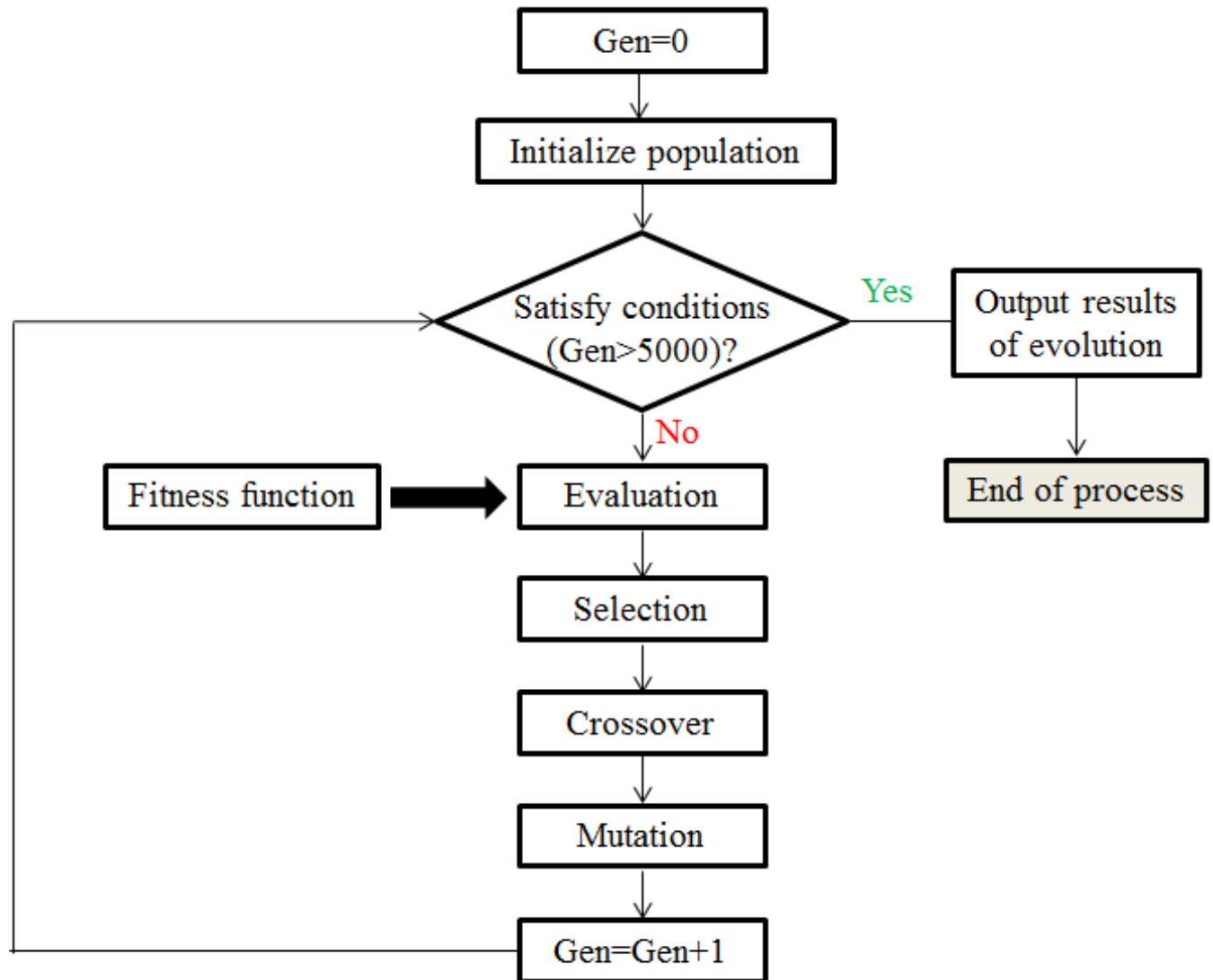**Figure 4-5 Framework of building surrogate model.**

Figure 4-6 Flowchart of Genetic Algorithm used on this research.

5 Results and discussion

5.1 Model validation and grid independence

Before any computational result can be deemed enough to illustrate the physical phenomenon, the computational results must be verified through a grid independence test. In order to validate the solution independence of grid number, the numerical set up was compared with experimental data from Kim and Bullard (2002), who experimentally studied the air-side heat transfer and pressure drop characteristics for multi-louvered fin and flat tube heat exchangers.

Three mesh sizes were investigated herein: coarse, intermediate and fine, corresponding to 9.9 million cells, 16.5 million cells and 23.7 million cells, respectively.

The accuracy of the present numerical approach was verified by comparing the average heat transfer coefficient (h) and average pressure drop (ΔP) for inlet velocity ranging from 0.75 m/s to 3 m/s (Figure 5-1). The results indicate that the coarse grid is enough to represent the pressure drop for all inlet air velocities, but it is not good enough to characterize the heat transfer. In turn, the maximum average heat transfer and pressure drop of the intermediate grid differs from that of the fine grid by 0.4% and 0.9%, respectively. Furthermore, the numerical predictions with those grids are in the range of measurement uncertainties, which are $\pm 12\%$ for heat transfer and $\pm 10\%$ for pressure drop.

The sensitivity analysis of the intermediate and fine grid refinements is also performed with the current geometry in order to evaluate the variation of heat transfer and pressure drop when the DWLs are placed in the core domain. Louver angle is set at 32º, $\theta_1 = 45º$, $\theta_2 = 45º$, $x_1 = 2.585$ mm and $x_2 = 7.725$ mm. The sensitivity analysis is performed for two Reynolds numbers: $Re_{Dh} = 120$ (corresponding to inlet velocity of 1.0 m/s) and $Re_{Dh} = 240$ (corresponding to inlet velocity of 2.0 m/s). For $Re_{Dh} = 120$, the variations in terms of heat transfer and pressure drop between

intermediate and fine grid refinements were 0.02% and 0.24%, respectively. For $Re_{Dh} = 240$, the variations were 0.17% and 0.02%, respectively. Based on these comparisons, the intermediate grid refinement, which can be seen in Figure 5-2, is considered enough for the purposes of this work.

(a)Heat transfer coefficient   (b)Pressure drop
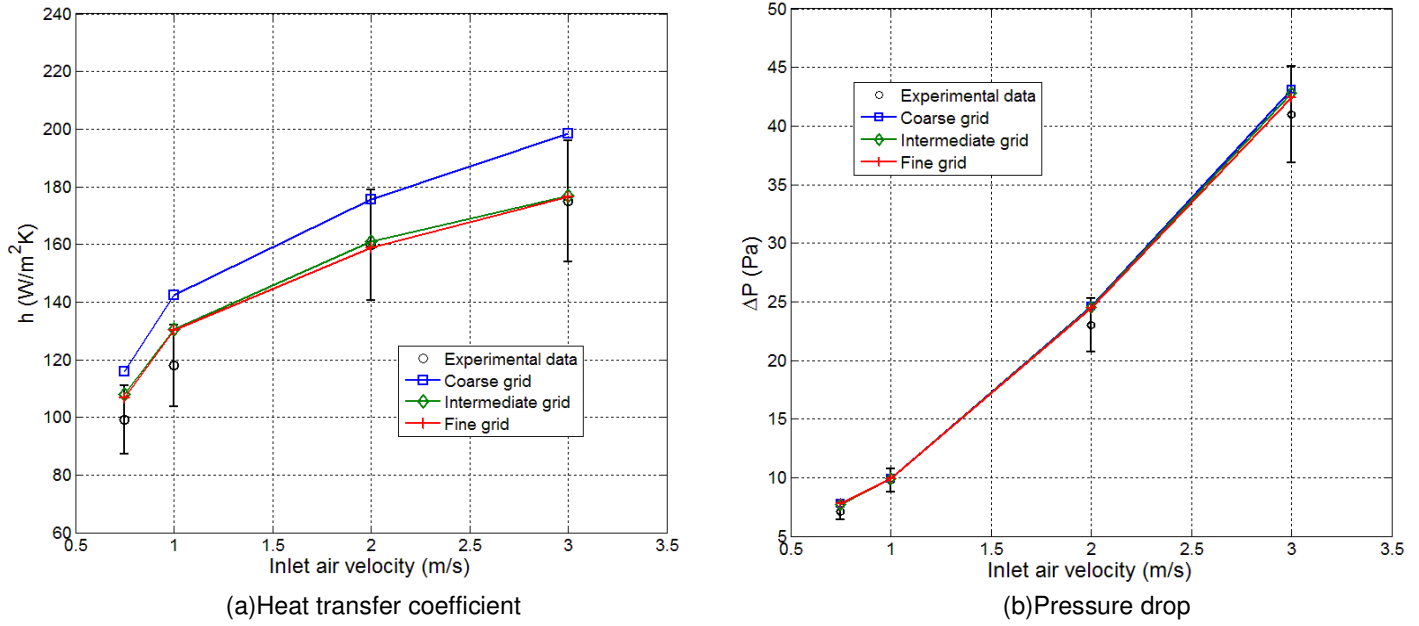
Figure 5-1 Comparison of heat transfer coefficient (a) and pressure drop (b) between experimental data and numerical results for some grid refinements.
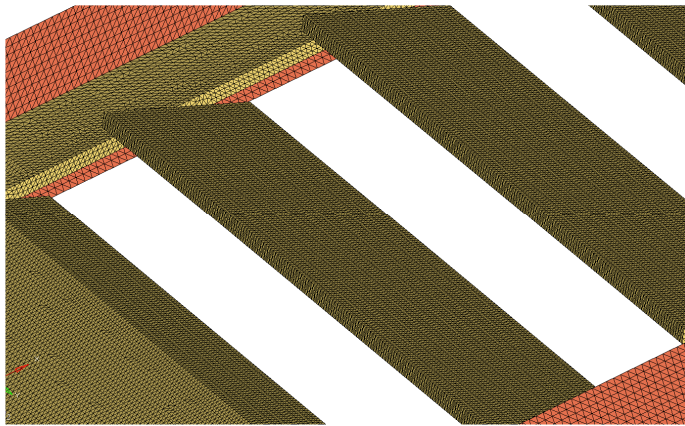
(a)Intermediate grid used for numerical validation   (b)Intermediate grid used in the current work
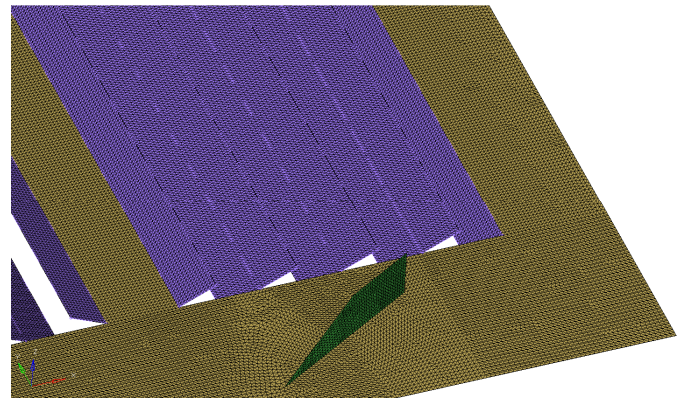
Figure 5-2 Grid topology for irregular meshing of the core region.

5.2 Screening analysis

The maximum collinearity indices for Colburn and friction factors were assessed and the process stopped when those indices were very close to the unity (maximum collinearity indice was 1.14 and 20 designs per input variable for GEO_1 and GEO_2, and for both $Re_{Dh} = 120$ and $Re_{Dh} = 240$).

However, we need to verify if the sample distribution of the input variables on design space was good enough. For this, we can use the scatter matrix chart to see all the pairwise scatter plots of the input variables, the correlation values between all the input variables and the Probability Density Function (PDF) chart for each input variable. Figure 5-3 shows the scatter matrix chart, which is exactly the same for GEO_1 and GEO_2, and for both $Re_{Dh} = 120$ and $Re_{Dh} = 240$.

For those five input variables, the scatter plot matrix have 5 rows and 5 columns and the ith row and wth column of this matrix (above the diagonal) is a scatter chart of the input variable i versus the input variable w. On the diagonal, at the ith row and wth column, it is plot the Probability Density Function chart for the ith input variable. Since the ith input variable versus the wth input variable is equivalent to wth input variable versus the ith input variable with the axes reversed, below the diagonal, on every cell of the matrix. It is print the correlation value between the ith input variable versus the wth input variable. Values close to zero value are expected for no correlation between the input variables.

From inspection of Figure 5-3, it can be seen in that the Probability Density Function (PDF) is practically uniform for all input variables and it is not observed any correlation between the 5 input variables. Based on this, we can assume that the sampling data distribution on the design space can be considered satisfactory to perform the screening analysis of those 5 input parameters in terms of heat transfer and pressure drop.
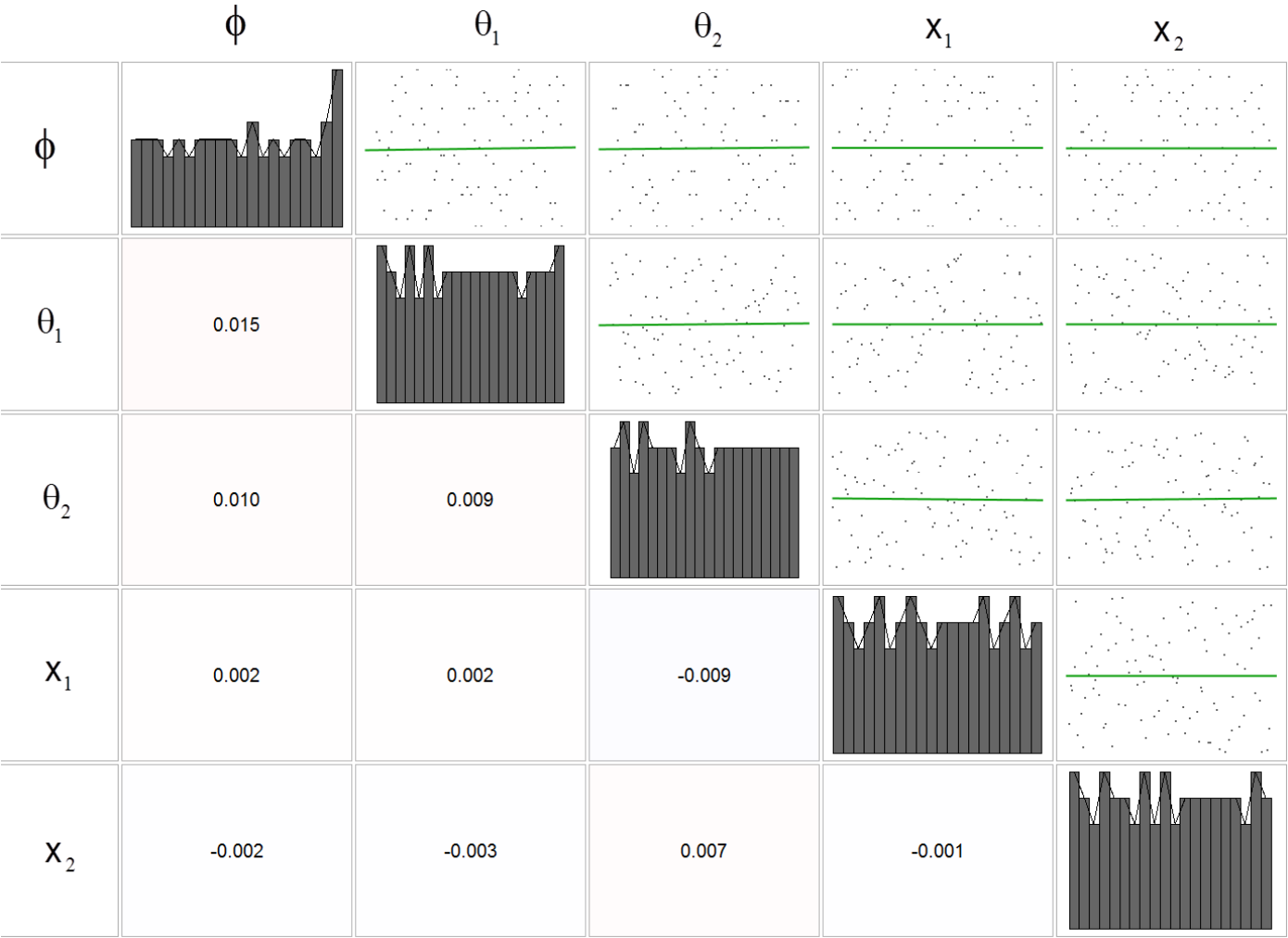
Figure 5-3 Scatter matrix chart for screening analysis of the input parameters.

5.2.1 Screening analysis from the GEO$_1$ parameters

Figure 5-4 (a) and (b) shows the contribution of main and interaction effects of the input parameters to f for $Re_{Dh} = 120$ and $Re_{Dh} = 240$, respectively. The results indicate that parameter ϕ is the major contributor to f for both Reynolds numbers, corroborating with the studies from Huisseune et al. (2013A) and Ameel et al. (2014) for round-tube multi-louvered fin heat exchangers. The effect of ϕ is higher because of the lower velocity and small louver angles, the flow passage between the louvers is blocked by the thick boundary layers making the flow duct-directed. As ϕ

increases, the duct diameter effectively decreases and the pressure drop for flow through the duct increases forcing the flow to pass between the louvers (louver-directed flow). In this case, the fluid particles travel long distances and, consequently, the pressure drop is increased. Since the Reynolds number is increased, the flow tends to be more louver-directed because the flow resistance between the louvers is decreased insofar as the boundary layers around the louvers are thinner. Thus, the influence of the louver angle is expected to be strong on pressure drop.

The impact on f due to DWL parameters is not observed and there are not any relevant interaction effects between the input variables for both Reynolds numbers. According to Huisseune et al. (2013A), the contribution of the DWL geometrical parameters is much smaller than louver angle for inlet velocity of 1.26 m/s, which is in accordance with the current results.

The influence of input variables on j for the lower and the upper Reynolds number is presented in Figure 5-5 (a) and (b), respectively. For $Re_{Dh} = 120$, the contribution of parameter ϕ is the highest (65%) followed by θ_1 (18%). As discussed, the increase of ϕ makes the flow more louver-directed, and is characterized by a higher heat transfer rate, since the fluid travel larger distances through the fin, improving the mixing of cold and hot air. Moreover, the boundary layers around the louvers are thinner; thus, the air flow velocity passing among them is increased, producing higher heat transfer rate. Two weak interactions are also observed, $\phi * x_1$ (6%) and $\theta_1 * x_1$ (5%). The effect of the second row (DWL_2 and DWL_4) of DWLs on heat transfer is negligible and, therefore, the first row of DWLs (DWL_1 and DWL_3) is the major contributor to heat transfer for $Re_{Dh} = 120$. For $Re_{Dh} = 240$, θ_1 is the major contributor (49%) to heat transfer followed by ϕ (13%), $x_1 * \theta_1$ (12%), θ_2 (8%), x_1 (6%), $\phi * x_1$ (5%) and x_2 (4%). Insofar as the angle of attack of DWLs is increased, the longitudinal vortices generated become stronger, and the swirling motion promotes a better mixing of hot and cold fluid regions, which increases heat transfer. The small contribution of θ_2 is due to the DWL_2 and DWL_4 placed on the second half of the fin, and thus their longitudinal vortices have a smaller heat exchange surface area than that created by DWL_1 and DWL_3.

Also for $Re_{Dh} = 240$, the contribution of each input variable on heat transfer is more pronounced. Increasing the inlet velocity makes the flow more louver-directed, and the impact of parameter ϕ is decreased. Significant contribution to heat transfer is observed due to DWLs, especially for those in the first row. The increase of the inlet flow velocity is evidently more beneficial to DWLs than louvers in terms of heat transfer. The contribution of the interaction $\phi * x_1$ to heat transfer has practically the same order of magnitude for both Reynolds numbers and could be taken as the only interaction (but still small) between louvers and DWLs. However, since the interaction effects are additive, the total contribution of main and interaction effects related to x_1 becomes important for this Reynolds number, differently of that occurred at $Re_{Dh} = 120$.

Overall, two distinct behaviors in heat transfer are observed. For the lower inlet velocity, the louver angle is the major contributor to heat transfer enhancement, while for the higher inlet velocity, the major contributors are the DWL parameters. Even though the GEO_1 is a kind of compound heat transfer technique, the results indicate that there are no important interactions between louvers and DWLs for either pressure drop and heat transfer. Thus, the flow phenomenology for each technique could be separately studied, according to key features already discussed by previous works regarding vortex generators and louvered fins.

By comparison of heat transfer and pressure drop for $Re_{Dh} = 120$, there is a clear evidence that ϕ has a greater impact on friction factor than heat transfer. In turn, θ_1 exerts considerable influence on heat transfer associated to negligible impact on pressure loss. For $Re_{Dh} = 240$, the contribution of θ_1 to heat transfer is about 40 times greater than its contribution to pressure drop, and the contribution of ϕ to pressure drop is about 8 times as great as its contribution to heat transfer. The parameters referred to the second row of DWLs are negligible for heat transfer and pressure drop for $Re_{Dh} = 120$. However, when the Reynolds number is increased, those parameters little contribute to heat transfer associated to almost negligible influence on pressure drop.

(a)Contribution to f for $Re_{Dh} = 120$ (b)Contribution to f for $Re_{Dh} = 240$
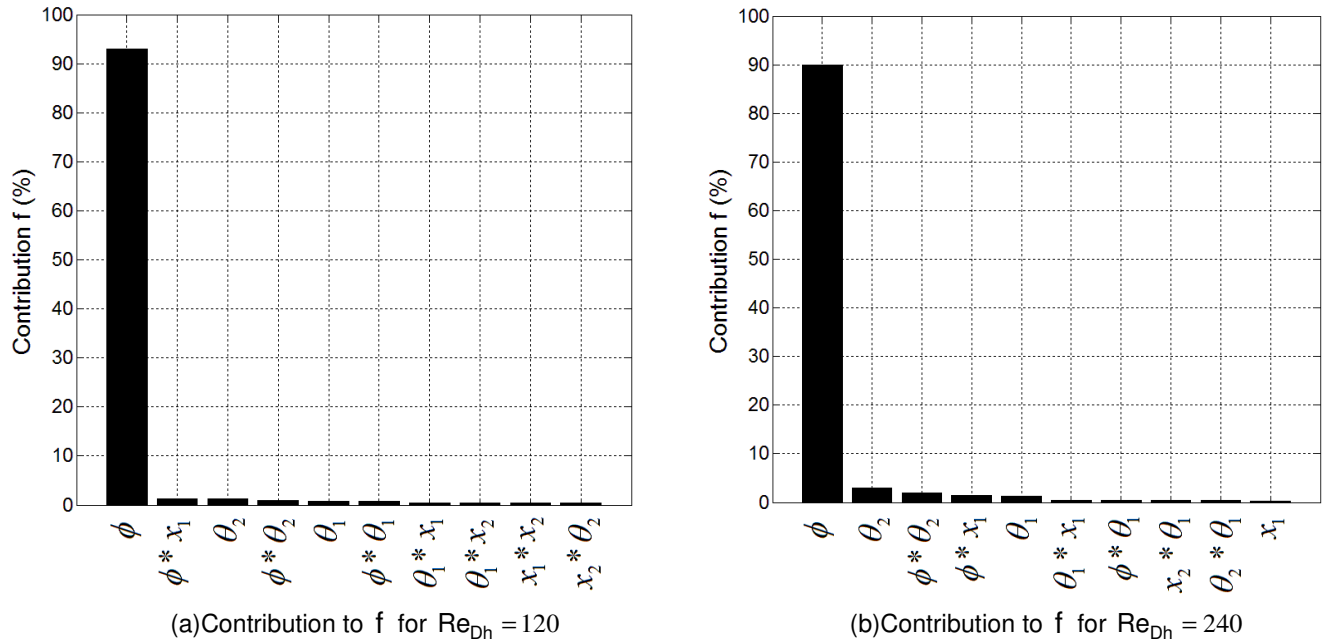
Figure 5-4 Contribution of input parameters to the friction factor.

(a)Contribution to j for $Re_{Dh} = 120$ (b)Contribution to j for $Re_{Dh} = 240$
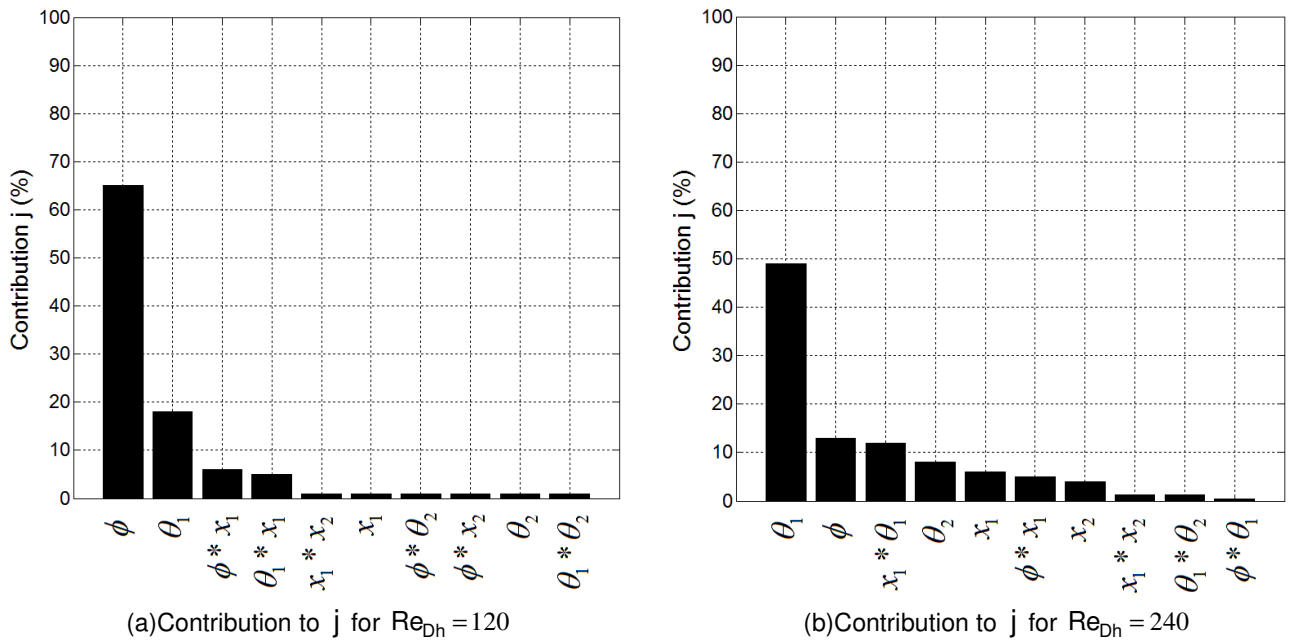
Figure 5-5 Contribution of input parameters to Colburn factor.

Figure 5-6 (a) presents the Friction factor as a function of parameter ϕ and Re_{Dh} for the GEO$_1$ baseline geometry (GEO$_1$ without DWLs) to show the effect of parameter

ϕ on the Friction factor, since that parameter is the major contributor for both Reynolds numbers. The Friction factor is strongly dependent of the parameter ϕ and the comparison between the Reynolds numbers show that the curves have similar formats. This explains the same order of magnitude of the contribution of ϕ on f for both Re_{Dh}.

Figure 5-6 (b) shows the influence of parameter ϕ on the heat transfer for the baseline geometry. The effect of parameter ϕ on the Colburn factor is higher for $Re_{Dh} = 120$ than for $Re_{Dh} = 240$. For $Re_{Dh} = 120$, the values of j increase sharply from $\phi = 15^{\circ}$ to $\phi = 25^{\circ}$ and reach stability within the range $25^{\circ} < \phi < 30^{\circ}$ and then decrease up to $\phi = 45^{\circ}$. For $Re_{Dh} = 240$, the heat transfer increases up to a critical value ($\phi = 20^{\circ}$), after which the heat transfer is independent of louver angle. Based on this, the contribution of the louver angle on heat transfer for the higher Reynolds number is expected to be smaller than for the lower Reynolds number, which corroborates with the screening analysis.

The major contribution of the parameter θ_1 to heat transfer for $Re_{Dh} = 240$ is discussed based on results presented in Figure 5-7, which shows the span-average Colburn factor along the fin at five different configurations for a constant louver angle:

1. Baseline geometry with $\phi = 25^{\circ}$
2. Geometry with $\phi = 25^{\circ}$ and $\theta_1 = \theta_2 = 5^{\circ}$
3. Geometry with $\phi = 25^{\circ}$ and $\theta_1 = \theta_2 = 10^{\circ}$
4. Geometry with $\phi = 25^{\circ}$ and $\theta_1 = \theta_2 = 30^{\circ}$
5. Geometry with $\phi = 25^{\circ}$ and $\theta_1 = \theta_2 = 40^{\circ}$

For configurations 1, 2 and 3, the distributions of the span-average Colburn factor behave similarly, while configurations 4 and 5 are very similar. From the Colburn factors for all configurations with the angle of attack in the first row of DWLs, the heat transfer is shown to increase because the strength of the longitudinal vortices increases with the increase in the DWL angle of attack. Configurations 4 and 5 behave differently from configurations 1, 2 and 3 at flow depth between positions 7.80 mm and 8.70 mm because of the longitudinal vortices generation from the second row of DWLs.

(a)Friction factor, f
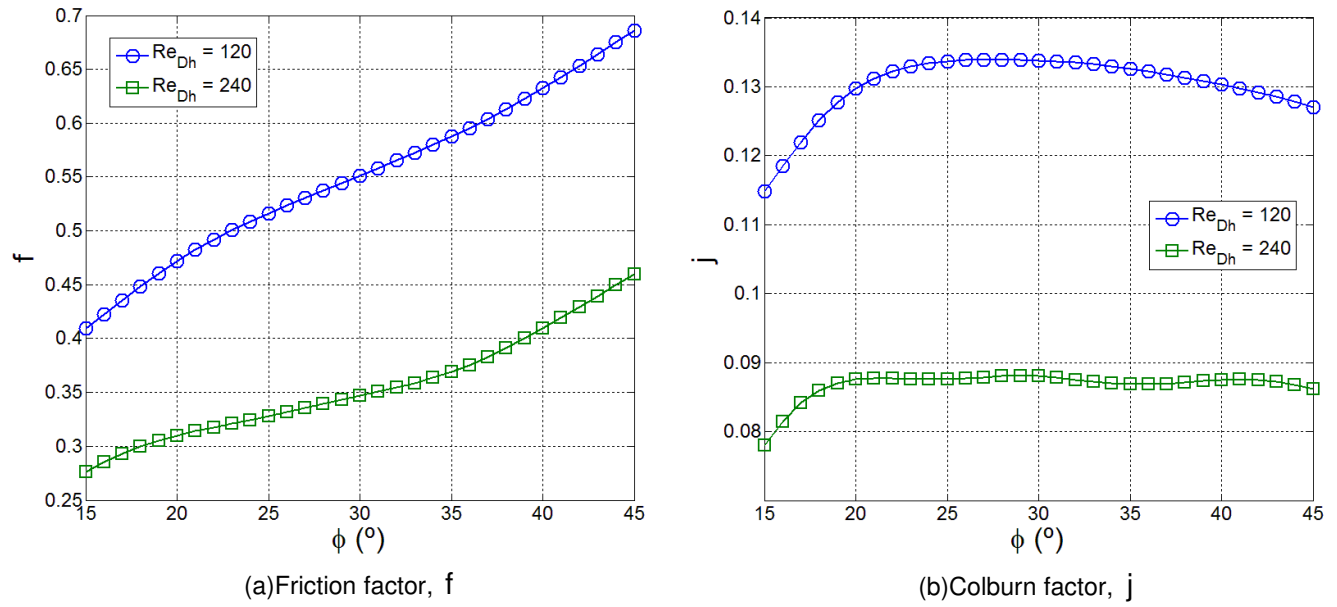
(b)Colburn factor, j

Figure 5-6 Variation of global Friction factor (a) and Colburn factor (b) for the GEO$_1$ baseline geometry as function of the louver angle.
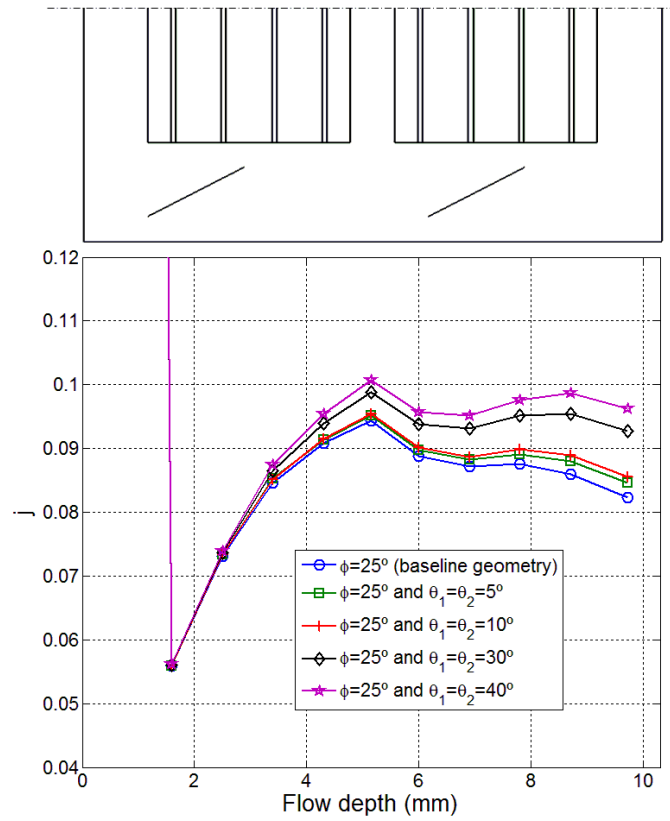
Figure 5-7 Distribution of span-average Colburn factor along the fin at different configurations of the GEO$_1$ at $Re_{Dh} = 240$.

5.2.2 Screening analysis from the GEO$_2$ parameters

The same analysis performed for GEO$_1$ is conducted for GEO$_2$. According to Figure 5-8 (a) and (b), for both Re$_{Dh}$, the major contributor to the friction factor is the parameter ϕ (about 95% of the total contribution) and, therefore, the contribution of the other parameters can be considered negligible. Thus, no influence of DWL parameters on pressure drop and no interactions between the input parameters are evidenced.

The effect of the parameters on the Colburn factor is shown in Figure 5-9 (a) and (b) for the lower and the higher Reynolds numbers, respectively. At the lower Reynolds number, the major contributor to heat transfer is the parameter ϕ, accounting for almost 90% of the total contribution. For Re$_{Dh} = 240$, the contribution of the parameters ϕ and θ_1 to heat transfer has practically the same order of magnitude (about 40% of the total contribution for each parameter). The contribution of parameter ϕ on the Colburn factor from Re$_{Dh} = 120$ to Re$_{Dh} = 240$ is mitigated since the flow tends to become more louver-directed for Re$_{Dh} = 240$. However, increasing the Reynolds number also increases the strength of the longitudinal vortices and as they are very persistent downstream, the effect of θ_1 on heat transfer is much more pronounced than that of θ_2. Increasing the Reynolds number is evidently beneficial to DWLs performance, i.e., the contribution of DWL parameters to heat transfer was about 10% for Re$_{Dh} = 120$ and about 55% for Re$_{Dh} = 240$. In other words, the effects of the vortex generator on Colburn factor are hidden by louvers for the lower Reynolds number and are revealed for the higher Reynolds number. Note that the louver is a passive technique that causes high heat transfer enhancement with high drop pressure penalty, and the vortex generators are also recognized to provide heat transfer enhancement with relatively small pressure drop penalty even for higher inlet velocity.

The heat transfer and pressure drop trade-off for Re$_{Dh} = 120$ indicated that ϕ is the major contributor. However, for Re$_{Dh} = 240$, the contribution of parameter θ_1 to heat transfer is higher than its contribution to pressure drop. Moreover, the DWLs have

shown to be the most contributors in terms of heat transfer than pressure drop when the inlet velocity is increased.

(a)Contribution of f for $Re_{Dh} = 120$ (b)Contribution of f for $Re_{Dh} = 240$
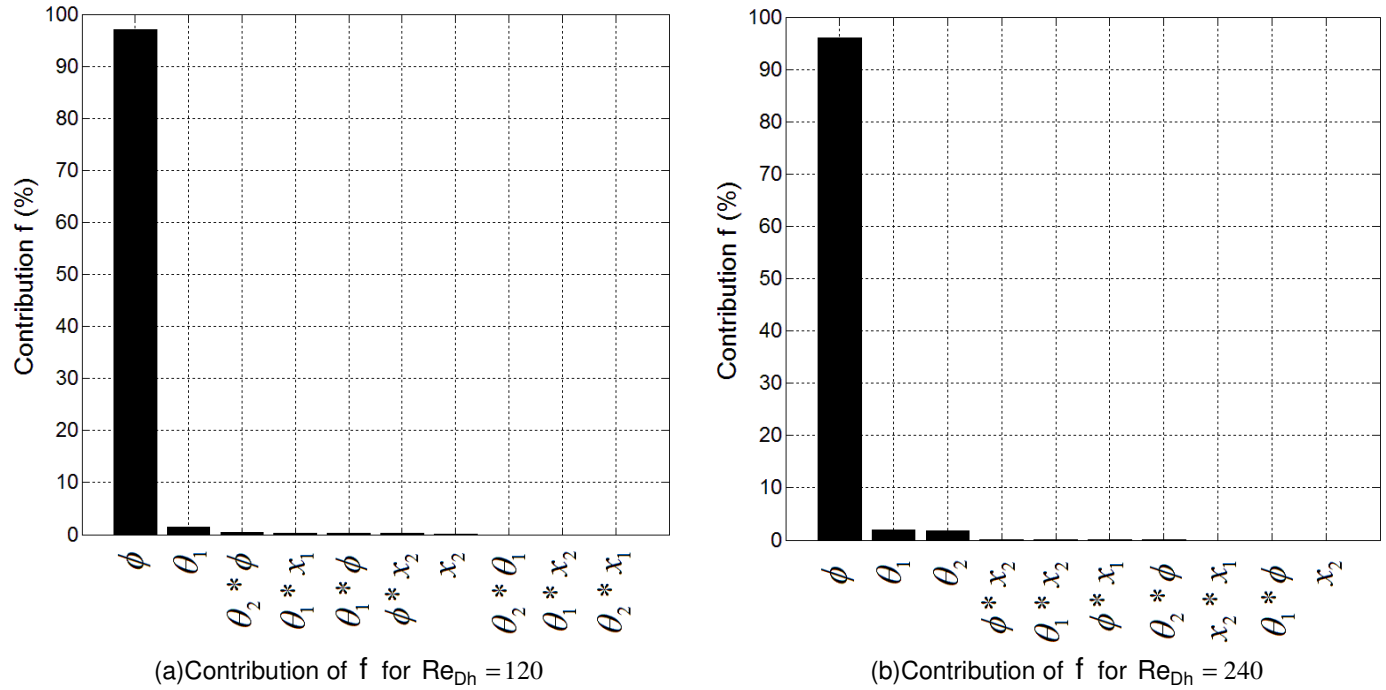
Figure 5-8 Contribution of input parameters to friction factor.

The next analysis is performed in order to evaluate the effects of louver angle and DWLs angle of attack on pressure drop and heat transfer for GEO_2. Figure 5-10 (a) allows verifying that the Friction factor behaves similarly for both Reynolds numbers as function of the louver angle for the GEO_2 baseline geometry (GEO_2 without DWLs). As occurred for GEO_1 baseline geometry, it seems that the friction factor varies quasi-linearly with the louver angle increasing and it has the same order of magnitude for both Reynolds numbers. Thus, the results summarized in Figure 5-10 (a) corroborate with the screening analysis for the friction factor.

In terms of heat transfer, the contribution of parameters ϕ and θ_1 are observed to have the same order of magnitude for $Re_{Dh} = 240$, while parameter ϕ is the major contributor for $Re_{Dh} = 120$. Figure 5-10 (b) presents the Colburn factor as function of the parameter ϕ for the baseline geometry. From that, the influence of the louver angle is higher for the lower Reynolds number, where the values of j increase rapidly

to $\phi = 25^{\circ}$, reaches a maximum value at $\phi = 30^{\circ}$ and then decrease up to 45°. On the other hand, the values of j increase slightly to $\phi = 20^{\circ}$ and then are kept practically constant up to $\phi = 45^{\circ}$, for the higher Reynolds number.
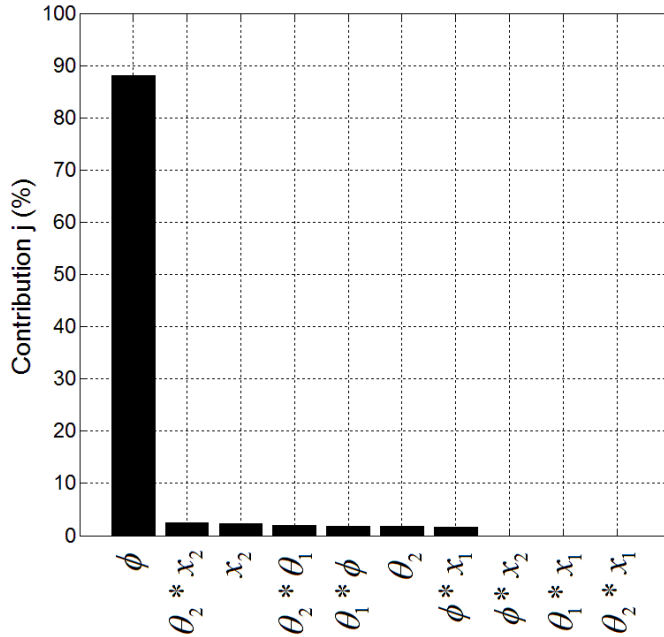
(a)Contribution of j for $Re_{Dh} = 120$ (b)Contribution of j for $Re_{Dh} = 240$
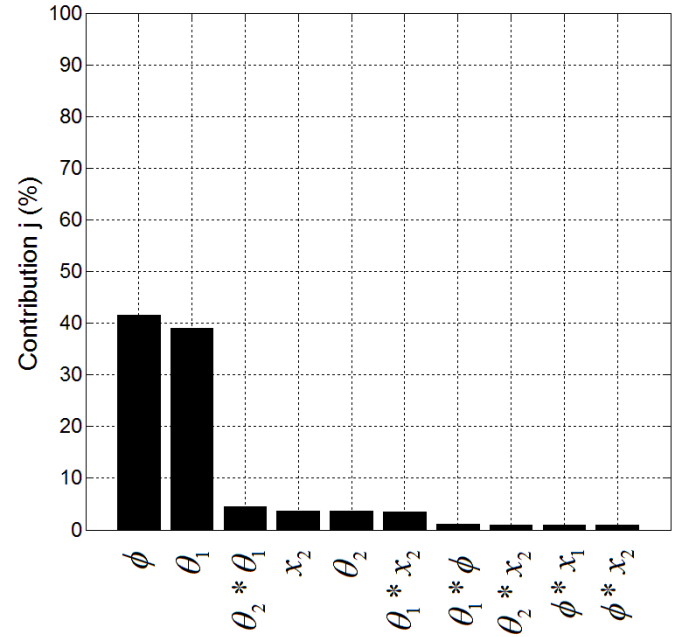
Figure 5-9 Contribution of input parameters to the Colburn factor.
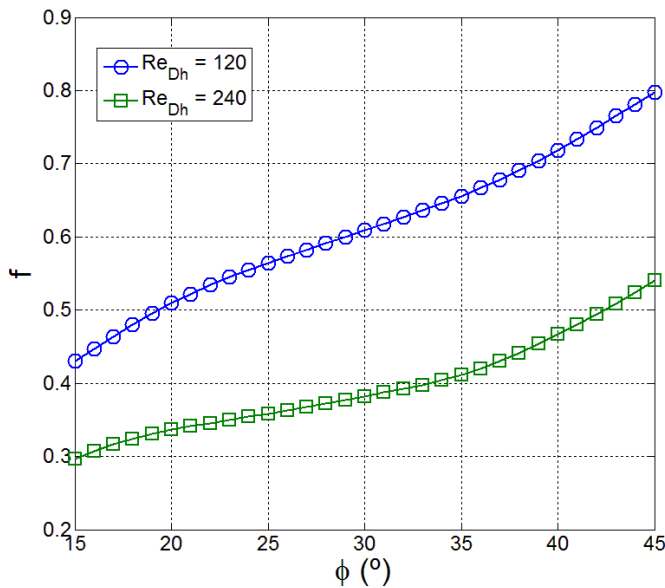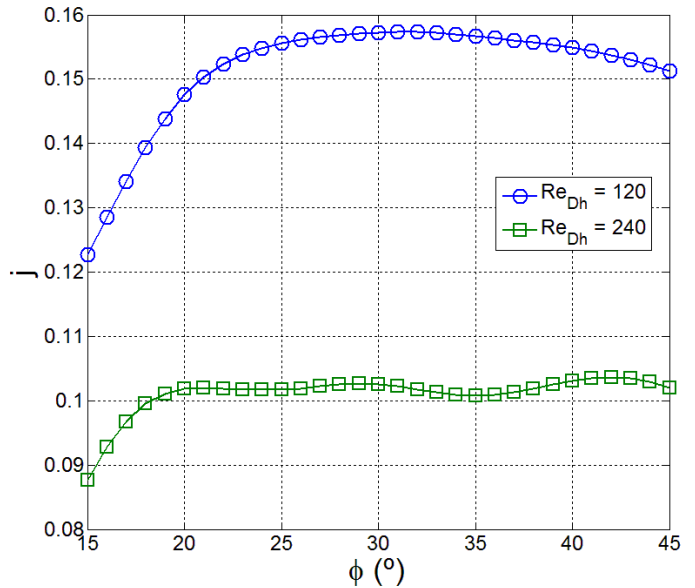
(a)Friction factor, f (b)Colburn factor, j

Figure 5-10 Variation of the global Friction factor (a) and Colburn factor (b) for the GEO$_2$ baseline geometry as a function of louver angle.

Figure 5-11 shows the span-average Colburn factor along the fin at six different configurations in order to investigate the conjugated contribution of parameters ϕ and θ_1 to heat transfer for $\mathrm{Re}_{Dh} = 240$. These configurations are:

6. Geometry with $\phi = 15^\circ$ and $\theta_1 = \theta_2 = 5^\circ$
7. Geometry with $\phi = 15^\circ$ and $\theta_1 = \theta_2 = 40^\circ$
8. Geometry with $\phi = 20^\circ$ and $\theta_1 = \theta_2 = 5^\circ$
9. Geometry with $\phi = 20^\circ$ and $\theta_1 = \theta_2 = 40^\circ$
10. Geometry with $\phi = 40^\circ$ and $\theta_1 = \theta_2 = 5^\circ$
11. Geometry with $\phi = 40^\circ$ and $\theta_1 = \theta_2 = 40^\circ$
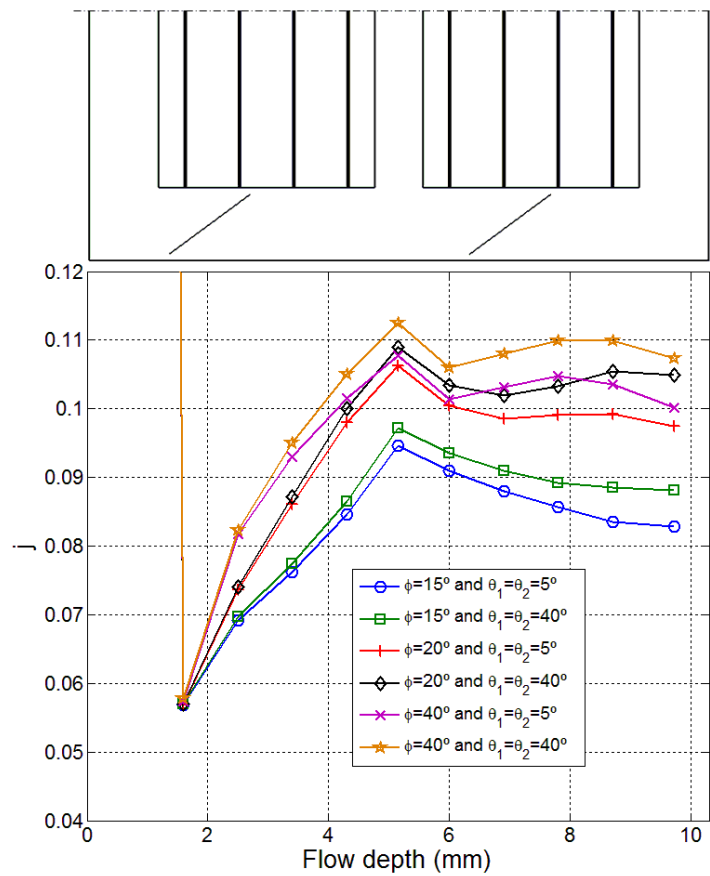
Figure 5-11 Distribution of span-average Colburn factor along the fin at different geometry configurations at $\mathrm{Re}_{Dh} = 240$**.**

The behavior of the curves for all the configurations is very similar up to the first half of the fin. After that, configurations 6 and 7 present a mitigation of heat transfer up to

the end of the fin, which is not observed in the other configurations. This occurs because at $\phi = 15^\circ$, the flow is predominately ducted, Figure 5-12 (a), and the heat transfer saturation in the first half of the array is reached, making the fin heat transfer performance poor. The other configurations present louver-directed regime, Figure 5-12 (b) and (c), which has a high heat transfer performance.

Figure 5-11 shows that there is a higher variation of Colburn factor, for the same DWLs angle of attack, between $\phi = 15^\circ$ and $\phi = 20^\circ$ along the fin, while the variation between $\phi = 20^\circ$ and $\phi = 40^\circ$ is very small. The strong influence of parameter ϕ on heat transfer is valid up to 20° and after this, its influence can be considered weak.

5.2.3 Comparison between GEO_1 and GEO_2

In the previous analyses, the effect of the input parameters on heat transfer depended on the type of geometry and on the Reynolds number, while the pressure drop is independent of type of geometry and Reynolds number. In this section, both geometries are compared to evaluate the impact of the louver and DWL surface areas on pressure drop and heat transfer. The total louver surface area of GEO_2 is 22.2% higher than of the GEO_1, while the total DWLs surface area of GEO_2 is 26.5% smaller than that of GEO_1.

The increase of louver surface area, or louver height, between GEO_1 and GEO_2 does not affect the influence of parameter ϕ on pressure drop for both Reynolds numbers. This behavior seems to be independent of the Reynolds number and the type of geometry. In turn, the contribution of each parameter to heat transfer is strongly associated with the type of geometry and Reynolds number. For GEO_1 at the lower Reynolds number, the DWLs have moderate influence on heat transfer and, when the DWLs surface area is decreased (GEO_2), their effect on heat transfer is negligible. For $Re_{Dh} = 240$, the contribution of DWL parameters for GEO_1 is higher than for GEO_2. Also at $Re_{Dh} = 240$, the parameters related to DWLs are the major contributors to heat transfer for GEO_2. These results are consistent with previous studies from Sanders and Thole (2006), who identified that the heat transfer

enhancement increased with DWL size and Reynolds number for flat-tube multi-louvered fin heat exchangers. Also, the authors concluded that for very low Reynolds numbers the influence of DWL parameters is much smaller than that for higher Reynolds numbers, which is in accordance to current results.

It is not identified any relevant effect for streamwise positions (x_1 and x_2) on heat transfer, except for GEO$_1$ at $Re_{Dh} = 240$, in which the parameter x_1 and their interactions accounted for about 25% of the overall contribution on heat transfer. This conclusion agrees with the results from Russel et al. (1982), who observed that the streamwise position between the vortex generators plays an important role on heat transfer for higher Reynolds numbers and higher DWL sizes than those used in the current work. However, the major part of the interaction effects of the parameter x_1 is with DWL parameters, not with the parameter ϕ.

In terms of interaction effects, the current results for GEO$_1$ and GEO$_2$ do not corroborate with screening analysis from Ameel et al. (2014), in which they identified important interactions between louver angle and DWL parameters for inlet velocity of 1.26 m/s. The main difference between the current work and Ameel et al. (2014) is that they used round-tubes and obviously DWLs do not cause any enhancement when they are placed in the tube wake, while if the trailing edge of the DWLs protrudes from the tube wake, heat transfer enhancement is verified.

Figure 5-13 and Figure 5-14 show the temperature profiles for GEO$_1$ and GEO$_2$, and for both Reynolds numbers. Furthermore, these figures compare the temperature profiles for the investigated geometries and their associated baseline geometry. On the louver regions, the temperature profiles can be considered similar at $Re_{Dh} = 120$ for each optimized geometry and its associated baseline geometry, while at $Re_{Dh} = 240$ there are very slight differences on temperature profiles only for the last two louvers. Moreover, at both Reynolds numbers the temperature profiles are quite different on a small region between louver and fin for GEO$_1$ and GEO$_2$ and baseline geometries, due to the fluid motion created by DWLs. However, this flow behavior is not sufficient to modify the temperature profiles on the most part of the louver array, and then we can conclude that there are no interactions between louver angle and DWLs parameters.

Finally, although these geometries can be considered a compound heat transfer enhancement technique, the contribution of the main effects seems to be much higher than that of the interaction effects for flat-tube multi-louvered fins with DWLs under laminar flow conditions.
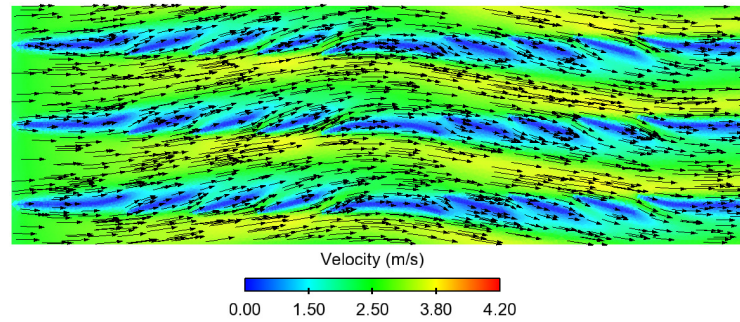
(a). $\phi = 15^\circ$
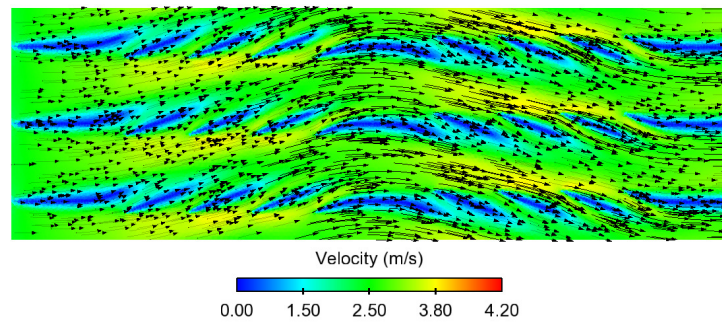
(b). $\phi = 20^\circ$
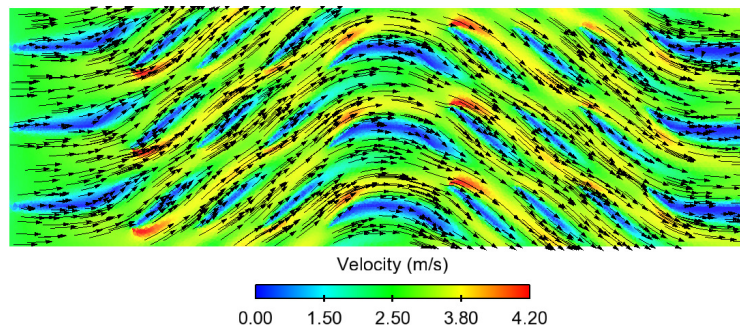
(b). $\phi = 40^\circ$

Figure 5-12 Velocity distribution and streamline contours for (a) $\phi = 15^\circ$ **, (b)** $\phi = 20^\circ$ **and (c)** $\phi = 40^\circ$ **at the mid-plane (** $F_P/F_H = 0.23$ **).**
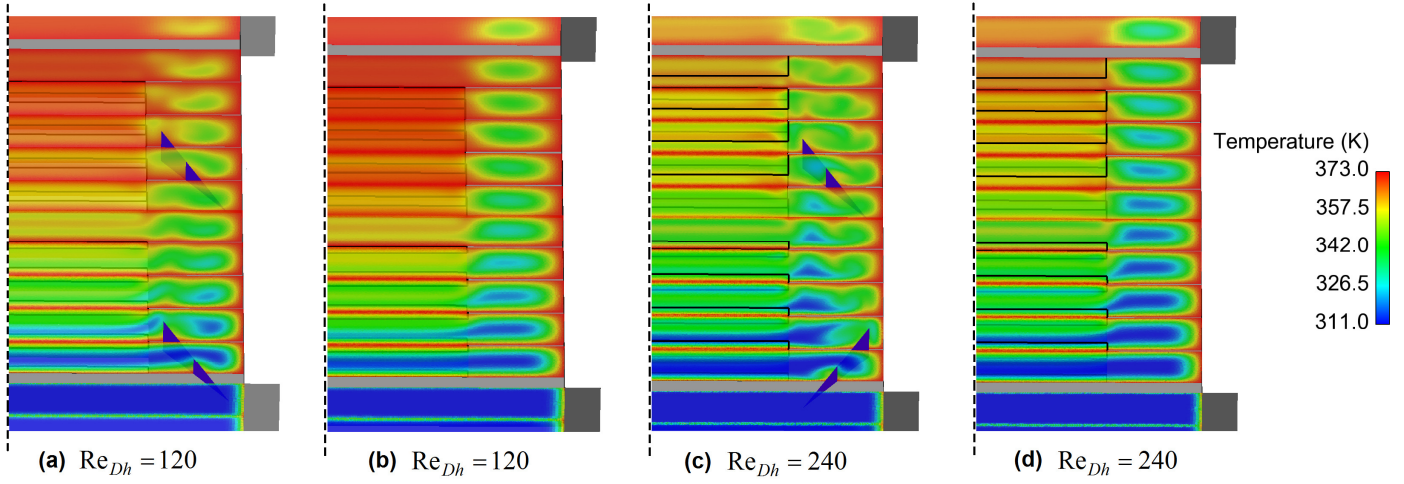
Figure 5-13 Temperature profiles at different cross sections for the GEO$_1$ and baseline geometry: (a) GEO$_1$ with $\phi = 32^\circ$ and $\theta_1 = \theta_2 = 45^\circ$; (b) Baseline geometry with $\phi = 32^\circ$; (c) GEO$_1$ with $\phi = 29^\circ$, $\theta_1 = -45^\circ$ and $\theta_2 = 45^\circ$; (d) Baseline geometry with $\phi = 29^\circ$.
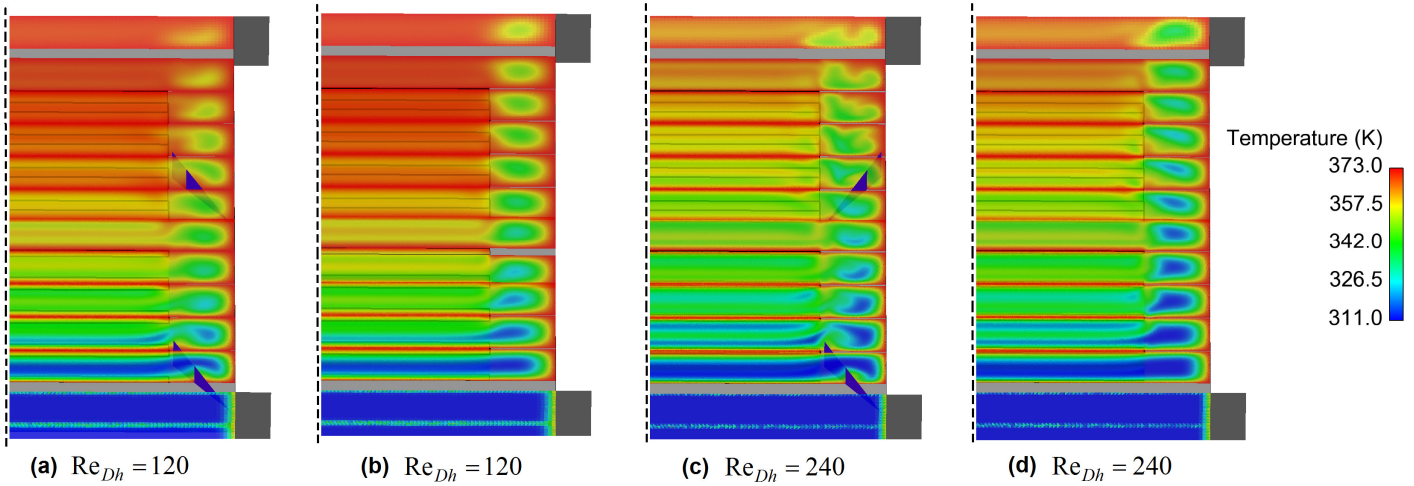
Figure 5-14 Temperature profiles at different cross sections for the GEO$_2$ and baseline geometry: (a) GEO$_2$ with $\phi = 32^\circ$ and $\theta_1 = \theta_2 = 45^\circ$; (b) Baseline geometry with $\phi = 32^\circ$; (c) GEO$_2$ with $\phi = 43^\circ$, $\theta_1 = 45^\circ$ and $\theta_2 = -45^\circ$; (d) Baseline geometry with $\phi = 43^\circ$.

5.3 Surrogate-based optimization

The objective function and design variables are firstly defined for the optimization procedure. The design space is then built by using Latin Hypercube Sampling, and the values of j are calculated using these design points. Finally, the ANN is trained and the optimization procedure is sought out by using NSGA-II. At the end of the optimization process, the highest value of j, called *predicted values*, is run on Fluent software (called *truth values*) and both j values are compared, in order to verify the accuracy of the surrogate model.

Thus, the optimization problem becomes:

GEO$_1$:
Find : ϕ, θ_1, θ_2, x_1, x_2
to Maximize : j
subject to :
$15^\circ \leq \phi \leq 45^\circ$
$-45^\circ \leq \theta_1 \leq 45^\circ$
$-45^\circ \leq \theta_2 \leq 45^\circ$
$1.090 \text{ mm} \leq x_1 \leq 4.060 \text{ mm}$
$6.240 \text{ mm} \leq x_2 \leq 9.210 \text{ mm}$

GEO$_2$:
Find : ϕ, θ_1, θ_2, x_1, x_2
to Maximize : j
subject to :
$15^\circ \leq \phi \leq 45^\circ$
$-45^\circ \leq \theta_1 \leq 45^\circ$
$-45^\circ \leq \theta_2 \leq 45^\circ$
$0.980 \text{ mm} \leq x_1 \leq 4.170 \text{ mm}$
$6.130 \text{ mm} \leq x_2 \leq 9.320 \text{ mm}$

In order to select the most accurate ANN surrogate model, neurons on hidden layer ranging from 1 to 50 are evaluated and the network configuration that provides the most accurate parameters for Colburn factor prediction is chosen. Table 5-1 presents the results and the network configurations for both lower and higher Reynolds numbers. The results have indicated that the model accuracy of the ANN, which is assessed by those three error measures shown on item 4.5, is in accordance with the suggested values from Forrester and Keane (2009) and Giunta (1997).

Table 5-1
Parameters of the surrogate model selection

	GEO$_1$		GEO$_2$	
	$Re_{Dh} = 120$	$Re_{Dh} = 240$	$Re_{Dh} = 120$	$Re_{Dh} = 240$
Network configuration	5-5-1	5-4-1	5-4-1	5-13-1
Number of hidden neuron	5	4	4	13
Number of hidden layers	1	1	1	1
Training data set	137 samples	137 samples	137 samples	137 samples
Testing data set	33 samples	33 samples	33 samples	33 samples
RMSE	0.91%	1.06%	0.65%	0.79%
Maximum absolute error	2.61%	2.11%	1.84%	2.32%
R^2	0.93	0.95	0.97	0.96

The optimized solutions for the lower and the higher Reynolds numbers for GEO$_1$ and GEO$_2$ are shown in Table 5-2. The maximum predicted values of Colburn factor for GEO$_1$ found by optimization procedure for the lower and the higher Reynolds numbers are 0.1625 and 0.1083, respectively; *truth values* are 0.1619 and 0.1082. Based on this, the absolute errors between *truth* and *predicted values* for the lower and the higher Reynolds number are 0.41% and 0.09%, respectively. Table 5-2 also presents the values of j for the respective baseline geometry with the same louver angle of the optimized solution for both Reynolds numbers in order to facilitate the evaluation of the heat transfer performance of this compound enhancement technique.

The maximum GEO$_2$ *predicted* values of j from the optimized solution for the lower and the higher Reynolds numbers are 0.1819 and 0.1183, respectively, and the *truth* values are 0.1785 and 0.1196. Thus, the absolute errors between *truth* and *predicted* values for the lower and the higher Reynolds number are 2.51% and 1.13%, respectively.

The configurations of DWLs are slightly different for both optimized solutions at the lower and the higher Re_{Dh}. For $Re_{Dh} = 120$ the aligned arrangement of DWL provides the highest heat transfer performance, while at $Re_{Dh} = 240$ the staggered arrangement provides the highest heat transfer. The angles of attack of the DWLs

found by the optimization procedure are exactly on the limits of the range. Furthermore, all DWLs are placed very close to their streamwise position (lower bound limits), i. e, the vortices generated by DWLs located more upstream propagate further downstream, which is accordance to previous results of Zhu et al. (2011), Wu and Tao (2008) and He et al.(2012). The optimized solutions present different louver angles for both type of geometry and Reynolds numbers, except for GEO_1 and GEO_2 at $Re_{Dh} = 120$, which presents the same value of the louver angle.

As the DWL angles of attack contribute to increase the heat transfer and they are placed on staggered and inline arrangements (as function os Reynolds numbers), a cross-check of the DWL arrangements become important to verify if the optimization procedure really found the best DWL arrangements. Table 5-3 and Table 5-4 present all available DWL arrangements which can be expected to provide the maximum Colburn factor, for GEO_1 and GEO_2, respectively. From inspection of these tables, the maximum Colburn factors found by the surrogate-based optimization procedure (in bold letters) are higher than those from the other arrangements.

Table 5-2
Optimized solution and baseline geometry for $Re_{Dh} = 120$ **and** $Re_{Dh} = 240$

Geometry	Re_{Dh}	ϕ	θ_1	θ_2	x_1	x_2	j	f
GEO_1 Optimized solution	120	32º	45º	45º	1.09 mm	6.27 mm	0.1619	0.7047
	240	29º	-45º	45º	1.12 mm	6.24 mm	0.1082	0.4387
GEO_1 Baseline geometry	120	32º	-	-	-	-	0.1335	0.5653
	240	29º	-	-	-	-	0.0876	0.3210
GEO_2 Optimized solution	120	32º	45º	45º	0.98 mm	6.15 mm	0.1785	0.7540
	240	43º	45º	-45º	0.98 mm	6.13 mm	0.1196	0.6298
GEO_2 Baseline geometry	120	32º	-	-	-	-	0.1573	0.6266
	240	43º	-	-	-	-	0.1034	0.5091

Based on previous screening analysis, the interaction effects between louver angle and DWL parameters can be neglected. Thus, it is expected that the optima louver angles should be very close to those ones which provides the highest Colburn factor

for the respective baseline geometry. From inspection of Figure 5-15 for GEO_1 and GEO_2 baseline geometries, it is clear that there is a large range where the maximum value of j can be found. Moreover, the maximum variation on Colburn factor on the four highlighted regions is less than 1%. Thus, the surrogate-based optimization used herein can be considered excellent, since the optima louver angles (Table 5-2) are very close to those louver angles which provide the highest Colburn factors in the baseline geometries (Figure 5-15).

Table 5-3
Different arrangements of DWLs – GEO_1

Re_{Dh}	θ_1, θ_2	j
	45º, 45º	**0.1619**
120	45, -45º	0.1568
	-45º, 45º	0.1586
	-45º, -45º	0.1530
	-45º, 45º	**0.1082**
240	45º, -45º	0.1062
	45º, 45º	0.1069
	-45º, -45º	0.1044

Table 5-4
Different arrangements of DWLs – GEO_2

Re_{Dh}	θ_1, θ_2	j
	45º, 45º	**0.1785**
120	45º, -45º	0.1743
	-45º, 45º	0.1778
	-45º, -45º	0.1725
	45º, -45º	**0.1196**
240	-45º, 45º	0.1188
	45º, 45º	0.1173
	-45º, -45º	0.1167

(a) GEO$_1$ baseline geometry   (b) GEO$_2$ baseline geometry

Figure 5-15 Variation of the global Colburn factor for the baseline geometries as function of louver angle and Reynolds number and expected regions where the GA can find the maximum values of louver angle.

The overall heat transfer enhancement provided by the optimized solutions at $Re_{Dh} = 120$ and $Re_{Dh} = 240$, in comparison with the respective baseline geometry can be seen on Table 5-5. The heat transfer performance is increased when the DWLs are placed on flat-tube louvered fin heat exchangers. At $Re_{Dh} = 120$ the heat transfer is augmented 21% and 13% with associated pressure loss of 24% and 20% for GEO$_1$ and GEO$_2$, while at $Re_{Dh} = 240$ the heat transfer is augmented 23% and 15% with associated pressure loss of 36% and 23%. These results have indicated that for very low Reynolds numbers, the combination of multi louvered fins and delta-winglet vortex generators can be regarded a promising strategy to enhance heat transfer with associated low pressure losses.

Sanders and Thole (2006) reported heat transfer enhancement of less than 4% for Reynolds number of 230 and Lawson and Thole (2008) reported just 3% for Reynolds number of 216, which are much lower than results provided by optimized solutions from the present work. These heat transfer augmentations are related to their baseline geometries (multilouvered fin without DWLs).

Table 5-5
Heat transfer enhancement and pressure drop for optimized solutions compared to the respective baseline geometry

Geometry	Re_{Dh}	$j_{optimized}/j_{baseline}$	$f_{optimized}/f_{baseline}$
GEO$_1$	120	1.2127	1.2466
	240	1.2352	1.3667
GEO$_2$	120	1.1348	1.2033
	240	1.1567	1.2370

5.4 Flow pattern and heat transfer characteristics

As already investigated that there are no relevant interactions between louver angle and DWL parameters, the flow pattern and heat transfer characteristics from optimized solutions can be evaluated separately.

The heat transfer coefficient on multilouvered fins is sensitive to the hydrodynamics of the flow pattern around the louver and to the absence or presence of the thermal wakes in the vicinity of the louvers.

In general, for low air flow velocity, the global motion of the fluid is duct-directed, which is characterized by very poor heat transfer performance. Also at low Reynolds numbers, the thermal wake of each upstream louver normally surrounds the downstream louver of the same fin and, as consequence, low heat transfer is observed. This flow pattern is called intra-fin thermal wake effect. As the air flow velocity is increased, the flow undergoes a transition from duct-directed flow to louver-directed flow, which normally presents high heat transfer performance. At louver-directed flow, the thermal wakes between fin rows interfere to each other; this behavior is known as inter-fin thermal wake effect. According to Zhang and Tafti (2003), large louver angles, small fin pitches, thin louvers and large louver pitches are conducive to louver-directed flow. However, as shown by Tafti et al. (2004), at Reynolds numbers higher than 100 the increasing of the louver angle above a certain value has a detrimental effect on heat transfer. The louver angle that produces the

maximum heat transfer coefficient depends on several flow and geometry conditions (Kim and Bullard (2002), Tafti et al. (2004), Tafti et al. (2001)).

From inspection of Figure 5-16 and Figure 5-17, the optimized solutions for both Re_{Dh} show that air flows straight over the louvers even for very low Reynolds numbers. In this case, the fluid particles travel larger distances through the fin, resulting an increase of heat exchange. Moreover, from inspection of Figure 5-18 and Figure 5-19, the thermal wake of the upstream louvers impinges the rear face of downstream louvers (inter-fin thermal wake effect) and cold free-stream fluid flows in the vicinity of the louvers, increasing the heat transfer.

(a) GEO$_1$ optimized solution at $Re_{Dh} = 120$ (b) GEO$_1$ optimized solution at $Re_{Dh} = 240$
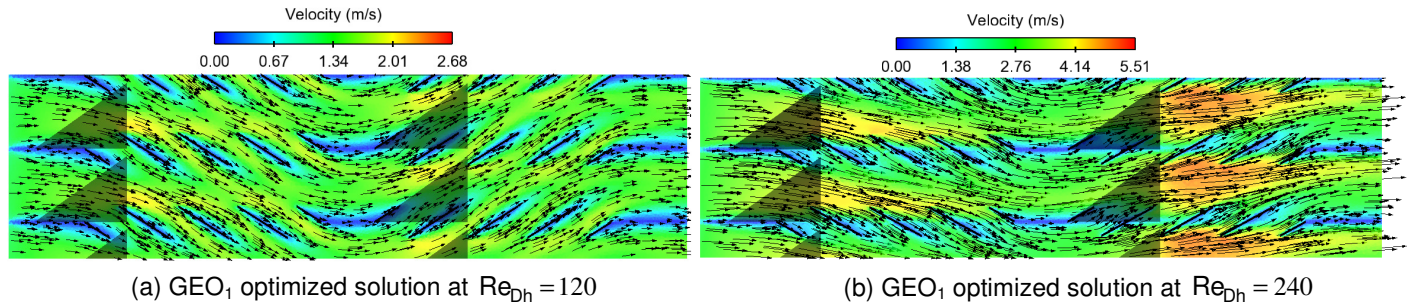
Figure 5-16 Velocity distribution and streamline contours for the GEO$_1$ optimized solutions with $Re_{Dh} = 120$ **and** $Re_{Dh} = 240$ $\left(F_P/F_H = 0.23 \right)$**.**

(a) GEO$_2$ optimized solution at $Re_{Dh} = 120$ (b) GEO$_2$ optimized solution at $Re_{Dh} = 240$
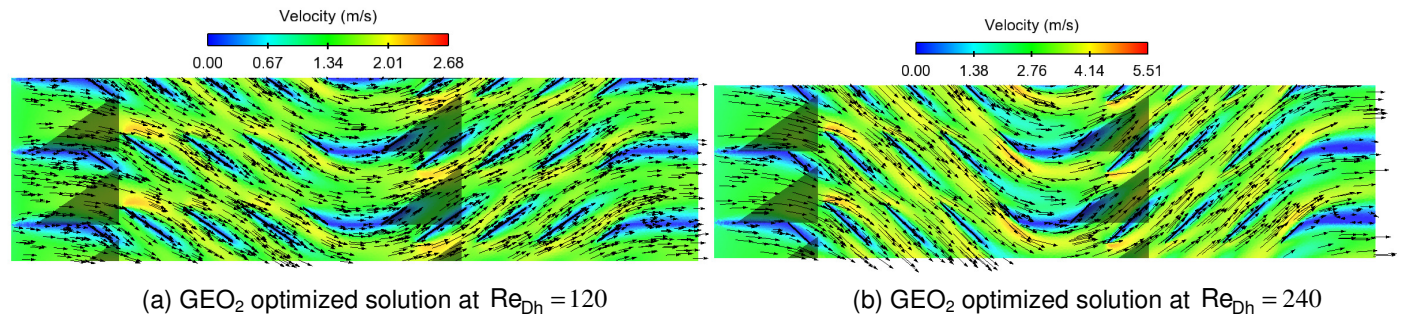
Figure 5-17 Velocity distribution and streamline contours for the GEO$_2$ optimized solutions with $Re_{Dh} = 120$ **and** $Re_{Dh} = 240$ $\left(F_P/F_H = 0.23 \right)$**.**

(a) GEO_1 optimized solution at $Re_{Dh} = 120$

(b) GEO_1 optimized solution at $Re_{Dh} = 240$
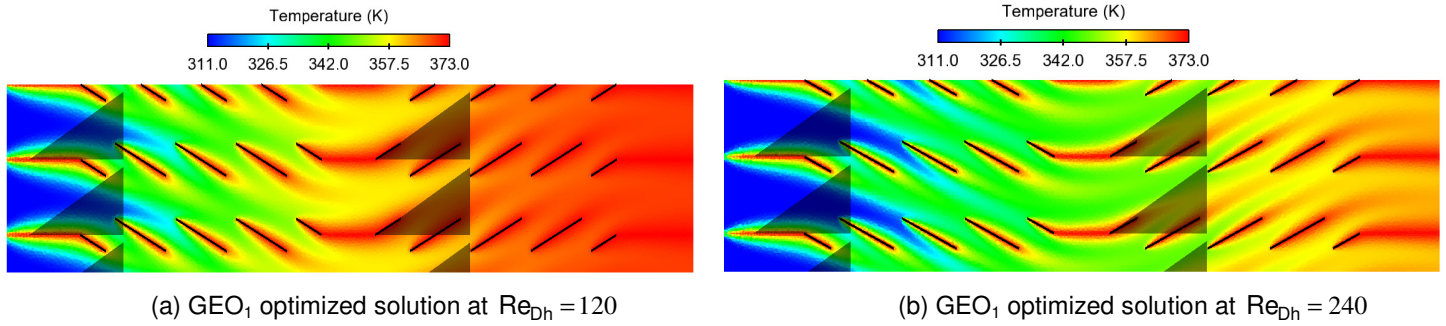
Figure 5-18 Temperature contours for the GEO_1 optimized solution with $Re_{Dh} = 120$ and

$Re_{Dh} = 240$ $(F_P/F_H = 0.23)$**.**

(a) GEO_2 optimized solution at $Re_{Dh} = 120$

(b) GEO_2 optimized solution at $Re_{Dh} = 240$
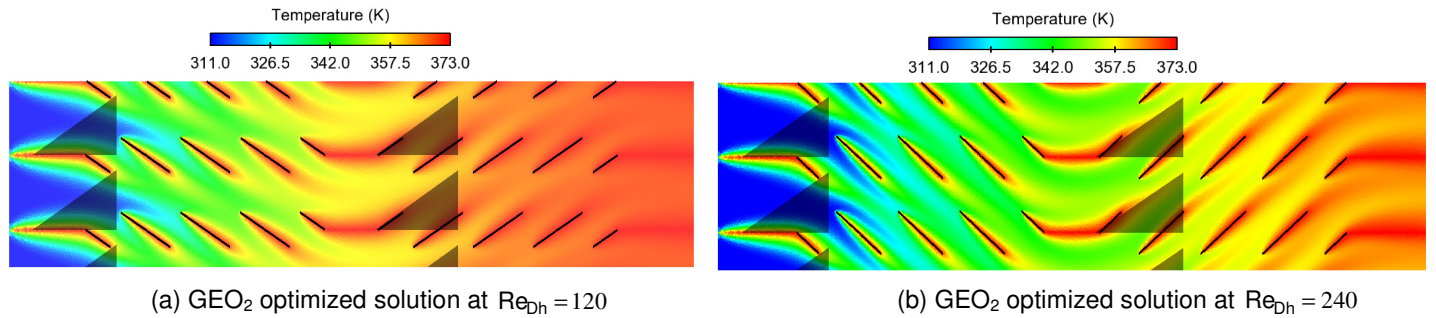
Figure 5-19 Temperature contours for the GEO_2 optimized solution with $Re_{Dh} = 120$ and

$Re_{Dh} = 240$ $(F_P/F_H = 0.23)$**.**

Figure 5-20 and Figure 5-21 show the temperature profiles at different cross-sections for GEO1 and GEO2 optimized solutions and the respective baseline geometries. The longitudinal vortices have significant influence on the temperature distribution on the fin-plate region (or non-louvered region) due to the mixing of the hot fluid adjacent to the channel walls and the cold fluid in the middle of the channel. Although the DWLs do not practically change the span-average temperature in the most part of the louver array for both Reynolds numbers and both optimized geometries, small changes of temperature profiles on the region between louvers and DWLs can be observed in comparison with the baseline geometry, especially on staggered arrangements. Figure 5-22 and Figure 5-23 show the flow pattern characteristics of this compound enhancement technique. These figures show typical results of the velocity contours and streamlines at different cross sections in the flow direction:

$F_D = 1.15$ mm, $F_D = 2.95$ mm, $F_D = 4.75$ mm, $F_D = 6.45$ mm and $F_D = 8.25$ mm. The generation and transport of the longitudinal vortices, eventual flattening of the vortex cores and their lateral movement towards the side boundaries are evident on these figures. At $F_D = 1.15$ mm and $F_D = 6.45$ mm the longitudinal vortices are generated from leading edges of the first and second rows of DWLs due to pressure difference between front and rear sides of the DWLs. At $F_D = 2.95$ mm, $F_D = 4.75$ mm and $F_D = 8.25$ mm, part of louver-directed flow is deflected towards non-louvered region, increasing the strength of the swirling flow. This flow behavior is because the flow resistance in the non-louver region is obviously less than the resistance due to the louvers. Especially at $F_D = 4.75$ mm the fluid motion close to the louver region is not a swirling motion due to the DWLs but due to the louver-directed flow, as can be seen in Figure 5-24. This fluid motion squeezes the longitudinal vortices from first row of DWLs, deflecting the longitudinal vortices towards tube walls. It is important to note that this type of analysis for flat-tube multiouvered fin with DWLs have never been shown before.

The longitudinal vortices generated by first and second rows of DWLs for inline arrangements ($Re_{Dh} = 120$) have the same rotation direction and their effects are aggregated after the second row of DWLs. When the DWLs are placed on staggered arrangements ($Re_{Dh} = 240$), the longitudinal vortices from first and second rows of DWLs present reversed rotation direction and thus the longitudinal vortices are not aggregated.

Figure 5-25 shows the streamlines and the air flow velocity around DWLs. The main vortices are formed by flow separation at the leading edge of the DWLs, while the corner vortices are formed by the deformation of the near vortex lines at the pressure side of the DWLs. It is notorious that the strength of the corner vortices is much weaker than of the main vortices. For GEO_1 optimized solutions, the corner vortex is normally carried out downstream of the fin by the main vortex, while for GEO_2 optimized solutions the corner vortex behaves differently for the first and second rows of DWLs. Part of the corner vortex formed by the first row of DWLs is mixed with the main vortex and another part is carried out by the louver-directed flow, while the corner vortex formed by the second row is fully mixed with the main vortex. The part

of the corner vortex from the first row of DWLs carried out by louver-directed flow is deflected towards the second row of DWLs from upstream turnaround louver and the second half of the louver array, and then it is mixed with the main vortex from the second row of DWLs. However, the heat transfer enhancement due to this flow pattern seems to be as effective as when the corner vortex is fully mixed in the main vortex, as occurred on GEO_1 optimized solutions. These flow mechanisms were never observed before.

Comparing the air flow velocity showed on Figure 5-25, although the velocity magnitude of the longitudinal vortices is relatively lower, the secondary flow is very strong and persistent downstream. The main vortex presents very low velocity when formed and it is accelerated downstream. The longitudinal vortices of the incoming flow is accelerated after the second row of DWLs, which works such as "boosters", corroborating with researches from Tiggelbeck et al (1993) and Russel (1982).

In order to quantitatively analyze the heat transfer enhancement from optimized solutions, Figure 5-26 (a) and (b) shows the span-average distribution of the Colburn factor along the main flow direction for the optimized solutions and their respective baseline geometries at $Re_{Dh} = 120$ and $Re_{Dh} = 240$, respectively. The heat transfer is very high at the inlet region and decreases gradually along the flow direction until a specified position immediately after the inlet for all geometries. For both Reynolds numbers and all geometries, the span-average Colburn factor abruptly increases in front of the second louver due to the acceleration and deflection of the fluid flow and reaches a maximum value at the first half of the array and then decreased up to the exit of the fin for all investigated geometries. However, for the optimized solutions the span-average Colburn factor increases again after the second row of DWLs and the Colburn factor on that region has practically the same order of magnitude of the maximum Colburn factor at the first half of the array, for both Reynolds numbers.

Since the louver angles for baseline and optimized geometries are exactly the same, the increasing of heat transfer is necessarily due to the DWLs. By comparison between optimized solution and its respective baseline geometry, the difference of heat transfer up to the first half of the array is due to the longitudinal vortices from the first row of DWLs. From inspection of Figure 5-25, when the oncoming flow impinges the second row of DWLs, the longitudinal vortices are formed and both oncoming

flow and longitudinal vortices from the first row of DWLs are accelerated. Thus, the increasing of heat transfer after the second row of DWLs is due to both incoming flow and longitudinal vortices from first row of DWLs, and longitudinal vortices formed by second row of DWLs.
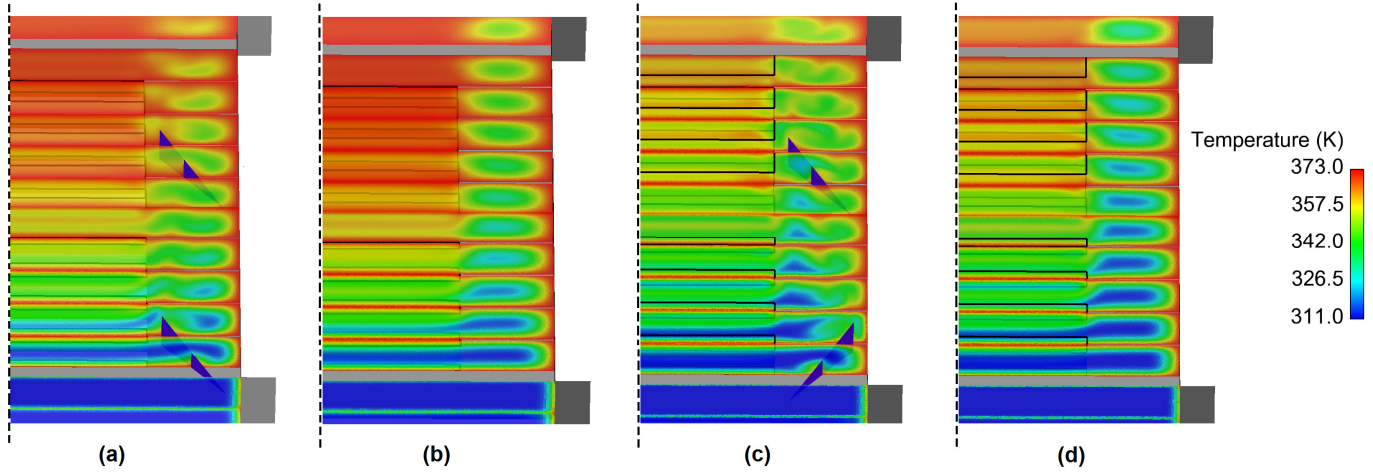
Figure 5-20 Temperature profiles at different cross sections for the GEO$_1$ and baseline geometry: (a) GEO$_1$ with $\phi = 32^\circ$ and $\theta_1 = \theta_2 = 45^\circ$; (b) Baseline geometry with $\phi = 32^\circ$; (c) GEO$_1$ with $\phi = 29^\circ$, $\theta_1 = -45^\circ$ and $\theta_2 = 45^\circ$; (d) Baseline geometry with $\phi = 29^\circ$.
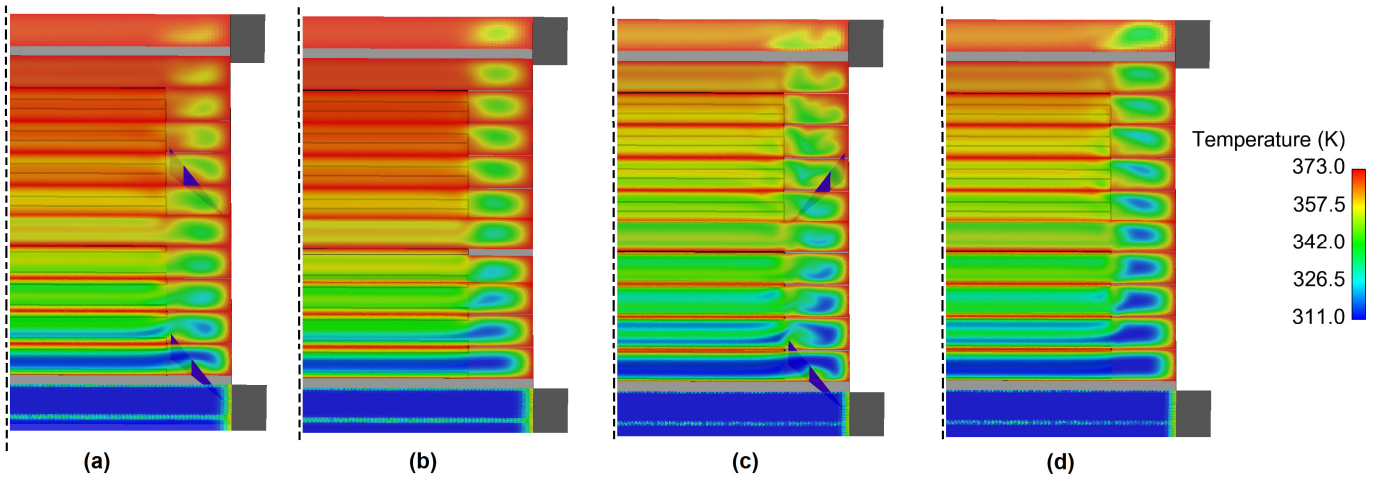
Figure 5-21 Temperature profiles at different cross sections for the GEO$_2$ and baseline geometry: (a) GEO$_2$ with $\phi = 32^\circ$ and $\theta_1 = \theta_2 = 45^\circ$; (b) Baseline geometry with $\phi = 32^\circ$; (c) GEO$_2$ with $\phi = 43^\circ$, $\theta_1 = 45^\circ$ and $\theta_2 = -45^\circ$; (d) Baseline geometry with $\phi = 43^\circ$.
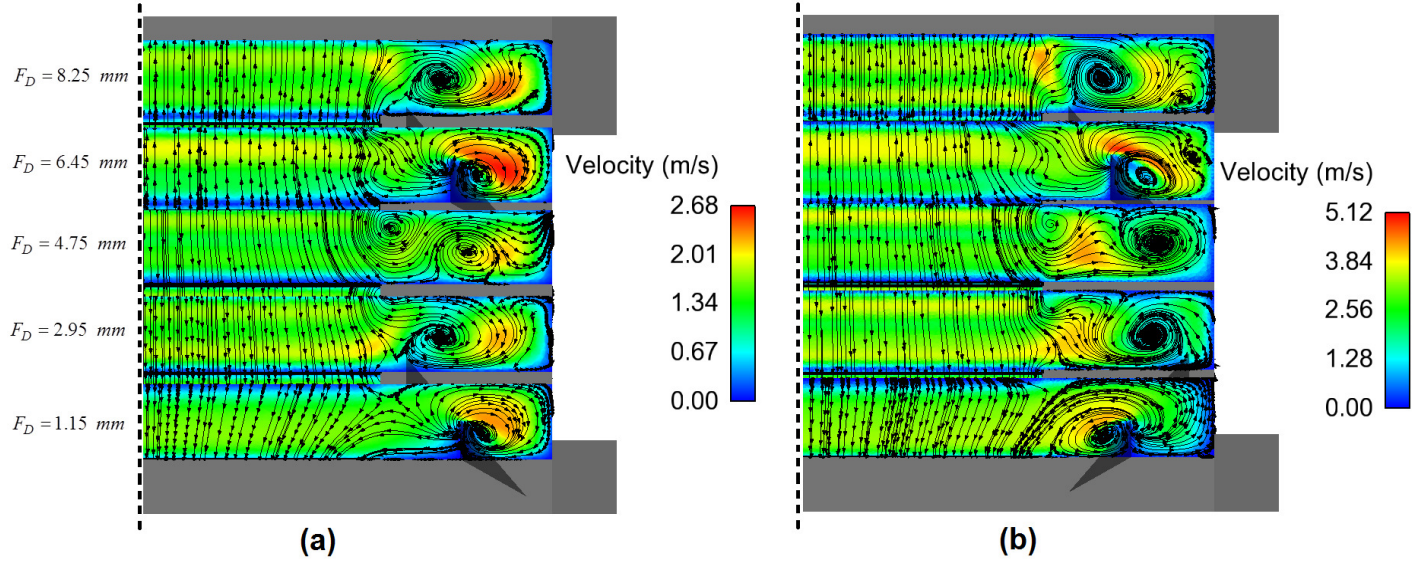
Figure 5-22 Velocity contours and streamlines generated by GEO$_1$ optimized solution at different cross sections: (a) $Re_{Dh} = 120$ **and (b)** $Re_{Dh} = 240$.
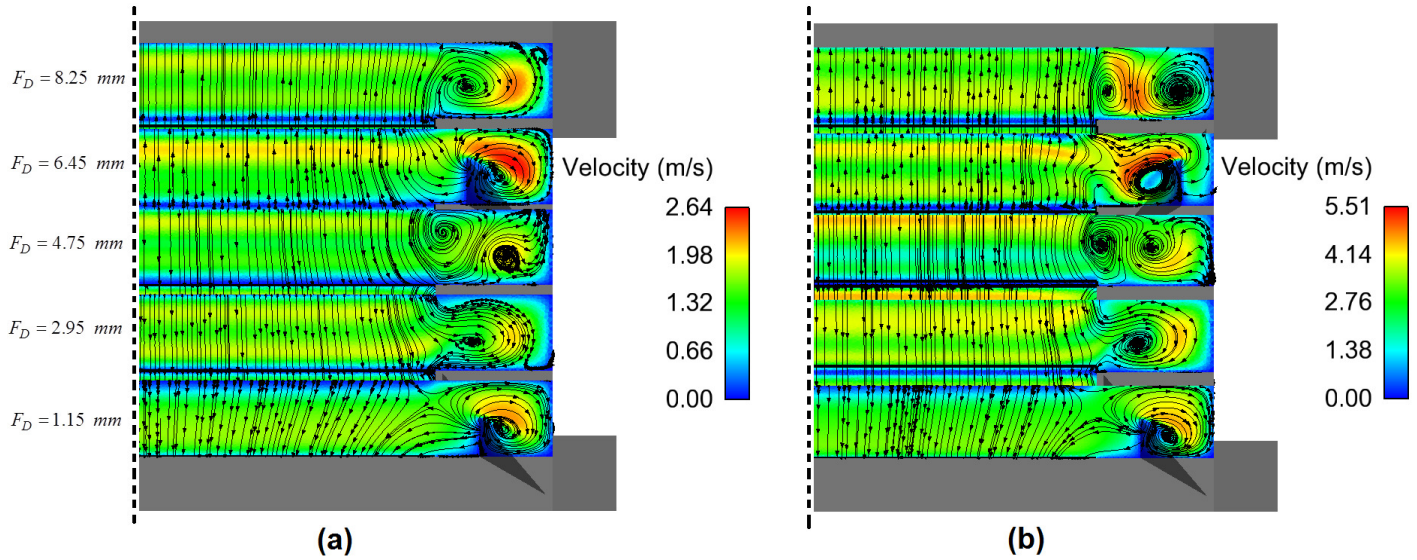
Figure 5-23 Velocity contours and streamlines generated by GEO$_2$ optimized solution at different cross sections: (a) $Re_{Dh} = 120$ **and (b)** $Re_{Dh} = 240$.

The Figures 5-27 and 5-28 show qualitatively the results of the local heat transfer coefficient for both GEO$_1$ optimized solution and baseline geometry for $Re_{Dh} = 120$ and $Re_{Dh} = 240$, respectively, while Figures 5-28 and 5-29 show the same analyses for GEO$_2$. The scale magnitude of the legend is adjusted in order to allow comparison

and to evidantiate the differences on heat transfer coefficient; the maximum values of the local heat transfer are not shown on these figures.
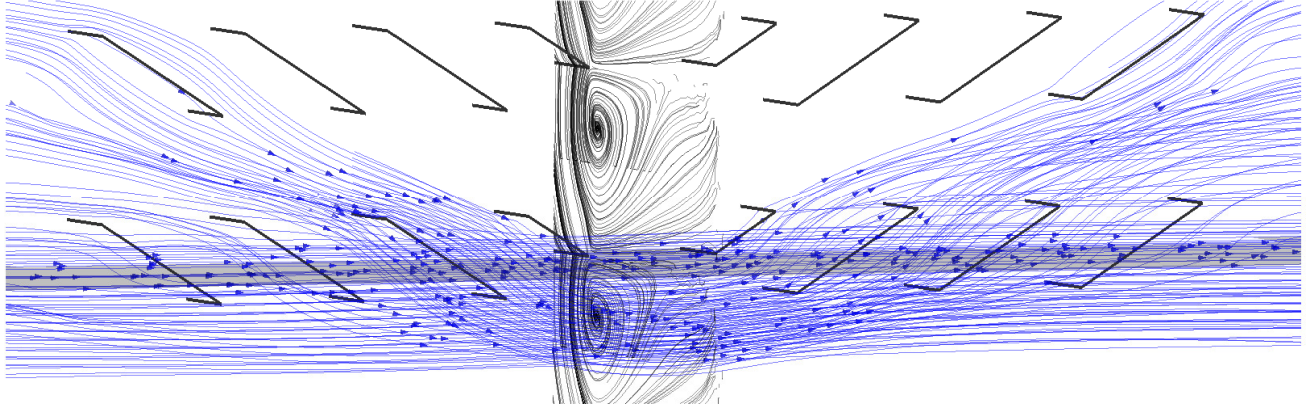
Figure 5-24 Fluid motion due to louver-direct flow at $F_D = 4.75$ mm **.**

Since a fixed temperature condition is applied at the walls (except on DWLs), the local heat transfer coefficient is calculated as

$$h_L = \frac{-K_f \left.\frac{\partial T}{\partial \xi}\right|_{\xi=0}}{(T_W - T_L)}$$ Eq.5-1

where

K_f is the thermal conductivity of the fluid (air)

$\left.\partial T / \partial \xi\right|_{\xi=0}$ is the temperature gradient normal to the wall

T_W is the wall temperature

T_L is the local fluid temperature
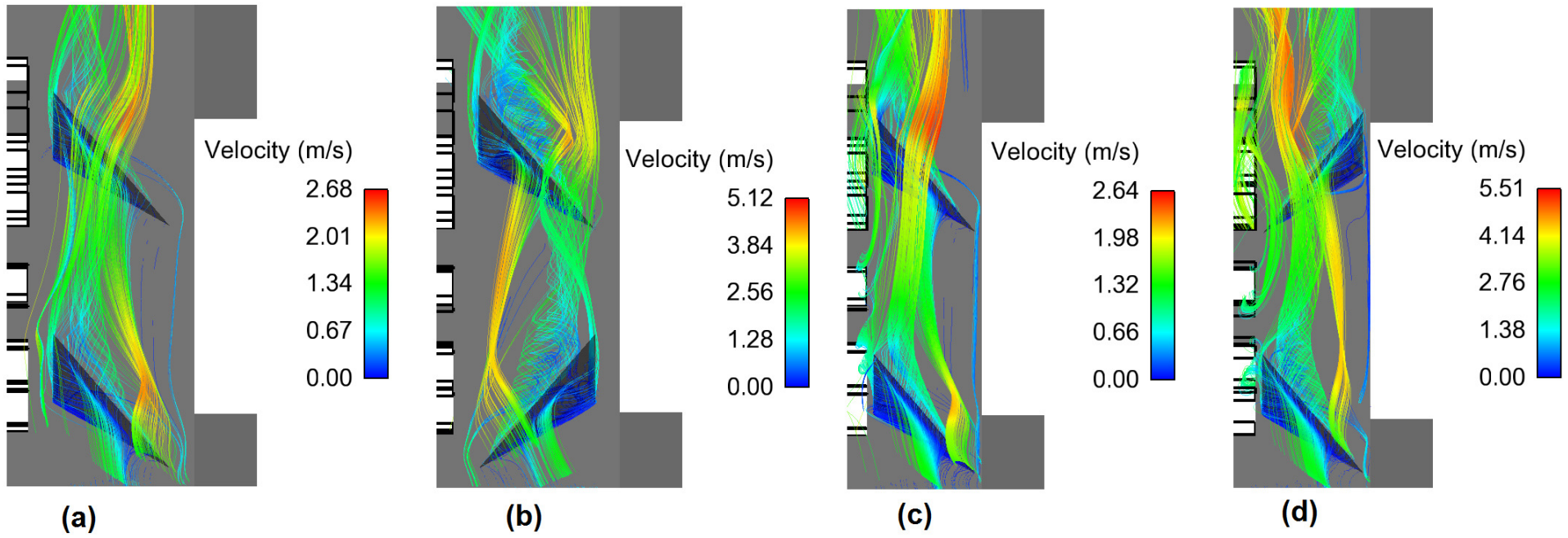
Figure 5-25 Streamlines showing the longitudinal vortices generated optimized solutions: (a) GEO$_1$ and $Re_{Dh} = 120$ **; (b) GEO$_1$ and** $Re_{Dh} = 240$ **; (c) GEO$_2$ and** $Re_{Dh} = 120$ **and; (d) GEO$_2$ and** $Re_{Dh} = 240$ **.**
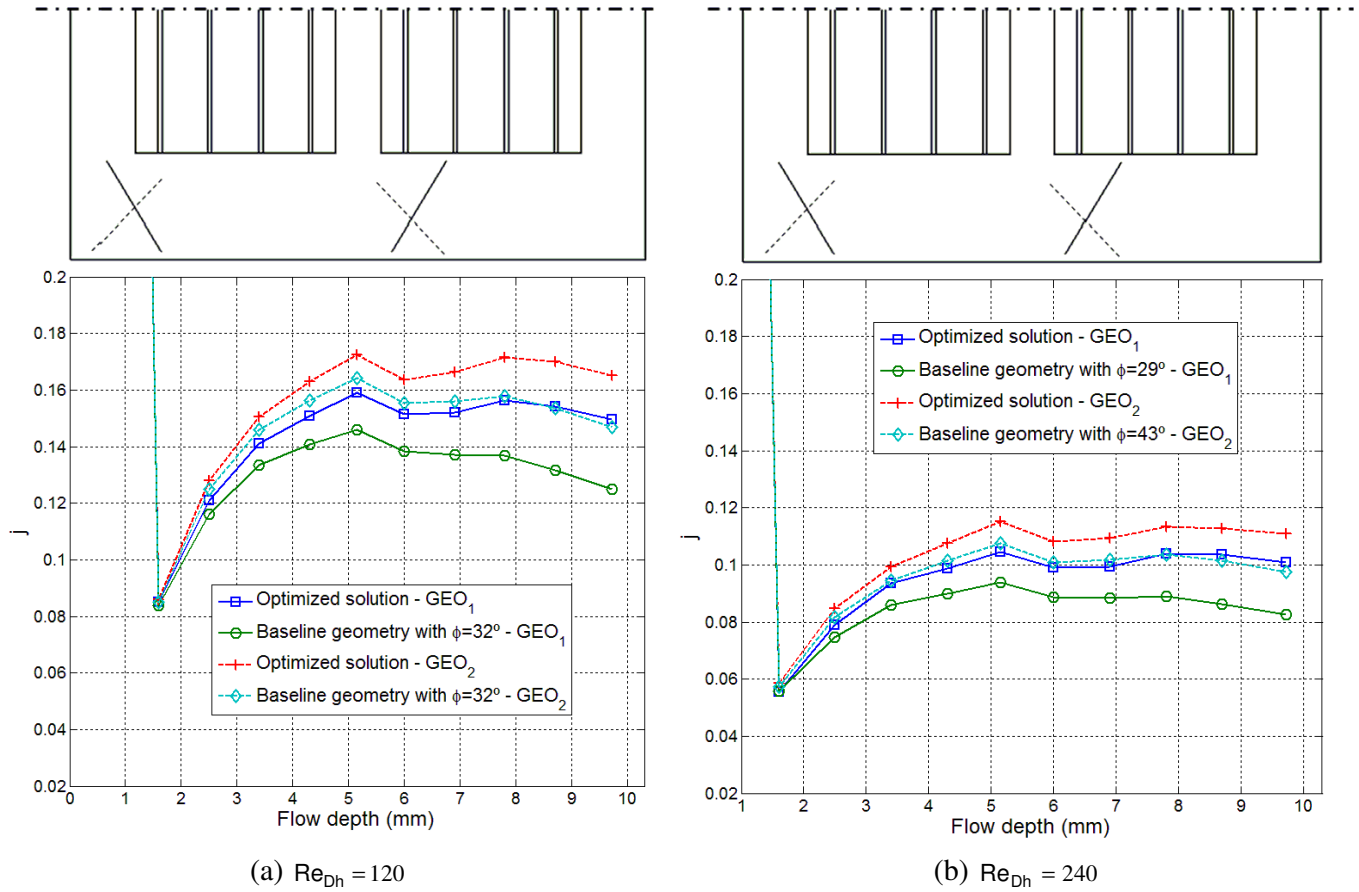
Figure 5-26 Distribution of span-average Colburn factor along the fin for GEO$_1$ and GEO$_2$ optimized solutions, and respective baseline geometries.

For all baseline and optimized geometries, it is observed a sharp increase in the local heat transfer coefficient on the lead edge of each louver and on the entrance of the fin and then it decreases rapidly on the flow direction. This occurs due to the development of the thermal boundary layers on the louver and fin surfaces. The local heat transfer is much higher on the first half than the second half. This is because as the air flow moves downstream, the temperature difference is considerably smaller.

In addition, on the louvered regions the local heat transfer is higher on the second louver for all geometries. This relevant heat transfer enhancement behavior is because the boundary layers and the thermal wakes that form at the leading edge of the second louver are thinner than the other louvers.

The presence of DWLs changes drastically the local heat transfer in the non-louvered and tube regions. On the lessened heat transfer zones (tube and second half of the fin), the addition of the DWLs increase the local heat transfer, especially for $Re_{Dh} = 240$. Furthermore, this heat transfer enhancement is more pronounced on the first row of DWLs than on the second row of DWLs, and when the frontal area of the DWLs is higher (GEO_1). It is well known that larger DWLs disturb the boundary layer more effectively than smaller ones and provide better air flow mixing.

The heat transfer enhancement along the tube wall by using DWLs is achieved by re-direction of cooler flow towards the tube wall and by formation of longitudinal vortices that serve to enhance flow mixing and heat transfer along the tube wall. When the rear side of the DWLs are positioned close to the tube (Figures 5-28(a) and 5-30(a)), the local heat transfer on the tube wall is higher only on the "nozzle" region, which is formed by DWLs and tube wall, and decreases abruptly downstream.

On the other hand, if the tip of DWLs is close to the tube wall, two distinct behaviors are observed: (a) on the first row of DWLs, the local heat transfer increases on that region and then decreases gradually downstream, which is much more evident for $Re_{Dh} = 240$ and; (b) on the second row of DWLs, very small local heat transfer is verified, independently of the Reynolds numbers. In these cases, the heat transfer enhancement is due to both flow acceleration and longitudinal vortices formed by DWLs. These two distinct behaviors are because the longitudinal vortices formed on the first row of DWLs move towards tube wall while the longitudinal vortices from second row of DWLs tend to move towards the louver array, as shown before. On the louvered region, the local heat transfer coefficient calculated for optimized solutions and their baseline geometries behaves similarly, corroborating with previous screening analysis. Meanwhile, slight changes on local heat transfer are caused by DWLs only on the intersection of louvers and fin on the second half of array.
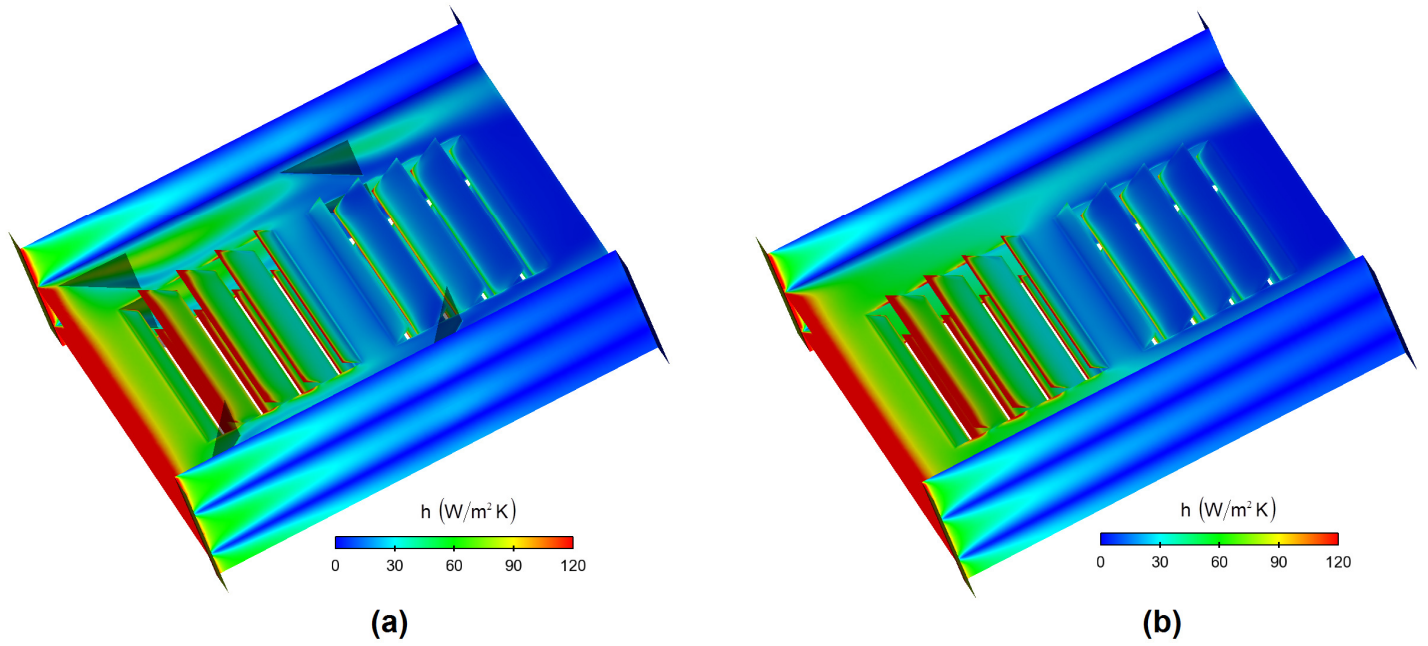
Figure 5-27 Local heat transfer coefficient for GEO$_1$ with $\mathrm{Re}_{Dh} = 120$: (a) Optimized solution and (b) Baseline geometry.
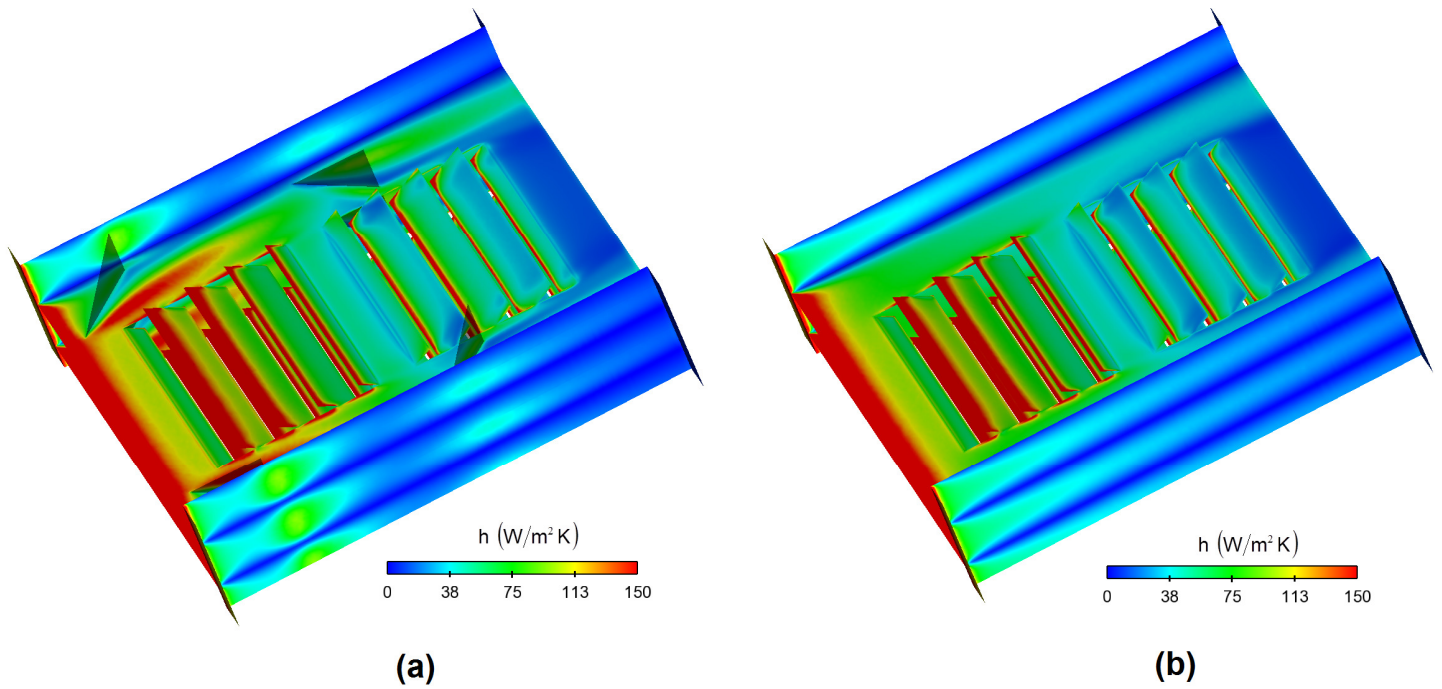
Figure 5-28 Local heat transfer coefficient for GEO$_1$ with $\mathrm{Re}_{Dh} = 240$: (a) Optimized solution and (b) Baseline geometry.
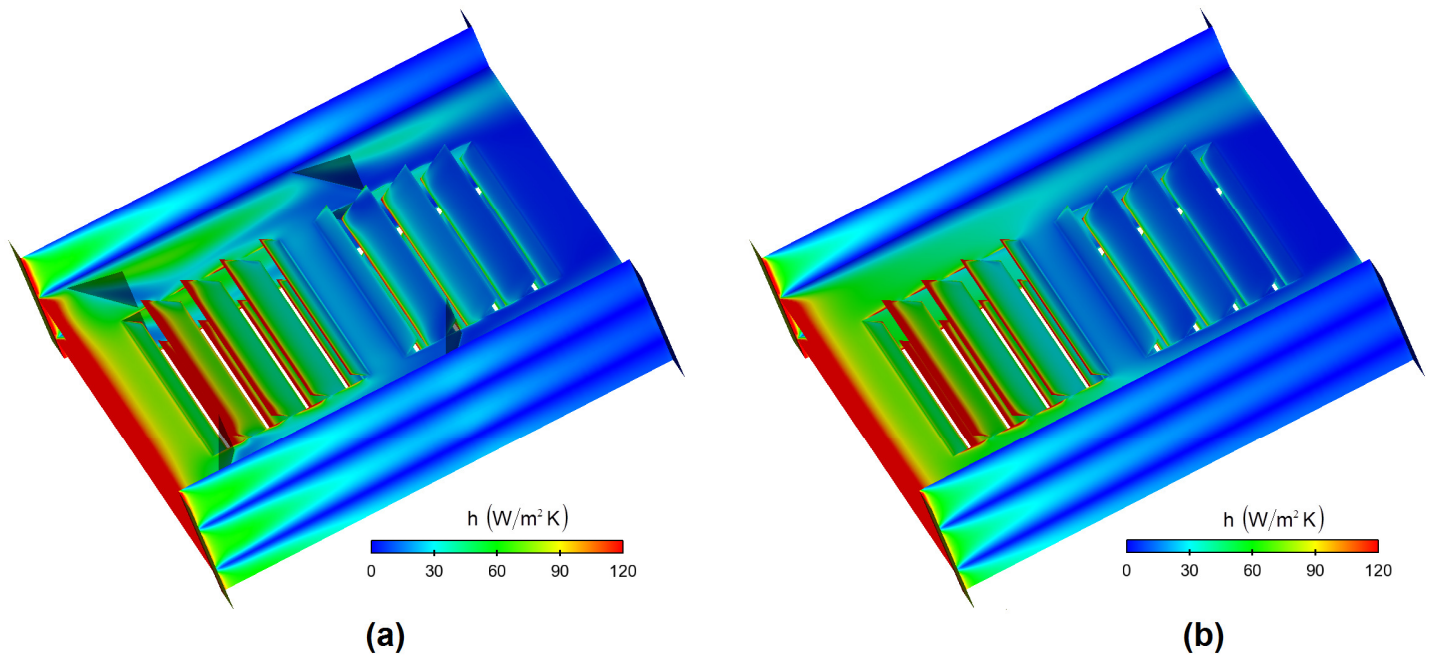
Figure 5-29 Local heat transfer coefficient for GEO$_2$ with $\mathrm{Re}_{Dh} = 120$: (a) Optimized solution and (b) Baseline geometry.
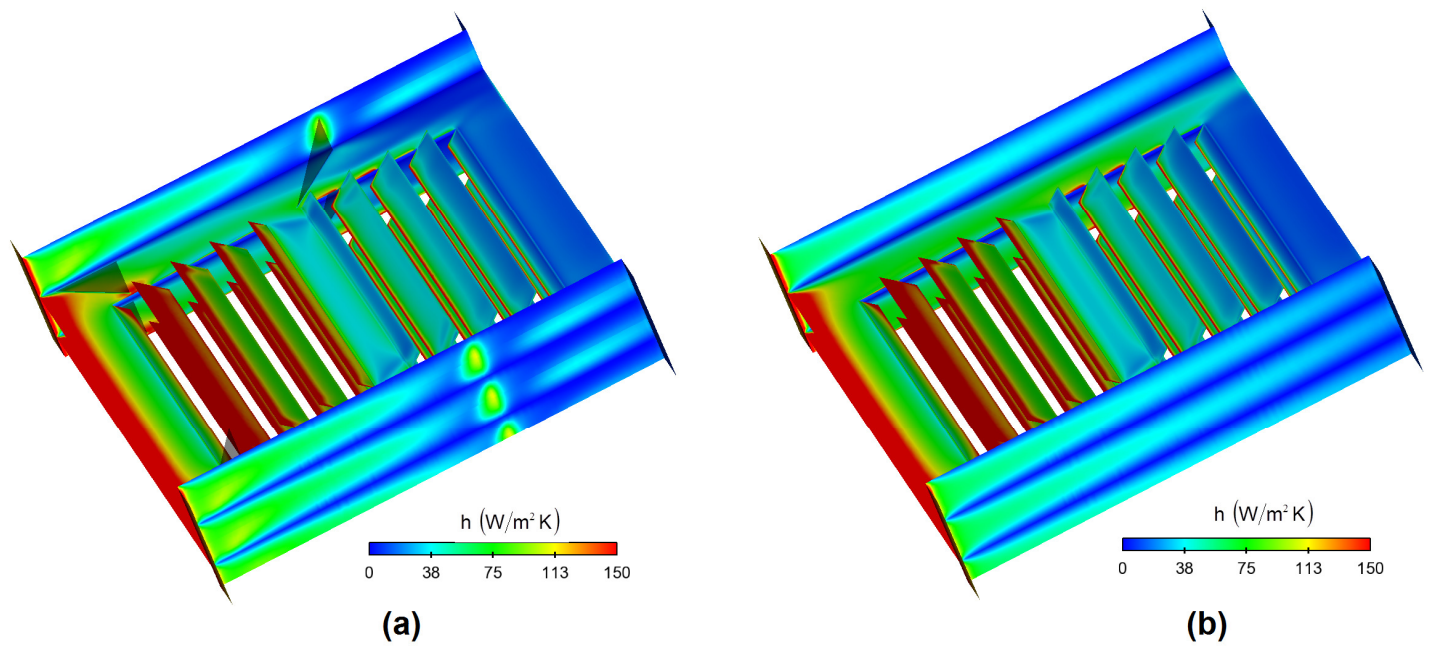
Figure 5-30 Local heat transfer coefficient for GEO$_2$ with $\mathrm{Re}_{Dh} = 240$: (a) Optimized solution and (b) Baseline geometry.

From Figure 5-31 (a) and (b), the introduction of DWLs resulted an increasing of pressure drop compared to the baseline geometries, mainly due to the additional form drag induced by DWLs. On the louver regions, the significant increase on pressure drop is also due to the form drag of the louvers. In few words, the form drag is related to the drag force due to pressure stress on the surface of the heat transfer enhancement device. The increasing of pressure drop on second row of DWLs is higher than on the first row. This occurs because the incoming flow to the second row of DWLs has higher vorticity and inhomogeneity than in the first row and the flow acceleration after the second row of DWLs. Moreover, as Reynolds number is increased, the flow becomes more louver-directed, which results on strong increase of pressure drop.

(a) $Re_{Dh} = 120$ (b) $Re_{Dh} = 240$
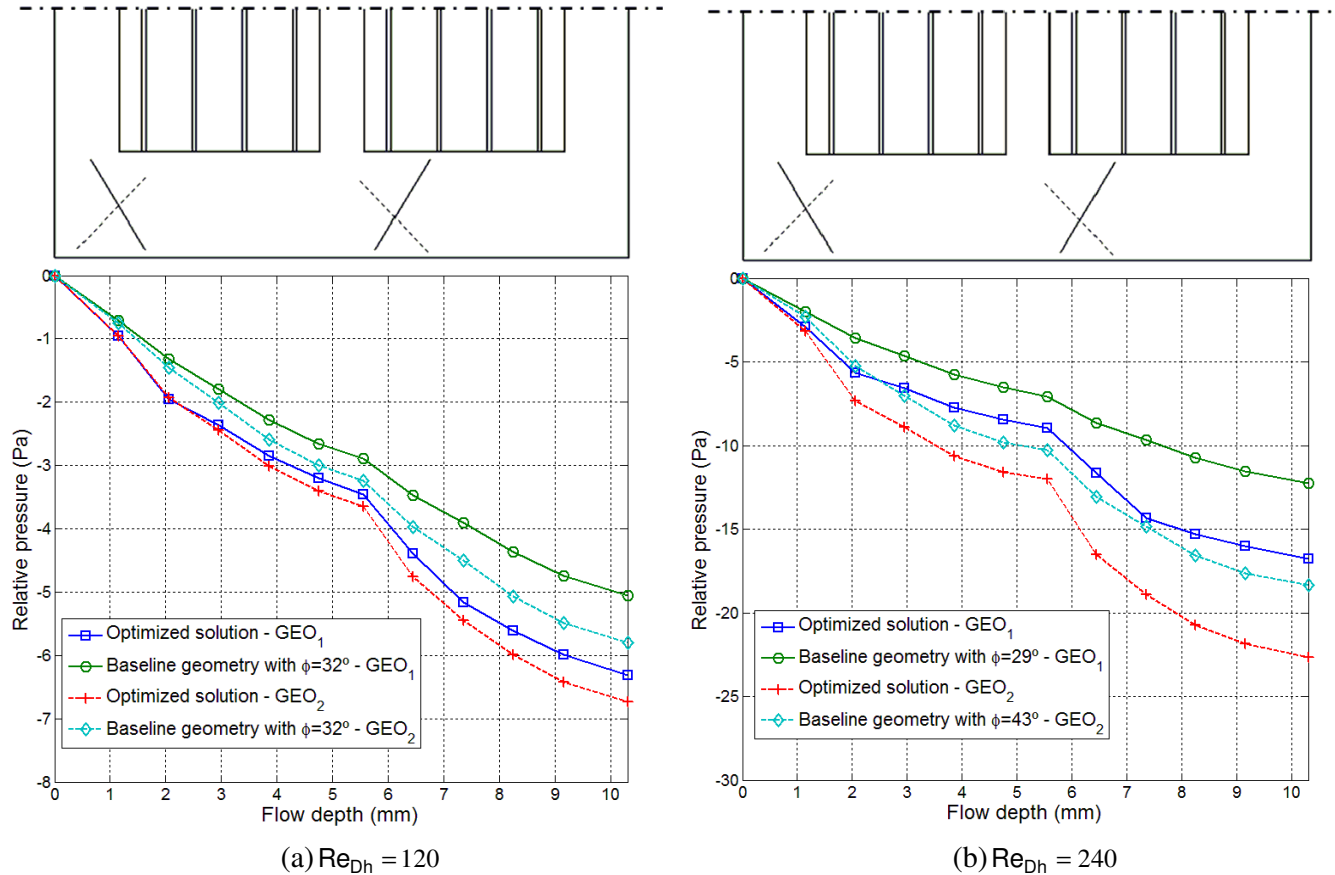
Figure 5-31 Distribution of span-average relative pressure of the GEO$_1$ and GEO$_2$ optimized solutions and respective baseline geometries along the main flow direction.

6 Conclusions and recommendations

6.1 Conclusion

This research has been focused on the use of flat-tube multilouvered fin compact heat exchangers combined with delta winglet vortex generators. Screening analysis of the input variables in terms of heat transfer and pressure drop, and heat transfer optimization of the proposed geometries were successfully completed.

A screening analysis of five parameters of multi-louvered fin heat exchanger with delta-winglet vortex generators was presented, taking into account the main and interaction effects on heat transfer and pressure drop, under laminar flow conditions. Two Reynolds numbers and two different geometries were investigated. Latin Hypercubes Sampling was used as DoE method to generate a random sample from some prior probability distribution of parameter space. The Smoothing Spline ANOVA methodology was used to run the analysis of variance and to evaluate the impact of the input parameters on heat transfer and pressure drop.

For both geometries and Reynolds numbers, the louver angle is the major contributor to the Friction factor; this behavior seems to be independent of the Reynolds number and type of geometry. No relevant interactions between the five input parameters were observed for the friction factor. In turn, the contribution of each parameter to heat transfer is strongly associated with the type of geometry and Reynolds number. For GEO_1 and $Re_{Dh} = 120$, the DWLs have moderate influence on heat transfer and, when the DWLs surface area is decreased (GEO_2), their effect on heat transfer is negligible. For $Re_{Dh} = 240$, the contribution of DWL parameters for GEO_1 is obviously higher than for GEO_2. Also at $Re_{Dh} = 240$, the parameters related to DWLs are the major contributors to heat transfer for GEO_2. In terms of heat transfer, two distinct behaviors are verified: for the lower Reynolds number, the major contributor is the louver angle for both geometries. At the higher Reynolds number, the angle of attack of the DWLs positioned on the first row of DWLs are the major contributors for GEO_1, whereas the contribution of the louver angle and angle of attack of the DWLs on the

first row of DWLs has the same order of magnitude. However, the contribution of the main effects is much higher than the interaction effects for flat-tube multi-louvered fins with DWLs. Furthermore, it is important to emphasize that this type of parametric evaluation was never reported in the open literature.

For the two optimized solutions, inline arrangements of the DWLs are found to provide the highest Colburn factor for the lower Reynolds number and staggered arrangement provide the highest Colburn factor for the higher Reynolds number.

The optimized solutions for the Colburn factor showed that heat transfer behind the second row of delta-winglets has the same order of magnitude that behind the first row for both Reynolds numbers. The flow patterns and heat transfer characteristics from optimized solutions presented some particular behavior, differently from the findings when those two heat transfer enhancement techniques are applied separately. The downstream propagation of the main vortex core depends on the configuration of the DWLs and their movement on spawise direction sometimes is towards flat-tube and sometimes is towards louvered region. Moreover, especially on the first half of the fin, part of louver-directed flow is deflected towards longitudinal vortices, increasing the strength of the vortical structure. Furthermore, for all optimized solutions, a swirling motion from louver-directed flow was observed on the first part of the louver arrays and it always squeezes the longitudinal vortices towards flat-tube. This flow behavior was not verified on the second part of the louver array.

The results showed that the addition of DWLs on GEO_1 increased the heat transfer on 21% and 23% with associated pressure loss increasing of 24% and 36% for the lower and the higher Reynolds numbers, respectively. For GEO_2, the heat transfer was increased 13% and 15% with an increase of the pressure drop 20% and 23%, for the lower and the higher Reynolds numbers, respectively. Finnaly, the solutions found by optimization procedure showed that surrogate-based optimization is a powerful tool to maximize the heat transfer of the multilouvered fin compact heat exchangers with delta winglet vortex generators.

6.2 Recommendations

During the execution of this research, a number of suggested future works appeared spontaneously, indicating the paths to a better understanding of the heat transfer characteristics and flow patterns related to louvered fin heat exchangers combined with longitudinal vortex generators. The most important recommendations for future investigations are listed below:

1. Conduct experimental researches to verify exactly how heat transfer characteristics and flow patterns behave due to the addition of longitudinal vortex generators on flat-tube multilouvered fin compact heat exchangers;

2. Extend this research through evaluation of the contribution effects of other input parameters such as fin pitch, louver pitch, flow depth, amount of louvers on the array, aspect ratio of DWLs on heat transfer and pressure drop;

3. Optimization of the heat transfer enhancement performance on multouvered fin compact heat exchangers with longitudinal vortex generators for other input parameters;

4. Investigations which take into account the addition of other types of vortex generators on multilouvered fin compact heat exchangers could be very interesting;

5. The results from the present research were obtained under laminar flow conditions. It is important the evaluation of the heat transfer enhancement and pressure drop on flat-tube multilouvered compact heat exchangers with vortex generators under turbulent flow conditions;

6. The present research used surrogate-based optimization procedure to find the maximum heat transfer enhancement on multilouvered fin compact heat exchangers with delta winglet vortex generators. The use of direct optimization can provide some interesting results which were not identified on this research.

7. The thickness of the louvered fin was neglected on this present research. It could be expected that if the thickness of louvered fin were considered on

numerical model, the results of the heat transfer and pressure drop could be different from those found by optimization procedure.

References

ABDOLLAHI, A., SHAMS, M. Optimization of shape and angle of attack of winglet vortex generator in a rectangular channel for heat transfer enhancement. Applied Thermal Engineering, vol. 81, pp. 376-387, 2015.

ACHAICHIA, A., COWELL, T. A. Heat transfer and pressure drop characteristics of flat tube and louvered plate fin surfaces. Exp. Thermal Fluid Sci., vol 1, pp. 147-157, 1988.

ALIABADI, M. K., SARTIPZADEH, O., ALIZADEH, A. An experimental study on vortex-generator insert with different arrangements of delta-winglets. Energy, vol. 82, pp. 629-639, 2015.

AMEEL, B., DEGROOTE, J., HUISSEUNE, H., DE JAEGER, P., VIERENDEELS, J., DE PAEPE, M. Numerical optimization of louvered fin heat exchanger with variable louver angles. 6th European Thermal Sciences Conference (Eurotherm 2012), 2012.

AMEEL, B., DEGROOTE, J., HUISSEUNE, H., DE JAEGER, P., VIERENDEELS, J., DE PAEPE, M. Interaction effects between parameters in a vortex generator and louvered fin compact heat exchanger. International Journal of Heat and Mass Transfer, vol. 77, pp. 247-256, 2014.

ANTONIOU, A. A., HEIKAL, M. R., COWELL, T. A. Measurements of Local Velocity and Turbulence Levels in Arrays of Louvered Plate Fins, In: Proceedings of the 9th International Heat Transfer Conference, Jerusalem, Paper No. 10-EH-18, pp. 105-110, 1990.

ARORA, A., SUBBARAO, P. M. V., AGARWAL, R. S. Numerical optimization of location of 'common flow up' delta winglets for inline aligned finned tube heat exchanger. Applied Thermal Engineering, vol. 82, pp. 329-340, 2015.

ATKINSON, A. C., COX, D.R. Planning experiments for discriminating between models, J. R. Statist. Soc., vol. B36, pp. 321-348, 1974.

BALDWIN, S. J., WHITE, P. R. S., AL-DAINI, A. J., DAVENPORT, C. J. Investigation of gas side flow field in multilouver ducts with flow reversal. 5th Int. Conf. on Numerical Methods in Laminar and Turbulent Flow, Montreal, pp. 482-495, 1987.

BEAUVAIS, F. N. An aerodynamic look at automobile radiators. SAE Paper No.650470, 1965.

BERGLES, A., E. ExHFT for fourth generation heat transfer technology. Experimental Thermal and Fluid Science, vol. 26, pp. 335-344, 2002.

BISWAS, G., TORII, K., FUJII, D., NISHINO, K. Numerical and experimental determination of flow structure and heat transfer effetcs of longitudinal vortices in a channel flow. International Journal of Heat and Mass Transfer, vol. 39, No. 16, pp. 3441-3451, 1996.

BUTTON, B. L., TURA, R., WRIGHT, C. C. Investigation of the air flow through louver rectangular ducts using laser Doppler anemometry. Proc. 2nd Int. Symp. On Applications of Laser Doppler Anemometry to Fluid Mechanics, Lisbon, 1984.

CARIJA, Z., FRANKOVIC, B., PERCIC, M., CAVRAK, M. Heat transfer analysis of fin-and-tube heat exchangers with flat and louvered fin geometries. International Journal of Refrigeration, vol. 45, pp. 160-167, 2014.

CHANG, L. M., WANG, L. B., SONG, K. W., SUN, D. L., FAN, J. F. Numerical study of the relationship between heat transfer enhancement and absolute vorticity flux along main flow direction in a channel formed by a flat tube bank fin with vortex generators. International Journal of Heat and Mass Transfer, vol. 52, pp. 1794-1801, 2009.

CHATWANI, A. U., TURAN, A. Improved pressure-velocity coupling algorithm based on global residual norm. Numer. Heat Transfer, vol. 20, pp. 115-123, 1991.

CHEN, Y., FIEBIG, M., MITRA, N. K. Conjugate heat transfer of a finned oval tube with punched longitudinal vortex generator in form of a delta winglet – parametric investigations of the winglet. International Journal of Heat and Mass Transfer, vol. 41, pp. 3961-3978, 1998.

CHEN, Y. S., KIM, S. W. Computation of turbulent flows using an extended turbulence closure model, NASA CR-179204, 1987.

CHU, P., HE, Y. L., LEI, Y. G., TIAN, L. T., LI, R. Three-dimensional numerical study on fin-and-oval-tube heat exchanger with longitudinal vortex generators. Applied Thermal Engineering, vol. 29, pp. 859-876, 2009.

CONNEL, S. D., STOW, P. The pressure correction methods. Comput. Fluids, vol. 14, pp. 1-10, 1986.

COWELL, T. A., HEIKAL, M. R., ACHAICHIA, A. Flow and heat transfer in compact louvered fin surfaces. Experimental Thermal and Fluid Science, vol. 10, pp. 192-199, 1995.

CYBENKO, G. Approximation by superposition of a sigmoidal function. Math. Contr. Signal Systems, vol. 2, pp. 303-314, 1989.

DAVENPORT, C. J. Heat transfer and flow friction characteristics of louvered heat exchanger surfaces, in Heat Exchangers: Theory and Practice, pp. 397-412, 1983.

DEB, K. A fast and elitist multiobjective genetic algorithm: NSGA-II. IEEE Transactions on Evolutionary Computation, vol 6, no 2, 2002.

DeJONG, N. C., JACOBI, A. M. Localized flow and heat transfer interactions in louvered-fin arrays. International Journal of Heat and Mass Transfer, vol. 46, pp. 443-455, 2003A.

DeJONG, N. C., JACOBI, A. M. Flow, heat transfer, and pressure drop in the near-wall region of louvered-fin arrays. Experimental Thermal and Fluid Sciences, vol. 27, pp. 237-250, 2003B.

DIEMER-LOPES, L. A. D., YANAGIHARA, J. I. Flat fin structure of fin type heat exchanger for air conditioners, Patentes BR9801850-A, JP11325776-A, US6079487-A, 1999.

DOGAN, B., ALTUN, O., UGURLUBILEK, N., TOSUN, M., SARIÇAY, T., ERBAY, L. B. An experimental comparison of two multi-louvered fin heat exchangers with different numbers of fin rows. Applied Thermal Engineering, vol. 91, pp. 270-278, 2015.

DONG, J., CHEN, J., CHEN, Z., ZHANG, W., ZHOU, Y. Heat transfer and pressure drop correlations for multi-louvered fin compact heat exchangers. Energy Conversion and Management, vol. 48, pp. 1506-1515, 2007.

FABBRI, G. Heat transfer optimization in corrugated wall channels. International Journal of Heat and Mass Transfer, vol. 43, pp. 4299-4310, 2000.

FANG, K. T., LI, R., SUDJIANTO, A. Design and modeling for computer experiments. Computer Science and Data Analysis Series. Taylor and Francis Group, 2006.

FEDOROV, V. V. Various discrepancy measures in model testing (two competing regression models). In: Y. Dodge, Statistical Data Analysis Based on the L_1-Norm and Related Methods, pp. 357-366, 1987.

FERRERO, M., SCATTINA, A., CHIAVAZZO, E., CARENA, F., PEROCCHIO, D., ROBERTI, M., RIVALTA, G. T., ASINARI, P. Louver finned heat exchangers for automotive sector: numerical simulations of heat transfer and flow resistance coping with industrial constraints. ASME Journal of Heat Transfer, vol. 135, 2013.

FERROUILLAT, S., TOCHON, P., GARNIER, C., PEERHOSSAINI, H. Intensification of heat-transfer and mixing in multifunctional heat exchangers by artificially generated streamwise vorticity. Applied Thermal Engineering, vol. 26, pp. 1820-1829, 2006.

FERZIGER, J. H., PERIC, M. Computational methods for fluid dynamics. 3rd ed., New York: Springer, 2002.

FIEBIG, M. Embedded vortices in internal flow: heat transfer and pressure loss enhancement. International Journal of Heat and Fluid Flow, vol. 16, pp. 376-388, 1995.

FIEBIG, M. Vortices, generators and heat transfer. Trans IChemE, vol. 76, Part A, 1998.

FLUENT INCORPORATION. FLUENT 6.3: user's guide. Documentation, 2006.

FORRESTER, A. I. J., KEANE, A. J. Recent advances in surrogate-based optimization. Progress in Aerospace Sciences, vol. 45, pp. 50-79, 2009.

FRIEDMAN, J., HASTIE, T., TIBSHIRANI, R. The elements of statistical learning. Second Ed., 2008.

GENTRY, M. C., JACOBI, A. M. Heat transfer enhancement by delta-wing vortex generators on a flat plate: vortex interactions with the boundary layer. Experimental Thermal and Fluid Science, vol. 14, pp. 231-242, 1997.

GIUNTA, A. A., WOJTKIEWICZ, J. S. F., ELDRED, M. S. Overview of modern design of experiments methods for computational simulations. AIAA paper 2003-649, 2001.

GIUNTA, A. A. Aircraft multidisciplinary design optimization using design of experimental theory and response surface modeling methods, Ph.D. dissertation, Virginia Polytechnin Institute and State University, Virginia, 1997.

GJESDAL, T., LOSSIUS, M. E. H. Comparison of pressure correction smoothers for multigrid solution of incompressible flow. Internat. J. Numer. Methods Fluids, vol. 25, pp. 393-405, 1997.

GUNNASEGARAN, P., SHUAIB, N. H., ABDUL JALAL, M. F. The effects of geometrical parameters on heat transfer characteristics of compact heat exchanger with louvered fins. International Scholarly Research Network, vol. 2012, Article ID: 832708, 2012.

HA, M. Y., KIM, K. C., KOAK, S. H., KIM, K. H., KIM K. I., KANG, J. K., PARK, T. Y. Fluid flow and heat transfer characteristics in multi-louvered fin heat exchanger. SAE Paper no. 950115, 1995.

HAN, Z. H., ZHANG, K. S. Surrogate-based optimization. Real-World Applications of Genetic Algorithms, Dr. Olympia Roeva Ed., 2012.

HASSOUN, M. H. Fundamentals of articial neural networks. The MIT Press, Cambridge, Massachussets, 1995.

HE, Y. L., CHU, P., TAO, W. Q., ZHANG, Y. W., XIE, T. Analysis of heat transfer and pressure drop for fin-and-tube heat exchangers with rectangular winglet-type vortex generators. Applied Thermal Engineering, vol. 40, pp. 1-14, 2012.

HE, Y. L., HAN, H., TAO, W. Q., ZHANG, Y. W. Numerical study of heat-transfer enhancement by punched winglet-type vortex generator arrays in fin-and-tube heat exchangers. International Journal of Heat and Fluid Flow, vol. 59, pp. 1016-1026, 2012.

HIRAVENNAVAR, S. R., TULAPURKARA, E. G., BISWAS, G. A note on the flow and heat transfer enhancement in a channel with built-in winglet pair. International Journal of Heat and Fluid Flow, vol. 28, pp. 299-305, 2007.

HSIEH, C. T., JANG, J. Y. 3-D thermal-hydraulic analysis for louver fin heat exchangers with variable louver angle. Applied Thermal Engineering, vol. 26, pp. 1629-1639, 2006.

HSIEH, C. T., JANG, J. Y. Parametric study and optimization of louver finned-tube heat exchangers by Taguchi method. Applied Thermal Engineering, vol. 42, pp. 101-110, 2012.

HUSAIN, A., KIM, K. Y. Enhanced multi-objective optimization of a microchannel heat sink through evolutionary algorithm coupled with multiple surrogate models. Applied Thermal Engineering, vol. 30, pp. 1683-1691, 2010.

HUISSEUNE, H., T'JOEN, C., DE JAEGER, P., AMEEL, B., DE SCHAMPHELEIRE, S., DE PAEPE, M. Performance analysis of a compound heat exchanger by screening its design parameters. Applied Thermal Engineering, vol. 51, pp. 490-501, 2013A.

HUISSEUNE, H., T'JOEN, C., DE JAEGER, P., AMEEL, B., DE SCHAMPHELEIRE, S., DE PAEPE, M. Performance enhancement of a louvered fin heat exchanger by using delta winglet vortex generators. International Journal of Heat and Mass Transfer, vol. 56, pp. 475-487, 2013B.

HUISSEUNE, H., T'JOEN, C., DE JAEGER, P., AMEEL, B., DE SCHAMPHELEIRE, S., DE PAEPE, M. Influence of the louver and delta winglet geometry on the thermal hydraulic performance of a compound heat exchanger. International Journal of Heat and Mass Transfer, vol. 57, pp. 58-72, 2013C.

ISSA, R. I. Solution of implicity discretized fluid flow equation by operator-splitting. Journal of Comput. Phys., vol. 62, pp. 40-65, 1985.

JACOBI, A. M., SHAH, R. K. Heat transfer surface enhancement through the use of longitudinal vortices: a review of recent progress. Experimental Thermal and Fluid Science, vol. 11, pp. 295-309, 1995.

JANG, J. Y., TSAI, Y. C. Optimum louver angle design for a louvered fin heat exchanger. International Journal of the Physics Sciences, vol. 6(28), pp. 6422-6438, 2011.

JANG, J. Y., CHEN, C. C. Optimization of louvered-fin heat exchanger with variable louver angles. Applied Thermal Engineering, vol. 91, pp. 138-150, 2015.

JAIBOON, W., PHOOCHAROEN, N., OKAWA, S., CHAREONSUK, J. Simulation of flow aerodynamics and transfer in a plate-fin radiator. 13th Annual Symposium on Computational Science and Engineering, 2013.

JEONG, W., SEONG, J. Comparison of effects on technical variances of computational fluid dynamics (CFD) software based on finite element and finite volume methods. International Journal of Mechanical Sciences, vol. 78, pp. 19-26, 2014.

JUNJANNA, G. C., KULASEKHARAN, N., PURUSHOTHAM, H. R. Performance improvement of a louver-finned automobile radiator using conjugate thermal CFD analysis. Int. Journal of Engineering Research & Technology (IJERT), vol. 1, ISSN: 2278-0181, 2011.

KAASTRA, I., BOYD, M. Designing a neural network for forecasting financial and economic time. Neurocomputing, vol. 10, pp. 215-236, 1996.

KAYS, W. M., LONDON, A. L. Compact heat exchangers. Third Edition, Mc-Graw-Hill, New York, 1984.

KIM, M. H., BULLARD, C. W. Air-side thermal hydraulic performance of multi-louvered fin aluminium heat exchangers. International Journal of Refrigeration, vol. 25, pp. 390-400, 2002.

KIM, W. J., PATEL, V. C. Influence of streamwise curvature on longitudinal vortices imbedded in turbulent boundary layers. Computer Fluids, vol. 23, No. 5, pp. 647-673, 1994.

KREITH, F., TIMMERHAUS, K., LIOR, N., SHAW, H., SHAH, R. K., BELL, K. J., DILLER, K. R., VALDANO, J. W. The Handbook of Thermal Engineering, CRC Press LLC, 2000.

KROSE, B., SMAGT, P. An introduction to neural networks. Eighth Ed., 2006.

LAWSON, J. M. and THOLE, K. A. Heat transfer augmentation along the tube wall of a louvered fin heat exchanger using practical delta winglets. International Journal of Heat and Mass Transfer, vol. 51, pp. 2346-2360, 2008.

LEARY, S., BASHKAR, A., KEANE, A. Optimal orthogonal array-based latin hypercubes. Journal Appl. Statist, vol. 30, pp. 585-598, 2003.

LEE, L. S., TZONG, R. Y. Artificial pressure for pressure linked equation. International Journal of Heat and Mass Transfer, vol. 35, pp. 2705-2716, 1992.

LEI, Y. G., HE, Y. L., TIAN, L. T., CHU, P., TAO, W. Q. Hydrodynamics and heat transfer characteristics of a novel heat exchanger with delta-winglet vortex generators. Chemical Engineering Science, vol. 65, pp. 1551-1562, 2010.

LEMOUEDDA, A., BREUER, M., FRANZ, E., BOTSCH, T., DELGADO, A. Optimization of the angle of attack of delta-winglet vortex generators in plate-fin-and-tube heat exchanger. International Journal of Heat and Mass Transfer, vol. 53, pp. 5386-5399, 2010.

LIN, J. C. Review of research on low-profile vortex generators to control boundary-layer separation. Progress in Aerospace Sciences, vol. 38, pp. 389-420, 2002.

LIN, Z. M., LIU, C. P., LIN, M., WANG, L. B. Numerical study of flow and heat transfer enhancement of circular tube bank fin heat exchanger with curved delta-winglet vortex generators. Applied Thermal Engineering, vol 88, pp. 198-210, 2015.

LI, W., WANG, X. Heat transfer and pressure drop correlations for compact heat exchangers with multi-region louver fins. International Journal of Heat and Mass Transfer, vol. 53, pp. 2955-2962, 2010.

LIU, A., QIN, L., STAUDENMAYER, J. M-type smoothing spline ANOVA for correlated data. Jounal of Multivariate Analysis, vol. 101, pp. 2282-2296, 2010.

LYMAN, A. C., STEPHAN, R. A., THOLE, K. A., ZHANG, L. W., MEMORY, S. B. Scaling of heat transfer coefficients along louvered fins. Experimental Thermal and Fluid Science, vol. 26, pp. 547-563, 2002.

MALAPURE, V. P., MITRA, S. K., BHATTACHARYA, A. Numerical investigation of fluid flow and heat transfer over louvered fins in compact heat exchanger. International Journal of Thermal Sciences, vol. 46, pp. 199-211, 2007.

McKAY, M. D., BECKMAN, R. J., CONOVER, W. J. A comparison of three methods for selecting values of input variables in the analysis of output from a computer code. Technometrics, vol. 42, no. 1, pp. 55-61, 2000.

MIN, C., QI, C., WANG, E., TIAN, L., QIN, Y. Numerical investigation of turbulent flow and heat transfer in a channel with novel longitudinal vortex generators. International Journal of Heat and Mass Transfer, vol. 55, pp. 7268-7277, 2012.

MISHRA, M., DAS, P. K., SARANGI, S. Second law based optimization of crossflow plate-fin heat exchanger design using genetic algorithm. Applied Thermal Engineering, vol. 29, pp. 2983-2989, 2009.

MOHAMMAD, A. E., ROZATI, A., TAFTI, D. K. Investigation of dimpled fins for heat transfer enhancement in compact heat exchangers. International Journal of Heat and Mass Transfer, vol. 51, pp. 1950-2966, 2008.

PAJOUH, S. K., RENAUD, O. An exact permutation method for testing any effect in balanced and unbalanced fixed effect ANOVA. Comput. Statist. And Data Analysis, vol. 54, pp. 1881-1893, 2010.

PARK, H. S., DANG, X. P. Structural optimization based on CAD-CAE integration and metamodeling techniques. Computer-Aided Design, vol. 42, pp. 889-902, 2010.

PATANKAR, S. V., SPALDING, D. B. A calculation procedure for heat, mass and momentum transfer in three-dimensional parabolic flows. International Journal of Mass and Heat Transfer, vol. 15, pp. 1787-1806, 1972.

PATANKAR, S. V. A calculation procedure for two-dimensional elliptic situations. Numer. Heat Transfer, vol. 4, pp. 409-425, 1981.

PAULEY, W. R., EATON, J. K. The fluid dynamics and heat transfer effects of streamwise vortices embeeded in a turbulent boundary layer, Report No. MD-51, Stanford University, 1988.

PENG, H., LING, X. Neural networks analysis of thermal characteristics on plate-fin heat exchangers with limited experimental data. Applied Thermal Engineering, vol. 29, pp. 2251-2256, 2009.

PERROTIN, T., CLODIC, D. Thermal-hydraulic CFD study in louvered fin-and-flat-tube heat exchangers. International Journal of Refrigeration, vol. 27, pp. 422-432, 2004.

QI, Z. G., CHEN, J. P., CHEN, Z. J. Parametric study on the performance of a heat exchanger with corrugated louvered fins. Applied Thermal Engineering, vol. 27, pp. 539-544, 2007.

RAMU, M., PRABHU, R. V. Metamodel based analysis and its application: a review. ACTA Technica Corvinienses – Bulletin of Engineering, Fascicule 2, ISSN 2067-3809, 2013.

RICCO, L. Smoothing Spline ANOVA Model Benchmark Tests, ESTECO TECHNICAL REPORT 2013-001, 2013.

RIGONI, E., RICCO, L. Smoothing spline ANOVA for variable screening. ESTECO TECHNICAL REPORT 2011-007, 2011.

RUSSEL, C. M. B., JONES, T. V., LEE, G. H. Heat transfer enhancement using vortex generators. Seventh Int. Heat Transfer Conf., vol. 3, pp. 283-288, 1982.

RYU, K., YOOK, S. J., LEE, K. S. Optimal design of a corrugated louvered fin. Applied Thermal Engineering, vol. 68, pp. 76-79, 2014.

RYU, K., LEE, K.S. Generalized heat-transfer and fluid-flow correlations for corrugated louvered fins. International Journal of Heat and Mass Transfer, vol. 83, pp. 604-612, 2005.

SAAD, S. B., AYAD, F., DAMOTTE, H. 3D CFD simulation of thermal hydraulic performances on louvered fin automotive heat exchangers. World Academy of Science and Technology, vol. 7, 2013.

SACKS, J., WELCH, W., MITCHELL, T. J., WYNN, H. P. Design and analysis of computer experiments. Statistical Science, vol. 4, pp. 409-435, 1989.

SAHA, P., BISWAS, G., SARKAR, S. Comparison of winglet-type vortex generators periodically deployed in a plate-fin heat exchanger – A synergy based analysis. International Journal of Heat and Mass Transfer, vol. 74, pp. 292-305, 2014.

SALVIANO, L. O., DEZAN, D. J., YANAGIHARA, J. I. Multi-Objective Optimization of Vortex Generators Position and Angles in Fin-Tube Compact Heat Exchanger at Low Reynolds Number Using Neural Network and Genetic Algorithm. Proceedings of the 15th International Heat Transfer Conference – IHTC 2014, Kyoto, 2014.

SALVIANO, L. O., DEZAN, D. J., YANAGIHARA, J. I. Optimization of Winglet-Type Vortex Generator Positions and Angles in Plate-Fin Compact Heat Exchanger: Response Surface Methodology and Direct Optimization. International Journal of Heat and Mass Transfer, Vol. 82, pp. 373-387, 2015

SANAYE, S., DEHGHANDOKHT, M. Modeling and multi-objective optimization of parallel flow condenser using evolutionary algorithm. Applied Energy, vol. 88, pp. 1568-1577, 2011.

SANDERS, P. A., THOLE, K. A. Effects of winglets to augment tube wall heat transfer in louvered fin heat exchangers. International Journal of Heat and Mass Transfer, vol. 49, pp. 4058-4069, 2006.

SHENG, Y., SHOUKRI, M., SHENG, G., WOOD, P. A modification to the simple method for buoyancy-driven flows. Numer. Heat Transfer, vol. 33, pp. 65-78, 1998.

SIEGEL, F. A., ANOVA: testing for differences among many samples, and much more. Practical Business Statistics, Sixth Ed., Chapter 15, 2012.

SINHA, A., RAMAN, K. A., CHATTOPADHYAY, H., BISWAS, G. Effects of different orientations of winglet arrays on the performance of plate-fin heat exchangers. International Journal of Heat and Mass Transfer, vol. 57, pp. 202-214, 2013.

TAN, C. K., WARD, J., WILCOX, S. J., PAYNE, R. A neural network modelling of the thermal performance of a compact heat exchanger. Applied Thermal Engineering, vol. 29, pp. 3609-3617, 2009.

TAFTI, D. K., WANG, G., LIN, W. Flow transition in multilouvered fin array. International Journal of Heat and Mass Transfer, vol. 43, pp. 901-919, 2000.

TAFTI, D. K., ZHANG, X. Geometry effects on flow transition in multilouvered fins – onset, propagation, and characteristic frequencies. International Journal of Heat and Mass Transfer, vol. 44, pp. 4195-4210, 2001.

TAFTI, D. K., ZHANG, X., GUO, D. Study of multilouvered heat exchangers at low Reynolds numbers. Chapter 2, Air Conditioning and Refrigeration Center, University of Illinois, 2004.

TAO, W. Q., QU, Z. G., HR, Y. L. A novel segregated algorithm for incompressible flow and heat transfer problems – clear (coupled equations algorithm revised) part 1: mathematical formulation and solution procedure. Numer. Heat Transfer, vol. 45, pp. 1-18, 2004.

TAO, W. Q., QU, Z. G., HR, Y. L. A novel segregated algorithm for incompressible flow and heat transfer problems – clear (coupled equations algorithm revised) part 2: application examples. Numer. Heat Transfer, vol. 45, pp. 19-48, 2004.

TAO, W. Q., HE, Y. L., LI, Z. Y., QU, Z. G. Some recent advances in finite approach and their applications in the study of heat transfer enhancement. Internat. J. Thermal Sciences, vol. 44, pp. 623-643, 2005.

TAYAL, M. C., FU, Y., DIWEKAR, U. M. Optimal design of heat exchangers: a genetic algorithm framework. Industrial & Engineering Chemestry Research, vol. 38, pp. 456-467, 1999.

TIAN, L. T., HE, Y. L., LEI, Y. G., TAO, W. Q. Numerical study of fluid flow and heat transfer in a flat-plate channel with longitudinal vortex generators by applying synergy principle analysis. International Communications in Heat and Mass Transfer, vol. 36, pp. 111-120, 2009.

TIGGELBACK, S., MITRA, N. K., FIEBIG, M. Experimental investigations of heat transfer and flow losses in a channel with double rows with longitudinal vortex generators. International Journal of Heat and Mass Transfer, vol. 36, pp. 2327-2337, 1993.

TIGGELBACK, S., MITRA, N. K., FIEBIG, M. Flow structure and heat transfer in a channel with multiple longitudinal vortex generators. Experimental Thermal Fluid Sciences, vol. 5, pp. 425-436, 1992.

TIWARI, S., MAURYA, D., BISWAS, G., ESWARAN, V. Heat transfer enhancement in cross-flow heat exchangers using oval tubes and multiple delta winglets. International Journal of Heat and Mass Transfer, vol. 46, pp. 2841-2856, 2003.

T'JOEN, C., HUISSEUNE, H., CANIÈRE, H., STEEMAN, H. J., WILLOCKX, A., PAEPE, M. DE. Interaction between mean flow and thermo-hydraulic behavior in inclined louvered fins. International Journal of Heat and Mass Transfer, vol. 54, pp. 826-837, 2011.

TORII, K., YANAGIHARA, J. I. The effects of longitudinal vortices on heat transfer of laminar boundary layers. JSME International Journal, Series II, vol. 32, no. 3, 1989.

TORII, K., YANAGIHARA, J. I. A review on heat transfer enhancement by longitudinal vortices. Jour. HTSJ, vol. 36, no. 142, 1997.

URBAN,N. M., FRICKER, T. E. A comparison of latin hypercube and grid ensemble designs for the multivariate emulation of an earth system model. Computers & Geosciences, vol. 36, pp. 746-755, 2010.

VAISI, A., ESMAEILPOUR, M., TAHERIAN, H. Experimental investigation of geometry effects on the performance of a compact louvered heat exchanger. Applied Thermal Engineering, vol. 31, pp. 1-10, 2011.

VAN DOORMAAL, J. P., RAITHBY, G. D. An evaluation of the segregated approach for predicting incompressible fluid flow. ASME Paper 85-HT-9, 1985.

VAN DOORMAAL, J. P., RAITHBY, G. D. Enhancement of simple method for predicting incompressible flows. Numer. Heat Transfer, vol. 7, pp. 147-163, 1984.

WAHBA, G. Improper priors, spline smoothing and the problem of guarding against model errors in regression. Journal of Royal Statistical Society, vol. 40, pp. 364-372, 1978.

WAHBA, G., WANG, Y., GU, C., KLEIN, R., KLEIN, B. Smoothing spline anova for exponential families, with application to the Wiscousin epidemiological study of diabetic retinopathy. The Annals of Statistics, vol. 23, pp. 1865-1895, 1995.

WANG, J. S. Flow around a circular cylinder using a finite-volume TVD scheme based on a vector transformation approach. Journal of Hydrodynamics, vol. 22, pp. 221-228, 2010.

WEBB, R. L., KIM, N. H. Principles of enhanced heat transfer. Second Edition, Taylor & Francis Routledge, 2005.

WEBB, R. L., TRAUGER, P. Flow structure in the louvered fin heat exchanger geometry. Experimental Thermal and Fluid Science, vol. 4, pp. 205-217, 1991.

WEN, X., INGHAM, D. B. A new method for accelerating the rate of convergence of the simple-like algorithm. Internat. J. Numer. Methods Fluids, vol. 17, pp. 385-400, 1993.

WU, J. M., TAO, W. Q. Effect of longitudinal vortex generator on heat transfer in rectangular channels. Applied Thermal Engineering, vol. 37, pp. 67-72, 2012.

WU, J. M., TAO, W. Q. Numerical study on laminar convection heat transfer in a rectangular channel with longitudinal vortex genetator. Part A: verification of field synergy principle. International Journal of Heat and Mass Transfer, vol. 51, pp. 1179-1191, 2008.

WU, J. M., TAO, W. Q. Investigation on laminar convection heat transfer in fin-and-tube heat exchanger in aligned arrangement with longitudinal vortex generator from the viewpoint of synergy principle. Applied Thermal Engineering, vol. 27, pp. 2609-2617, 2007.

XIE, G., SUNDEN, B., WANG, Q., TANG, L. Performance predictions of laminar and turbulent heat transfer and fluid flow of heat exchangers having large tube-diameter and large tube-row by artificial neural networks. International Journal of Heat and Mass Transfer, vol. 52, pp. 2484-2497, 2009.

YANAGIHARA, J. I., TORII, K. Enhancement of laminar boundary layer heat transfer by a vortex generator. JSME International Journal, series II, vol. 35, no. 3, 1992.

YANAGIHARA, J. I., TORII, K. Heat transfer augmentation by longitudinal vortices rows. Experimental Heat Transfer, Fluid Mechanics and Thermodynamics, pp. 560-567, 1993.

YANAGIHARA, J. I. and RODRIGUES Jr., R. Numerical Study of the Heat Transfer Enhancement of Fin-Tube Channels by Vortex Generations, In: Heat Transfer 1998, Vol. 5, pp. 409-414, 1998.

YANG, J. S., LEE, D. W., CHOI, G. M. Numerical investigation of fluid flow and heat transfer characteristics by common-flow-up. International Journal of Heat and Mass Transfer, vol. 51, pp. 6332-6336, 2008.

YANG, J. S., SEO, J. K., LEE, K. B. A numerical analysis on flow field and heat transfer by interaction between a pair of vortices in rectangular channel flow. Current Applied Physics, vol. 1, pp. 393-405, 2001.

YANG, K. S., LI, S. L., CHEN, I. C., CHIEN, K. H., HU, R., WANG, C. C. An experimental investigation of air cooling thermal module using various enhancements at low Reynolds number region. International Journal of Heat and Mass Transfer, vol. 53, pp. 5675-5681, 2010.

YANG, X. S., KOZIEL, S., LEIFSSON, L. Computational optimization, modeling and simulation: recent trends and challenges. Procedia Computer Science, vol. 18, pp. 855-860, 2013.

YANG, X. S., GANDOMI, A. H. Bat algorithm: a novel approach for global engineering optimization. Engineering Computations, vol. 29, no. 5, pp. 464-483, 2013.

YEN, R. H., LIU, C. H. Enhancement of the simple algorithm by an additional explicit corrector step. Numer. Heat Transfer, vol. 24, pp. 127-141, 1993.

YU, B., OZOE, H., TAO, Q. A modified pressure-correction scheme for the simpler method, msimpler. Numer. Heat Transfer, vol. 39, pp. 439-449, 2001.

ZHANG, X., TAFTI, D. K. Classification and effects of thermal wakes on heat transfer in multilouvered fins. International Journal of Heat and Mass Transfer, vol. 44, pp. 2461-2473, 2001.

ZHANG, X., TAFTI, D. K. Flow efficiency in multi-louvered fins. International Journal of Heat and Mass Transfer, vol. 46, pp. 1737-1750, 2003.

ZHU, C., LIANG, H., SUN, D., WANG, L., ZHANG, Y. Numerical study of interactions of vortices generated by vortex generators and their effects on heat transfer enhancement. Numerical Heat Transfer, Part A, vol. 50, pp. 345-360, 2006.